DEVELOPMENT OF A THREE WAY CATALYTIC CONVERTER FOR ELIMINATION OF HYDROCARBONS, CARBON MONOXIDE AND NITRIC OXIDE IN AUTOMOTIVE EXHAUST

A THESIS SUBMITTED TO
THE GRADUATE SCHOOL OF NATURAL AND APPLIED SCIENCES
OF
MIDDLE EAST TECHNICAL UNIVERSITY

BY

NUR KANDİLLİ

IN PARTIAL FULFILLMENT OF THE REQUIREMENTS
FOR
THE DEGREE OF MASTER OF SCIENCE
IN
CHEMICAL ENGINEERING

SEPTEMBER 2010

Approval of the thesis:

DEVELOPMENT OF A THREE WAY CATALYTIC CONVERTER FOR ELIMINATION OF HYDROCARBONS, CARBON MONOXIDE AND NITRIC OXIDE IN AUTOMOTIVE EXHAUST

submitted by **NUR KANDİLLİ** in partial fulfillment of the requirements for the degree of **Master of Science in Chemical Engineering Department, Middle East Technical University by,**

Prof. Dr. Canan Özgen _____
Dean, Graduate School of **Natural and Applied Sciences**

Prof. Dr. Gürkan Karakaş _____
Head of Department, **Chemical Engineering**

Prof. Dr. Işık Önal _____
Supervisor, **Chemical Engineering Dept., METU**

Examining Committee Members:

Prof. Dr. Canan Özgen _____
Chemical Engineering Dept., METU

Prof. Dr. Işık Önal _____
Chemical Engineering Dept., METU

Prof. Dr. İnci Eroğlu _____
Chemical Engineering Dept., METU

Assist. Prof. Dr. Görkem Külah _____
Chemical Engineering Dept., METU

Dr. Mehmet Ferdi Fellah _____
Chemical Engineering Dept., Yüzüncü Yıl University

Date: (13 / 09 / 2010)

I hereby declare that all information in this document has been obtained and presented in accordance with academic rules and ethical conduct. I also declare that, as required by these rules and conduct, I have fully cited and referenced all material and results that are not original to this work.

Name, Last name : Nur, KANDİLLİ

Signature :

ABSTRACT

DEVELOPMENT OF A THREE WAY CATALYTİC CONVERTER FOR ELIMINATION OF HYDROCARBONS, CARBON MONOXIDE AND NITRIC OXIDE IN AUTOMOTIVE EXHAUST

Kandilli, Nur

M.Sc., Department of Chemical Engineering

Supervisor : Prof. Dr. Işık ÖNAL

September 2010, 172 pages

In this work, slurries of powder catalysts are washcoated on 22 mm diameter and 13 mm height cordierite monoliths. CeO_2-ZrO_2 (CZO) and CeO_2-ZrO_2-Al_2O_3 (CZAO) mixed oxides are synthesized by co-precipitation and sol-gel methods respectively, to be used as support materials of Pd and Rh metals. Metal loaded CZO is mixed with gamma phase alumina. Powder catalysts and their slurries are characterized by XRD, BET, ICP-MS and the monolithic catalysts are imaged by SEM. Catalytic activities of monolithic catalysts are tested in dynamic test system which is computerized and basically composed of gas flow control and conditioning units, split furnace, quartz reactor, mass spectrometer and CO analyzer. Gas mixture containing CO, C_3H_6, C_3H_8, NO, H_2, O_2, CO_2, SO_2, H_2O and N_2 is used to simulate the exhaust gas of gasoline vehicles. O_2 is oscillated at 1 Hz frequency around the stoichiometric condition. Monolithic catalyst in the reactor is heated and cooled between 150 ºC and 600 ºC. Gas composition data from mass

spectrometer and CO analyzer and temperature data from thermocouple at the monolith entrance, are converted to conversion versus temperature graphs. Results of 26 activity tests are compared. Catalyst containing co-impregnated CZO support material with metals, showed the lowest loss of catalytic performance after exposure to SO_2 during activity tests. Catalyst containing separately impregnated CZO support material, showed the highest resistance against thermal aging at 900 ºC and 1000 ºC, and even improved catalytic activity after aging. These catalysts showed higher resistances against the applied procedures than the commercial catalyst.

Keywords: Three Way Catalytic Converter, Automotive, Catalyst, Catalytic Activity, Aging

ÖZ

OTOMOBİL EGZOZUNDAKİ HİDROKARBONLAR, KARBON MONOKSİT VE NİTRİK OKSİT BİLEŞİKLERİNİN ARITILMASI İÇİN ÜÇ YOLLU KATALİTİK KONVERTÖR GELİŞTİRİLMESİ

Kandilli, Nur
Yüksek Lisans, Kimya Mühendisliği Bölümü
Tez Yöneticisi : Prof. Dr. Işık ÖNAL

Eylül 2010, 172 sayfa

Bu çalışmada, toz katalizörlerin sulu karışımı 22 mm çap ve 13 mm yüksekliğindeki kordierit monolitlerin üzerine kaplanmıştır. Pd ve Rh metallerinin destek malzemeleri olarak, CeO_2-ZrO_2 (CZO) ve CeO_2-ZrO_2-Al_2O_3 (CZAO) karışık oksitleri, sırasıyla beraber çöktürme ve sol-jel yöntemleri ile sentezlenmişlerdir. Metal yüklenmiş CZO, gama fazındaki alumina ile karıştırılmıştır. Toz katalizörler ve sıvıları XRD, BET, ICP-MS ile karakterize edilmiş ve monolitik katalizörler SEM ile görüntülenmiştir. Monolitik katalizörlerin katalitik aktiviteleri, bilgisayarla donatılmış ve temel olarak gaz akış kontrolü ve şartlandırma üniteleri, split fırın, kuvars reaktör, kütle spektrometresi ve CO analizöründen oluşan test sisteminde test edilmiştir. CO, C_3H_6, C_3H_8, NO, H_2, O_2, CO_2, SO_2, H_2O ve N_2 içeren gaz karışımı benzinli araçların egzoz gazını simule etmek için kullanılır. O_2 stokiometik durum etrafında 1 Hz frekansında salınım yapılır. Reaktör içindeki monolitik katalizör 150 ºC ve 600 ºC arasında ısıtılır ve soğutulur. Kütle spektrometre ve CO analizöründen gaz kompozisyon verileri ve monolit

girişindeki sıcaklık ölçerden sıcaklık verileri, dönüşüme karşılık sıcaklık grafiklerine dönüştürülür. 26 aktivite testinin sonuçları karşılaştırılmıştır. Metallerin beraber emdirildiği CZO destek malzemesini içeren katalizör, aktivite testleri süresince SO_2' ye maruz kaldıktan sonra en düşük katalitik performans kaybını göstermiştir. Metallerin ayrı ayrı emdirildiği CZO destek malzemesini içeren katalizör, 900 ºC ve 1000 ºC' de termal yaşlandırmaya karşı en yüksek direnci ve hatta yaşlandırmadan sonra iyileşmiş katalitik aktivite göstermiştir. Bu katalizörler, uygulanan prosedürlere ticari katalizörden daha fazla direnç göstermişlerdir.

Anahtar Sözcükler: Üç Yollu Katalitik Konvertör, Otomotiv, Katalizör, Katalitik Aktivite, Yaşlandırma

To My Fiancé

ACKNOWLEDGEMENTS

I would like to express my deepest gratitude to my supervisor Prof. Dr. Işık Önal for his guidance, advice, criticism, encouragements and insight throughout the research.

It is a pleasure to thank Ministry of Industry and Trade of Turkish Republic and Tofaş Türk Otomobil Fabrikası A.Ş. since this study is supported as SAN-TEZ Project No:00207.STZ.2007-2.

I would like to acknowledge the technical services supported by TERRALAB A.Ş.

I would like to thank TERRALAB A.Ş.Bilal Bayram, Selahattin Uysal and Turgut Aksakal for their technical assistances.

I would also like to thank Pelin Yetişemiyen and Elif Seda Şayin for their advice and help.

I gratefully acknowledge the scholarship demanded by TÜBİTAK during my graduate education.

My parents deserve more than I can give in return for their all kinds of supports.

Finally I owe my hearthfelt gratitude to my Fiancé, Emrah, for his endless patience.

TABLE OF CONTENTS

APPENDICES

LIST OF TABLES

TABLES

LIST OF FIGURES

FIGURES

LIST OF SYMBOLS

Symbol	Definition	Units
A, B, C	Antoine Equation Constants	-
C_{A_0}	İnitial Concentration	ppm
C_A	İnstant Concentration	ppm
P^{sat}	Saturation Pressure	torr
S	Stoichiometric Number	-
T	Temperature	ºC
V_{eff}	Effective Volume	cm^3
T50	Light-off Temperature	ºC
X	Conversion	%
γ	Gamma Phase	-
v_0	Flow Rate	mL/min

LIST OF ABBREVIATIONS

AO	Aluminum Oxide
ATSB	Aluminum Tri Sec Butoxide
A/F	Air to Fuel Ratio
CZAO	Cerium Zirconium Aluminum Oxide
CZO	Cerium Zirconium Oxide
GHSV	Gas Hourly Space Velocity
HC	Hydrocarbon
HDPE	High Density Polyethylene
MFC	Mass Flow Controller
MS	Mass Spectrometer
NOx	Nitrogen Oxides
OSC	Oxygen Storage Capacity
TWC	Three Way Catalyst

CHAPTER 1

INTRODUCTION

1.1 Exhaust Gases

Automotive exhaust gases exiting from the gasoline vehicles consist of many harmful compounds causing air pollution. These compounds are originated from the combustion chamber where incomplete combustion of fuel and high temperatures take place. The major pollutants in the exhaust gas are unburned or partially burned hydrocarbons (HCs), carbon monoxide and nitrogen oxides (NOx), especially nitric oxide. Besides these, it mainly contains oxygen, hydrogen, nitrogen, water and carbon dioxide as combustion products and sulphur oxides formed from the sulphur in the fuel (Kaspar et al., 2003a; Ulla, 2003). As the world attention increased to air pollution, limits of harmful compounds in exhaust gas become more stringent by environmental legislations (Fornasiero et al., 2008). For the abatement of emissions from exhaust gases, automobiles are equipped with a three way catalytic converter. Three way catalytic converters can convert harmful HCs, CO and NOx simultaneously and efficiently into partially harmless CO_2, H_2O and N_2 (Ulla, 2003).

1.2 Catalytic Reactions

Engine exhaust gases are very complex mixtures and in the catalytic converter both the oxidation and reduction reactions take place as well as many other side reactions. In Table 1.1, the most general desired reactions on the three way catalytic converter are given, which contribute to the abatement of pollutants in the exhaust gases. To promote these desired reactions three way catalytic converter has to be highly selective (Kaspar et al., 2003a; Ulla, 2003).

Table 1. 1 Main Reactions Occurring on the Three Way Catalytic Converter (Ciambelli et al., 2003; Ulla, 2003; Kaspar et al., 2003a).

Oxidation

$$2CO + O_2 \rightarrow 2CO_2$$
$$4C_xH_y + (4x + y)O_2 \rightarrow 4xCO_2 + 2yH_2O$$
$$2H_2 + O_2 \rightarrow 2H_2O$$

Reduction

$$2CO + 2NO \rightarrow 2CO_2 + N_2$$
$$4C_xH_y + (8x + 2y)NO \rightarrow (4x + y)N_2 + 4xCO_2 + 2yH_2O$$
$$2H_2 + 2NO \rightarrow 2H_2O + N_2$$

Water Gas Shift

$$CO + H_2O \rightarrow CO_2 + H_2$$

Steam Reforming

$$2C_xH_y + 4xH_2O \rightarrow 2xCO_2 + (4x + y)H_2$$

1.3 Air to Fuel Ratio

Emissions from automobiles depend on air to fuel ratio (A/F). Under fuel rich conditions higher power is obtained consuming higher amounts of fuel. On the other hand, under fuel lean conditions due to the lower combustion temperatures NOx emissions are reduced. However, HC emissions increase through higher A/F ratios. In order to achieve high conversion rates of pollutants, A/F ratio need to be at stoichiometric condition which is 14.6 on weight basis (Kaspar et al., 2003a; Fornasiero et al., 2008). For the efficient operation of three way catalytic converter, A/F ratio in the engine is controlled by an O_2 sensor and oscillated around the stoichiometric value at a frequency of 0.5 or 1 Hz (Farrauto & Heck, 1999).

1.4 Light – Off Temperature

The light-off temperature is defined as the temperature at which the conversion of a specific reactant is 50% (Noh et al., 1999). A three way catalyst (TWC) shows typical light-off type behavior on conversion vs. temperature curves which can be described as a steady increase of conversion from 0% to 100% (Kaspar & Fornasiero, 2003). The light-off characteristic of a TWC is a sign of its performance efficiency. Lower light-off temperature indicates higher TWC activity and performance (Di Monte et al., 2002; Yucai, 2006). At cold start of an engine catalytic activity is low since the light off temperatures are generally not reached and most of the total emission is released during this period. Therefore TWCs with lower light-off temperatures are needed especially for the abatement of cold start emissions (Wang et al., 2004).

1.5 Mechanical Structure of a Three Way Catalytic Converter

A three way catalytic converter composed of a stainless steel container and a honeycomb structured monolith mounted in the container. The catalyst is washcoated on this monolith by dipping the monolith into the slurry prepared with the catalyst precursors. The excess washcoat in the channels are blown out with air and after calcination of the monolith the three way catalyst is obtained. The monoliths can be metal or ceramic made of cordierite. Ceramic monoliths are porous, making the washcoating process easy. Besides, the ceramic monoliths can be produced at lower cost. On the contrary, metal monoliths are non-porous but have walls with lower thickness (Kaspar et al., 2003a).

1.6 TWC Components

The primary components of the washcoat are alumina, cerium-zirconium mixed oxides, noble metals and stabilizers. Honeycomb monolith has a very limited surface area and alumina is used to provide high surface area for the dispersion of noble metals. In addition, alumina, especially γ-alumina shows high stability against the hydrothermal conditions of the exhaust gases. To increase the stability of surface area stabilizers such as lanthanum, barium, cerium and zirconium oxides are used (Kaspar et al., 2003a). Cerium and zirconium oxides are used as promoters. Cerium oxide is reported to stabilize the noble metal dispersion, increase the thermal stability of alumina support, promote the water-gas shift and steam reforming reactions at low temperatures and provide oxygen storage capacity (OSC) by storing and releasing oxygen under lean and rich conditions respectively (Kaspar et al.,

2003a; Yao et al., 1997). On the other hand, adding zirconium oxide to cerium oxide improves the thermal stability, oxygen storage capacity and low temperature catalytic activity (Yingying et al., 2007).

1.7 Catalyst Deactivation

Thermal deactivation is the major deactivation pathway for a TWC. High temperatures reached by TWC cause the sintering of the oxygen storage component and loss of its redox property. Sintering and alloying of noble metals, metal losses and metal-support interactions are other deactivation mechanisms caused by high temperatures (Fornasiero et al., 2000; Granados et al., 2006). Foreign components such as S and Pb present in the fuel additives and P, Zn and Ca present in the lubricant oil additives deposit on TWCs and interact with the components of TWC causing chemical deactivation (Lambrou et al., 2005).

1.8 Objective of the Study

The objective of this study is to develop three way catalysts which have low light-off temperatures, high stability against SO_2 exposure and high thermal stability. In order to determine the light-off temperatures of the catalysts, it is aimed to perform dynamic catalytic activity tests using simulated exhaust gas. In this study, several powder catalysts are synthesized and washcoated on cordierite monoliths to obtain monolithic catalysts. The catalytic activities of the monolithic catalysts are tested in dynamic test system. First, the effect of SO_2 exposure on a set of monolithic catalysts are determined during a

series of catalytic activity tests. Then, a second set of monolithic catalysts are aged at high temperature and the effect of high temperature aging is determined by comparing the catalytic activities of the catalysts before and after aging. The samples of commercial catalyst are also subjected to same treatments and the results are compared with the research catalysts.

CHAPTER 2

LITERATURE SURVEY

2.1 Support Material

Kaspar and Fornasiero (2003) stated that noble metals can perform highest conversions of pollutants in exhaust as the stoichiometric composition is maintained against air-to-fuel oscillations with the help of OSC of a TWC. CeO_2-ZrO_2 mixed oxides serve as oxygen storage/release components under fuel lean and fuel rich conditions respectively. However, due to the sintering of OSC component at high temperature, OSC property is lost. So OSC components with high thermal stability are needed in order to overcome this deactivation mechanism. CeO_2-ZrO_2 mixed oxides are used in TWCs because of their high redox behavior and high thermal stability compared to pure CeO_2.

Di Monte et al. (1998) proved that the ZrO_2 doped CeO_2 has improved redox property (oxygen storage capacity) and catalytic activity. In the bulk of the solid solution these mixed oxides have high oxygen mobility, so the redox processes are no more dependent on surface area. As a result, even after severe sintering, no deactivation is observed making the catalysts thermally stable.

Rossignol et al. (1999a) indicated that the $Ce_xZr_{1-x}O_2$ mixed oxides with “x” value larger than 0.5 have high thermal stability. In another study by

Rossignol et al. (1999b), the $Ce_{0.75}Zr_{0.25}O_2$ mixed oxide with improved thermal stability and promoted OSC is investigated.

Kaspar et al. (2003b) synthesized $Ce_xZr_{1-x}O_2$ by citrate complexation method for a range of compositions and studied the textural properties. They have concluded that the composition of the $Ce_xZr_{1-x}O_2$ effects the sintering of the particles. For the use in catalytic applications, compositions which are rich in cerium are better for catalytic applications up to 1000 ºC. Di Monte et al. (2005) indicated that $Ce_{0.8}Zr_{0.2}O_2$ is found as the most texturally stable $Ce_xZr_{1-x}O_2$ composition.

Gennari et al. (2008) synthesized $Ce_{0.8}Zr_{0.2}O_2$ solid solutions with two different techniques of co-precipitation and microemulsion. With both techniques, homogenous $Ce_{0.8}Zr_{0.2}O_2$ with high surface area were prepared. Co-precipitation technique resulted in higher surface areas.

Kaspar and Fornasiero (2003a) stated that in order to improve the thermal stability, the CeO_2-ZrO_2 mixed oxide is dispersed over Al_2O_3 support. However, homogeneous products can not be produced by impregnating of Al_2O_3 with ceria and zirconia nitrates since the ZrO_2 spreads over the Al_2O_3 surface. Also when the CeO_2 is obtained by impregnating the Al_2O_3 support, high temperatures result in formation of $CeAlO_3$ which deactivates the OSC component. For this reason, in usual practice, the mixed oxide is previously synthesized and then suspended with Al_2O_3 and other components for washcoating process. In three way catalytic applications γ- Al_2O_3 is employed rather than other transition aluminas due to its high surface area property. The use of CeO_2-ZrO_2 mixed oxides which are rich in ZrO_2 content are reported to stabilize the alumina thermally. To improve the thermal stability of the alumina, sol-gel techniques are also employed.

Considering the use of thermally stable CeO_2-ZrO_2-Al_2O_3 system as three way catalyst in automotive industry, Zahir et al. (2007) investigated the use of hydrothermally stable mesoporous CeO_2-ZrO_2-Al_2O_3 system for hydrogen separation membrane where high temperature and high steam atmosphere is present. They have synthesized CeO_2-ZrO_2-γ-Al_2O_3 mixed oxide by sol-gel method and studied the relationship between the molar composition and textural and structural properties of the system. XRD, SEM and TEM characterizations displayed that a single solid solution phase is observed only for the CeO_2-ZrO_2-γ-Al_2O_3 system with a molar ratio of 10:10:80 mol%, as $Zr_{0.32}Ce_{0.68}O_2$. In addition, N_2 adsorption/desorption experiment showed that this sample has a mesopore structure. The most important part of the study was that they have treated their samples under severe hydrothermal condition of 75% steam at 500 ºC and the same sample is found to be highly hydrothermally stable against the treatment for more than 20 h with negligible change in pore size structure.

2.2 Monolith Coating

The most used catalyst carrier for the three way catalytic converters is ceramic monolith made of cordierite ($2MgO.2Al_2O_3.5SiO_2$). Cordierite has high mechanical strength and low thermal expansion coefficient, that allow the monolith stand against high temperature and temperature differences. Cordierite monoliths can be produced up to 900 cells/in^2 cell densities. The coating of the monolith with the catalyst called as washcoating. Washcoating of catalyst slurry can be done by dipcoating of the monolith. In this process, the monolith is first dipped into the washcoating slurry containing the catalyst for a short time. After removing it from the slurry, most of the liquid in the channels of the monolith is shaken out and the rest is blown out by

pressurized air. Then it is horizontally dried and calcined to fix the coating on the monolith. In the slurry, large particles exist and after coating, with the evaporation of liquid these particles start to touch each other. However the interaction between these large particles is insufficient to have a stable coating. Small binder particles provide the necessary contact surface for larger particles. For the coating of alumina, pseudo-boehmite can be used as a binding agent. The binder amount in the slurry should be around 10 wt% where the total solid content of the slurry should be 40-50 wt% (Nijhuis et al., 2001). In case of using boehmite as binder, nitric acid is used to activate the boehmite as binder (U.S. Patent No. 5,212,130). U.S. Patent No. 5,292,991 discloses the use of pseudoboehmite alumina as binder in the slurry. Nguefack et al. (2003) synthesized hydrated pseudoboehmite by the hydrolysis of aluminum-tri-sec-butoxide with water. XRD diffractograms showed that boehmite phase remains present up to calcination temperature of 380 ºC.

2.3 Catalytic Activity Measurements

Several studies including catalytic activity measurements are examined and important parameters of the measurement methods are listed in Table 2.1. Among them, Beck et al. (1994) evaluated their pellet size catalysts for light-off and isothermal activity. The composition of the feedstream is chosen to simulate the vehicle exhaust and it is alternated between the reducing and oxidizing feedstream conditions using a switching valve controlled by computer. Since the alkenes are the most abundant hydrocarbon species in the exhaust, propylene is chosen as the representative of the hydrocarbon emissions. For light-off tests, the sample is stabilized in nitrogen flow at 600

ºC and then exposed to simulated exhaust gas while the sample is cooled to 100 ºC at a rate of 20 ºC/min .

Agrafiotis et al. (2001) tested the coated honeycombs in a tubular oven heated up to 700 ºC at a rate of 3 ºC/min and kept at this temperature for 30 min. They used a mixture of gas from a cylinder at stoichiometric condition. Apart from the species listed in Table 2.1, this mixture also contained toluene, methane, ethylene, ethane, butadiene, pentane and benzane as hydrocarbons. The feedstream and product gases are sampled and analyzed later.

Gonzales-Velasco et al. (2001) performed four different activity measurements for the pellet size catalysts; stationary light-off, cycled light-off, stoichiometric windows and performance for the water gas shift and steam reforming reactions. The product gases were removed from the steam and the remaining CO, CO_2, NH_3 and N_2O were analyzed by nondispersive infrared, C_3H_6 by flame ionization, O_2 by magnetic susceptibility and NO and NO_2 by chemiluminiscence. Before stationary light-off tests, the sample is kept under N_2 flow at 100 ºC for 4 h. With the flow of stoichiometric gas composition the sample is heated from 100 ºC to 600 ºC with a rate of 3 ºC/min. For the cycled light-off tests, the feed stream is cycled between the oxidizing and reducing conditions around the stoichiometric condition. During the stoichiometric windows tests, the selectivity and the conversion of the nitrogen containing compounds are measured at 500 ºC but at different A/F ratios. In order to determine the performance of water gas shift and steam reforming reactions, the sample exposed first to stoichiometric gas composition composed of CO, H_2O and N_2 and then to gas composition composed of C_3H_6, H_2O and N_2. Between the change in gas composition, the sample is exposed to N_2 flow. At each conditions, the conversion is

measured after 10 min stabilization at different temperatures of 200 ºC, 300 ºC, 400 ºC and 500 ºC.

Tanaka et al. (2003) determined the catalytic activity of the powder catalysts for propane oxidation in a fixed bed flow reactor. Before the activity measurement, the sample is pretreated with O_2 at 300 ºC for 1 h. After 1 h of reaction with the reaction gas consisting of C_3H_8, O_2 and N_2, the product gas is analyzed with gas chromatography. On the other hand, the three way catalytic activity is measured with the compositions in Table 2.1. Pretreatment of the sample is performed with the gas mixture at stoichiometric condition for 15 min at 550 ºC.

Yamazaki et al. (2004) used fixed bed reactor and cycled feed stream around the stoichiometric ratio for the catalytic activity measurement of the powder catalysts. The exit product is removed from the water vapor and analyzed continuously by nondispersive infrared spectrophotometer for CO and CO_2, by flame ionization detector for hydrocarbons, by magnetic susceptibility for O_2, and by chemiluminescence equipped with an automotive gas analyzer for NOx. They performed two experiments for light-off performance and for conversion efficiency at different stoichiometric numbers. For the light-off performance, the feed stream is cycled and the sample is heated over 600 ºC at a rate of 5 ºC/min.

Shinjoh et al. (2004) also used fixed bed reactor for the catalytic activity measurements of the powder samples. The exit product, removed from water, is analyzed continuously by nondispersive infrared for CO and CO_2, flame ionization for hydrocarbons, flame photometry for SO_2, magnetic susceptibility for O_2 and chemiluminescence for NOx. Catalytic activity is measured both as a function of O_2 concentration and temperature. Temperature is changed between 200 ºC and 500 ºC at every 50 ºC and the

O_2, C_3H_6 and CO composition of the gas mixture is changed for various measurements.

Granados et al. (2005) used fixed bed flow reactors for grinded commercial monolithic three way catalyst. The CO, H_2 and O_2 concentrations was cycled between the values in Table 2.1. The temperature is raised from 100 ºC to 700 ºC at a rate of 5 ºC/min and the exit product is analyzed continuously by chemiluminescence detector for NO, by dispersive infrared detectors for CO and CO_2, by paramagnetic detector for O_2 and by quadrupole mass spectrometer for C_3H_6 , H_2 and O_2.

Suopanki et al. (2005) tested the coated metallic foil sample under stoichiometric gas composition. The sample is heated to 400 ºC at a rate of 11.5 ºC/min and the conversion values at 400 ºC are evaluated.

Apart from these studies, at METU, Zoarob (1991) studied with monolithic TWC and made a mathematical model of monolithic reactor. This model is used for effective diffusivity measurements, applying pulse testing method with an optimization procedure. In his study, he found that the effective diffusivity is not depended on the gas velocity, however it is highly depended on entrance shape of the reactor.

	Beck et al. (1994)	Agrafiotis et al. (2001)	Gonzales-Velasco et al. (2001)	Tanaka et al. (2003)	Yamazaki et al. (2004)	Shinjoh et al. (2004)	Granados et al. (2005)	Suopanki et al. (2005)
C_3H_6	300 ppm	30 ppm	900 ppm	500 ppm	0.053 %	1200 ppm (as C)	900 ppm	375 ppm
C_3H_8	-	5 ppm	-	133 ppm	-	-	-	125 ppm
CO	0.77%	1 %	0.4-1.6 %	0.70-2.20 %	0.72-1.83 %	0.015 %	0.4-1.6 %	1 %
CO_2	10 %	9,5 %	10 %	8 %	8 %	6.7 %	10 %	10 %
O_2	0.2-1.0 %	0.75 %	0.46-1.26 %	0.67-1.67 %	0.65-1.40 %	0.1-10 %	0.77-1.37 %	0.65 %
NO	500 ppm	-	900-1700 ppm	1700 ppm	0.12 %	230 ppm	900 ppm	1500 ppm
SO_2	0.5,10,20,30 ppm	-	-	-	-	25 ppm	25 ppm	-
H_2O	10 %	-	10 %	4 %	5 %	5 %	10 %	10 %
H_2	0.2 %	-	-	0.23 %	0.24-0.61 %	-	0.13-0.53 %	-
N_2	Balance	Balance	Balance	Balance	Balance	Balance	Balance	Balance
GHSV (h^{-1})	135,000	50,000	125,000	81,000	90,000	-	100,000	50,000
Perturbation	± 0.5 A/F	-	± 0.5 A/F	± 4 % λ	S: 0.36-1.65	-	± 0.03 A/F	± 0.22 % O_2
Frequency	0.5 Hz	-	1 Hz	0.5 Hz	-	-	-	1 Hz

Table 2.1 Summary of the Literature Survey on Catalytic Activity Tests

CHAPTER 3

EXPERIMENTAL

3.1 Catalyst Preparation

In this study, catalysts are initially prepared as powder. Powder catalysts are composed of support material and precious metals added onto these support materials. Two kinds of support materials are used in this study, ceria-zirconia and ceria-zirconia-alumina mixed oxides. Later these powder catalysts are slurried with the addition of pseudoboehmite as binder material and nitric acid. The slurry is washcoated on cordierite monoliths to have monolithic catalysts. Preparation of support materials and binder, metal addition methods, preparation of washcoating slurry and monolith washcoating process are explained below in details.

3.1.1 Preparation of Ceria – Zirconia Mixed Oxide

Co-precipitation technique is used to synthesize the ceria - zirconia mixed oxide (CZO) described by Gennari et al. (2008). An aqueous solution of cerium (III) nitrate hexahydrate ($CeN_3O_9.6H_2O$) (Aldrich, 99 %) and zirconyl nitrate hydrate ($N_2O_7Zr.aq$) (Fluka, ~27 % Zr (gravimetric)) is prepared with Ce/Zr atomic ratio of 4/1. H_2O_2 (J.T.Baker, 30 % v/v) is added into the solution for the complete oxidation and the solution is stirred for 1 h. Then the solution is added dropwise into the excess ammonium hydroxide solution

(NH_4OH) (Aldrich, 33 % NH_3) and kept 12 h to have complete precipitation. The product is washed and filtered with 2-propanol ($CH_3CHOHCH_3$) (J.T. Baker), then refluxed in $CH_3CHOHCH_3$ for 6 h. The product is dried at 150 ºC for 12 h. The powder sample is grounded and calcined in an oven under dry air at 550 ºC for 1 h.

3.1.2 Preparation of Ceria – Zirconia – Alumina Mixed Oxide

Ceria – zirconia – alumina mixed oxide (CZAO) is synthesized by sol – gel method described by Zahir et al. (2007) and Germani et al. (2005). Aluminum tri-sec-butoxide (ATSB), ($Al(OC_4H_9)_3$) (Aldrich, 97 %) is hydrolyzed with deionized water in excess molar ratio of H_2O/ATSB=100 at 85 ºC under vigorous stirring for 1 h. The mixture is cooled to to 60 ºC and nitric acid (HNO_3) (Merck, 65 %) is added for peptization with a molar ratio of HNO_3/ATSB=0.07. Then the temperature is increased again to 85 ºC and refluxed for 12 h. An aqueous solution of $.CeN_3O_9.6H_2O$ (Aldrich, 99 %) and $N_2O_7Zr.aq$ (Fluka, ~27 %Zr) is prepared with an atomic ratio of 1.0. The gel is dried at 150 ºC for 48 h. The powder sample is grounded and calcined in an oven under dry air at 600 ºC for 3 h with a heating rate of 1 ºC/min.

3.1.3 Preparation of Pseudoboehmite

Hydrated pseudoboehmite is synthesized by sol – gel method described by Nguefack et al. (2003). $Al(OC_4H_9)_3$ (Aldrich, 97 %) is hydrolyzed with deionized water at 60 ºC under vigorous stirring for 2 h. For peptization, aqueous HCl (Aldrich, min 37 %) is added and the sol is stirred for 1 h after

increasing the temperature to 80 ºC. The gel is dried at 150 ºC for 48 h. The powder sample is grounded and calcined in an oven under dry air at 300 ºC for 5 h with a heating rate of 5 ºC/min.

3.1.4 Addition of Metals

The deposition of metals onto the support materials can be carried out using one of the methods of impregnation, ion-exchange co-precipitation or vapor deposition. Vapor deposition method is not economical. Co-precipitation method is generally used for the preparation of base metal catalysts and co-precipitation of metals with the support material is not efficient since the recovery of the metals during the recycling process is not possible. Thus, ion-exchange and impregnation methods are used usually for preparing precious metal catalysts (Cooper et al., 1987). Impregnation method is used generally for addition of metals into the pre-synthesized support materials. In this method, the solution of the metal salt is impregnated on the support material and the impregnated support material is dried and calcined for the decomposition of the metal salts (Graham & Vedrine, 2003).

3.1.4.1 Impregnation of Metals

The mixed oxides synthesized by co-precipitation or sol-gel technique is impregnated with metals using rotary vacuum evaporator. Based on the total catalyst weight, Pd and Rh metals are impregnated on the support material with a Pd/Rh ratio of 6.5 as 0.1 and 0.65 wt% respectively. Palladium (II) chloride solution (Aldrich, Pd_2Cl, 5 wt% solution in 10 wt% HCl) and rhodium

(III) nitrate solution (Aldrich, ~10 wt% Rh in >5 wt% nitric acid) are used as metal sources. In order to use the necessary water for the impregnation process, the water capacity of the support sample is determined first. A 1 g of support sample is put in a pot with a flat surface and water is added slowly until the sample is able to absorb. The amount of water that the sample can take is noted as the water capacity of the sample as mL water/1 g of sample. The metal to be impregnated is dissolved in 1.2 times of the water capacity of the support to have a homogeneous mixture in a flask. The mixture is mixed for 30 min in rotary vacuum evaporator without any vacuum or heating. Then the support sample is added to the mixture. The flask is immersed in the water bath at 80 ºC while rotating under vacuum. When all the liquid in the flask is evaporated, the flask is placed in an oven and the sample is dried at 150 ºC for 12 h. The powder sample is grounded and calcined in an oven under dry air at 550 ºC for 1 h. Two kinds of impregnation methods are used in the synthesis of metal supported catalysts; co-impregnation (CI) or separate impregnation (SI). In co-impregnation, palladium and rhodium metals are present in the same aqueous solution and they are impregnated together onto the support material. On the other hand, in separate impregnation the aqueous solutions of palladium and rhodium metals are prepared separately and these solutions are used for the impregnation of metals onto separate support materials. In this study co-impregnated support materials are named as CZO-CI and CZAO-CI whereas the separate impregnated CZO support material is named as CZO-SI.

3.1.4.2 Addition of Metals in Sol

Addition of metals into the sol of CZAO is performed as follows. The aqueous solution of metals is added into the sol after the reflux and stirred for 30 min.

The resulting gel is dried at 150 ºC for 48 h. The powder sample is grounded and calcined in an oven under dry air at 600 ºC for 3 h with a heating rate of 1 ºC/min. This powder catalysts is named as CZAO-S.

The details of the catalyst preparation processes that are described so far are given with examples in Appendix A.

3.1.5 Preparation of Washcoating Slurry

The wascoating slurry is prepared as follows: in case of using impregnated CZO support materials (CZO-CI or CZO-SI), they are mixed with gamma phase aluminum oxide (γ-Al_2O_3)(AO) and named as CZO-CI+AO or CZO-SI+AO. Also pseudoboehmite is added to mixture as binder, as Ce is 19 wt% of the total catalyst and pseudoboehmite is 10 wt% of γ-Al2O3. CZAO support material already contains alumina so the metal loaded CZAO support materials (CZAO-CI or CZAO-S) are directly used to make slurry.

The slurry of the powder catalysts are used to washcoat the monoliths. The resulting monolithic catalysts are subjected to two different catalytic activity test procedures that will be explained in following sections. So the catalysts are classified as first and second set according to the catalytic activity test procedures that they are subjected after washcoated on monoliths. The catalysts included in the first and second tests are indicated with (1) and (2) after their names respectively. In the first set, CZO-CI+AO-(1), CZAO-S-(1) and CZAO-CI-(1) are included. Before the preparation of CZO-CI+AO-(1) catalyst slurry, the CZO and AO are mixed in deionized water as 40 wt% solid content, ball-milled for 24 hours and then dried at 150 ºC for 12 h and calcined in an oven under dry air at 550 ºC for 1 h, to obtain a complete

powder catalyst. The CZAO-CI-(1) and CZO-CI+AO-(1) catalysts are resynthesized and included in second set as CZAO-CI-(2) and CZO-CI+AO-(2). In addition, CZO-SI+AO-(2) catalyst is also included in second set of catalysts. Binder material is started to be used after the coating processes of CZO-CI+AO-(1) and CZAO-S-(1) catalysts, so the slurries of CZO-CI+AO-(1) and CZAO-S-(1) catalysts do not contain binder material.

For all kinds of catalysts, all the ingredients are mixed with a deionized water so as the total solid content of the slurry is 40 wt%, in a high density polyethylene (HDPE) mortar with 3 mm alumina bills. The slurry is ball milled at 275 rpm for 30 min. Nitric acid is added into the slurry and the slurry is ball milled again for 3 h at the same speed.

3.1.6 Monolith Coating

Laboratory scale monoliths which are 22 mm in diameter and 13 mm in height and having 600 cells/in^2, are washcoated by dipcoating technique. Before the coating the bare monoliths are weighted. The monolith is dipped into the slurry, removed, turned upside down and dipped again. After removing from the slurry, the liquid in the monolith channels are shaken out and the remaining is blown out with pressurized air. Monoliths placed horizontally in the oven and dried at 150 ºC for 12 h. Then they are calcined in an oven under dry air at 550 ºC for 1 h. After calcinations excess coating on the outer walls of the monolith is cleaned and weighted again. If the coated catalyst amount is not necessary, the whole washcoating process is repeated. In the case of the coating process of CZO-I+AO and CZAO-S catalyst slurries which do not contain binder material, instead of 12 h drying

and calcination, monoliths are dried at 150 ºC for 30 min and dipcoating proceses repeated for three times and calcinated after.

3.2 Catalyst Characterization

The BET surface area of the catalysts are determined using a “Quantachrome Corporation, Autosorb-6” instrument. The crystal structure of the catalysts are identified by XRD technique using Cu X-ray radiation at 40 kV and 40 mA with scan speed of 2 degrees / min. The Pd and Rh metal content of the prepared wascoating slurries are analyzed by “Perkin Elmer DRC II” model inductively coupled plasma mass – spectrometer (ICP-MS). The washcoated monolits are screened by ”QUANTA 400F” model field emission scanning electron microscope (SEM). Adherence test is performed by keeping monoliths 15 min in ultrasound bath. After drying at 150 ºC for 12 h the weight loss is determined.

3.4 Catalytic Activity Tests in Dynamic Test System

To decide whether a monolithic catalyst can be used as a three way catalyst or not, its catalytic activity has to be tested at similar conditions with automotives. For this purpose, a test system is constructed simulating the operating conditions in automotives. Catalytic activity of a three way catalyst is evaluated according to percent conversion of pollutants and the corresponding temperatures. A mixture of gases is used to simulate the exhaust gases and passed through the reactor. The reactor with the monolithic catalyst placed inside, is heated and cooled back to simulate the

temperature changes of three way catalytic converters. The temperature at the entrance of the monolithic catalyst is controlled by a thermocouple. With this system the product gases from the reactor can be analyzed dynamically by mass spectrometer and CO analyzer. Finally the gas composition and temperature data are combined to obtain conversion vs. temperature graphs for each type of gas species.

3.4.1 Dynamic Test System

Dynamic test system, illustrated in Figure 3.1, is completely computerized and it is basically composed of gas flow control and conditioning units, a split furnace, a quartz reactor, a Hiden HPR-20 Q/C Mass Spectrometer (MS) and a Teledyne model 7600 non-dispersive infrared CO Analyzer. A gas mixture composition is used to simulate the exhaust gas exiting from gasoline vehicles, using five gas cylinders. Using mixture of gases reduces the fixed and operating costs of the test system. In addition, rather than controlling the low flow rates of each pure gas species, combination of these species results in a higher flow rate and makes the flow control easier. The first cylinder contains mixable hydrocarbons of C_3H_6, C_3H_8, CO, CO_2 and H_2 together with the percentages of 0.33, 0.11, 8.87, 2.04 and 88.65 respectively. The composition of this cylinder is determined so as to satisfy the final composition of simulated exhaust gas. The second cylinder is a mixture of NO and N_2 with 50 % each. The third cylinder contains 100 ppm SO_2 in N_2. Because of the corrosive nature of NO and SO_2 and the low flow rates of these species needed during the tests, they are diluted with N_2. Pure oxygen and nitrogen gases are contained in separate cylinders. 1/8 inch teflon pipes are used to carry the gases from cylinders. Using a computer program, predefined values of gas flow rates from five cylinders are input and the flow

rates of gases are controlled by five mass flow controllers (MFCs). In order to have an oxygen oscillation, a separate oxygen pipe is directly sent to the inlet of the reactor. The oxygen is sent through this pipe by a selenoid valve working at a frequency of 1 Hz and the necessary flow rate is regulated by the help of a flow reducer. In order to have 10 % of water vapor in the simulated exhaust gas, the nitrogen gas from MFC5 is used to carry water vapor to the system from the water bath kept at 54 ºC. All the gases from MFC1, MFC2, MFC3 and MFC4 are mixed in a manifold and at the exit of the manifold, these mixture of gases are combined with the saturated nitrogen gas. The pipes where water vapor is passing are all heated electrically to prevent the condensation. Using the valves VTP6 and VTP7, the mixture of gases are either sent through the reactor or by-passed. The quartz reactor is 80 cm in height and composed of several quartz sections. It is placed vertically in the split furnace. The reactor is designed to test the monolithic catalysts only 2.2 cm in diameter and 1.3 cm in height. Feed stream enters the reactor through 4 mm inner diameter and vertically 27.5 cm long spiral quartz pipe. A thermocouple is placed in the reactor, through a quartz pipe, at just the entrance of the monolith where the feed stream meets the monolith. The temperature of the oven is controlled according to this thermocouple, so the temperature data corresponds to the monolith exactly. Monolithic catalyst is placed inside a quartz capsule which is located 30 cm from the top of the reactor. A quartz filter is placed under the monolith for keeping the impurities and the product gases are removed from a 4 mm inner diameter quartz pipe. Product gases are first conditioned to remove water and then approximately 1 L of it regulated by rotameter is sent to the MS and CO analyzer and the rest is vented. All the data from the thermocouple placed inside the reactor, CO analyzer and MS are collected by the MAS-SOFT computer program linked to MS.

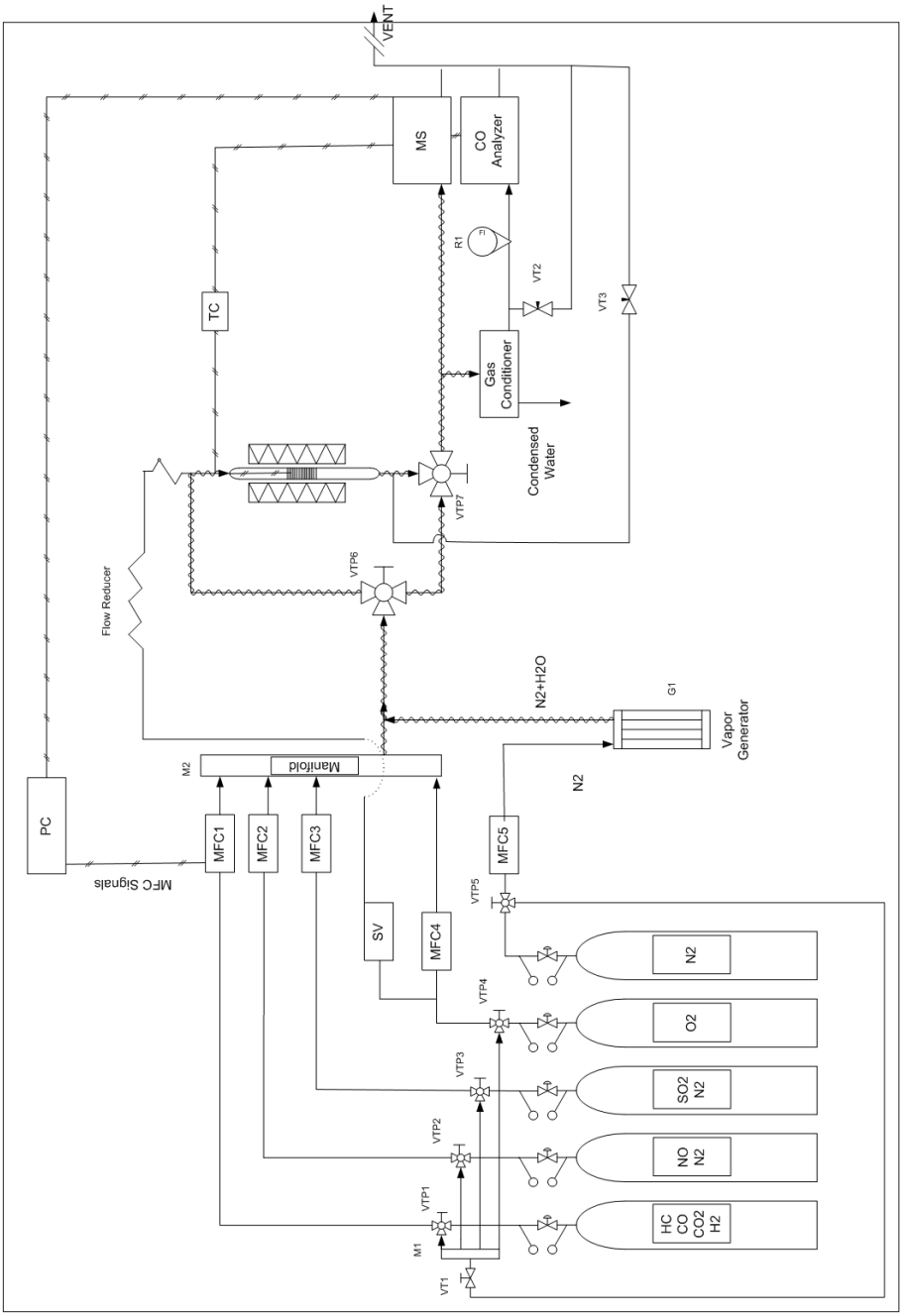

Figure 3.1 Dynamic Test System

3.4.2 Catalytic Activity Tests

A sample monolith catalyst having 600 cells/in^2 and which is 22 mm in diameter and 13 mm in height, is placed in the reactor and heated to 150 ºC. The temperature of catalyst is measured with a thermocouple placed at gas entrance to monolith sample. As the monolith in the oven is kept at 150 ºC, the simulated exhaust gas composition given in Table 3.1 or in Table 3.2 is passed through the by-pass line and analyzed by MS and CO Analyzer. Data from thermocouple, MS and CO analyzer are collected every 40 seconds simultaneously in MAS-SOFT computer program. When the MS and CO analyzer data are stabilized for each species, these data are noted as initial data and used for the conversion calculations at the end of the test. Then the gases are passed through the reactor using valves VTP6 and VTP7, and at the same time the oven is started to be dynamically heated from 150 ºC to 600 ºC at a rate of 5 ºC/min and cooled again to 150 ºC naturally. During the test GHSV is 50,000 h^{-1} and O_2 is oscillated at 1 Hz frequency between the reducing and oxidizing composition around the stoichiometric feedstream. The data collected by the MAS-SOFT computer program is converted to conversion versus temperature graphs using the zero data and MS calibration equations for each species. In Appendix B, calculations of concentrations and flow rates of the gases and sample analysis of catalytic activity test data are given.

Table 3. 1 Simulated Exhaust Gas Mixture Composition without SO_2

Species	Gas Mixture Composition (%)		
	Reducing	**Stoichiometric**	**Oxidizing**
C_3H_6	0.037	0.037	0.037
C_3H_8	0.012	0.012	0.012
CO	1.002	1.001	0.999
H_2	0.231	0.230	0.230
CO_2	10.018	10.000	9.981
NO	0.150	0.150	0.150
SO_2	0.000	0.000	0.000
O_2	0.585	0.767	0.949
N_2	Balance	Balance	Balance

Table 3. 2 Simulated Exhaust Gas Mixture Composition with SO_2

Species	Gas Mixture Composition (%)		
	Reducing	**Stoichiometric**	**Oxidizing**
C_3H_6	0.037	0.037	0.037
C_3H_8	0.012	0.012	0.012
CO	1.002	1.001	0.999
H_2	0.231	0.230	0.230
CO_2	10.018	10.000	9.981
NO	0.150	0.150	0.150
SO_2	0.002	0.002	0.002
O_2	0.585	0.767	0.949
N_2	Balance	Balance	Balance

For the optimization of the catalytic activity test conditions, over 50 activity tests are performed with samples of commercial monolithic catalyst. However, the results of these tests are not shown and discussed here. In order to evaluate the catalytic activity of catalysts, two different approaches are followed as explained below.

3.4.2.1 Effect of Exposure to SO_2 during Catalytic Activity Tests

To determine the effect of exposure to SO_2 on monolithic catalysts during the catalytic activity tests, four separate tests are performed subsequently. The monolithic catalysts which are classified as first set are subjected to these tests. Test 1 is performed with the simulated exhaust gas composition without SO_2 given in Table 3.1. During the following two tests, Test 2 and Test 3, simulated exhaust gas composition with SO_2 given in Table 3.2 is used. Finally Test 4 is performed with the same conditions of Test 1, that is without SO_2. As a result, the effect of exposure to SO_2 during Test 2 and Test 3 is seen in the difference between the catalytic activities of catalysts during Test 1 and Test 4.

3.4.2.2 Effect of Thermal Aging

To determine the effect of high temperature aging, monolithic catalysts which are classified as second set, are aged thermally in an oven under 650 mL/min dry air flow, either at 900 ºC or 1000 ºC for 1 h. Monoliths are placed horizontally in the oven through the air flow. Before the aging treatment, monolithic catalysts are tested as fresh with the gas composition given in Table 3.2. After the aging treatment, the catalysts are tested as aged, with the same gas composition. The difference between the catalytic activities of monolithic catalysts as fresh and aged shows the effect of aging at high temperatures.

3.5 Calibrations

Calibration is needed to determine the accuracy of an instrument. In dynamic test system, flow rates of the gases are regulated using MFCs which are linked to a computer program. Accuracy of a MFC is related to the actual flow and the input of an MFC, so calibration is necessary for establishing relation between the actual and input flow.

The calibration of MS is used to determine the concentration of a species in the product gas. Data is obtained from MS in terms of pressure, so this data is needed to be calibrated according to the concentration in the gas mixture. After the catalytic activity tests, conversion vs. temperature graphs are plotted for CO, C_3H_6, C_3H_8, H_2, NO and O_2 species. CO is analyzed by CO analyzer and the CO concentration is directly read as “ppm”. For this reason MS calibration is made for C_3H_6, C_3H_8, H_2, NO and O_2 species only. All the calibration data for MFCs and MS are given in Appendix C.

3.5.1 Mass Flow Controller Calibrations

Each MFC is calibrated with nitrogen gas and gas correction factor is used for each type of gas to be used with MFC during the tests. Certain flow rates are set in the computer program of MFCs and the actual flow rate is measured by a soap bubble flowmeter. This measured flow rate is multiplied by the gas correction factor of the gas to be used with the MFC. Gas correction factor is specific for each species however for the mixture of gases in cylinders, gas correction factor is taken as the average value or as the one

for the highest concentration. Then the set flow rate values vs. the measured flow rate values are plotted and a calibration constant is determined.

3.5.2 Mass Spectrometer Calibration

During the calibration of MS, calibration gas mixture is sent through the by-pass line of the dynamic test system. Calibration gas mixture is composed of the calibration gas, nitrogen and water vapor. Three lines are used during the calibration process. From one line the gas that will be calibrated is sent with different flow rates with known composition and the other two lines are used for nitrogen gas. Nitrogen flow from MFC5 is kept constant during the calibration and carries water vapor and the nitrogen flow rate from the other line is changed according to the flow rate of the calibrated gas, to keep the total gas flow rate constant as used during the catalytic activity test. At the end of the calibration, concentration of the calibrated gas vs. the MS data is plotted and a calibration equation is obtained. Three different calibrations are used for the catalytic activity tests; Calibration-1 for the catalytic activity tests of first set of catalysts, Calibration-2 for the second set of catalysts that are aged at 900 ºC and for their fresh tests and Calibration-3 for the second set of catalysts that are aged at 1000 ºC and for their fresh tests.

CHAPTER 4

EFFECT OF EXPOSURE TO SO_2 DURING CATALYTIC ACTIVITY TESTS

4.1 Support Materials

In this study, two different support materials are synthesized. The first one is cerium - zirconium oxide (CZO), synthesized by co-precipitation method. The atomic ratio of Ce/Zr is kept as 4/1 to obtain $Ce_{0.8}Zr_{0.2}O_2$. This support material is used to impregnate the metals and then it is physically mixed with γ-Al_2O_3. The second support material is cerium - zirconium - aluminum oxide (CZAO) synthesized by sol - gel method. The atomic ratio of Ce/Zr is kept as 1/1 to obtain CeO_2 - ZrO_2 - Al_2O_3 with molar composition of 10:10:80. This support material is also used to impregnate the metals.

4.1.1 Catalyst Characterizations

The XRD pattern of CZO sample illustrated in Figure 4.1 is similar to that of XRD pattern of $Ce_{0.8}Zr_{0.2}O_2$ given by Larese et al. (2004).

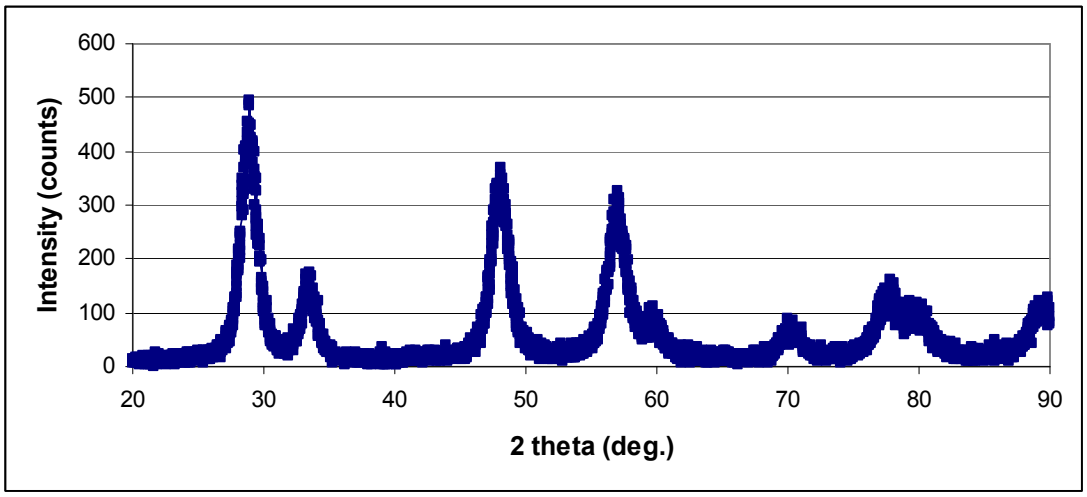

Figure 4. 1 XRD Diffractogram of CZO

The XRD pattern of CZAO sample illustrated in Figure 4.2 is similar to that of XRD pattern of CZAO with the molar ratio of 10:10:80 given by Zahir et al. (2007). In the study of Zahir et al. (2007), it is mentioned that the XRD pattern of this sample revealed the presence of single solid solution phase of $Zr_{0.32}Ce_{0.68}O_2$.

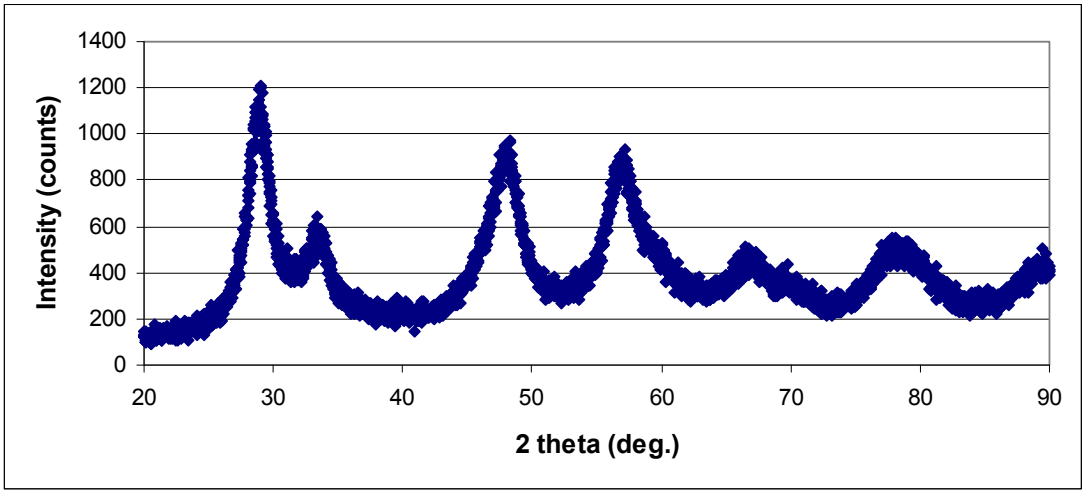

Figure 4. 2 XRD Diffractogram of CZAO

The BET surface areas of the synthesized support materials given in Table 4.1 show that, the CZAO sample synthesized by sol-gel method has higher surface area than the CZO sample.

Table 4. 1 BET Surface Areas of CZO and CZAO Support Materials

Catalyst	CZO	CZAO
BET Surface Area (m^2/g)	143.8	390.9

4.2 Metal Loaded Catalysts

Using the support materials of CZO and CZAO, three kinds of metal loaded powder catalysts are prepared and these catalysts are named as the first set of catalysts indicated as (1) after their names as explained in Chapter 3. The

CZO-CI+AO-(1) catalyst is prepared by co-impregnating the CZO support material with Rh and Pd metals and then mixing with γ-Al_2O_3. The CZAO-S-(1) catalyst is prepared by adding Rh and Pd metal solutions into the sol of CZAO. The CZAO-CI-(1) catalyst is prepared by co- impregnating the CZAO support material with Rh and Pd metals. All the catalysts are loaded to have Rh content of 0.1% and Pd content of 0.65% with the Pd/Rh ratio of 6.5.

4.2.1 Catalyst Characterizations

The metal contents of prepared powder catalysts are analyzed by ICP-MS and the results are given in Table 4.2. The importance of knowing the metal content of a powder catalyst is to calculate the total metal loaded on a monolith with a specific volume, as "g metal / ft^3". With this information, the catalytic activities of the monolithic catalysts can be compared since the noble metals are the active metals responsible for the catalytic reactions. The metal contents of the prepared powder catalysts are around the targeted values of 0.1% Rh and 0.65% Pd. Lower contents can be resulted from material losses during the addition of metals, as well as the miscalculation of total catalyst weight which is probably the case also for higher metal content values.

Table 4. 2 ICP-MS Results of Powder Catalysts

Catalyst	CZO-CI+AO-(1)	CZAO-S-(1)	CZAO-CI-(1)
Rh Content (%)	0.112±0.001	0.078±0.002	0.080±0.001
Pd Content (%)	0.731±0.008	0.550±0.008	0.651±0.008

The BET surface areas of the prepared powder catalysts are given in Table 4.3. As expected, like the support material of CZAO, the metal loaded catalysts prepared with CZAO support material have higher surface area than the catalyst with CZO support material. Adding metal solutions into the sol of CZAO support material give higher surface area than impregnating this support material with metals. The number of calcinations while preparing a catalyst is also a cause for surface area loss. During the catalyst preparations, after each process, drying and calcination steps are carried out. High temperature treatments cause loss in the surface area of the catalysts. CZAO-S-(1) sample contains the metals already in the sol, so this catalyst is calcinated once. On the other hand, the preparation of CZAO-CI-(1) catalyst includes two drying and calcination steps; one after the synthesis of support material and the second is after the impregnation process. For the CZO-CI+AO-(1) catalyst there is one more mixing step with alumina which needs drying and calcination also, making this number three. These approaches explain the surface area difference between the powder catalysts.

Table 4. 3 BET Surface Areas of Powder Catalysts

Catalyst	CZO-CI+AO-(1)	CZAO-S-(1)	CZAO-CI-(1)
BET Surface Area (m^2/g)	81.2	217.5	177.5

The powder catalysts are slurried and washcoated on monoliths. The total loaded metal content is calculated as g metal in the washcoated catalyst, depending on the ICP-MS results of powder catalyst, per volume of the monolith as ft^3 and given in Table 4.4. Different washcoating procedures are performed for the catalysts as explained in Chapter 3, so the final total loaded metal contents are paid importance in the evaluation of catalytic

activities. Although the metal contents of the powder catalysts are different from each other, the total metal content is very small in weight percent for all, less than 1%. So the differences in metal contents of monolithic catalysts mainly result from the washcoat amounts. So, higher washcoat amount on monoliths results in higher amount of metal content.

Table 4. 4 Total Metal Content of Catalysts

Catalyst	CZO-CI+AO-(1)	CZAO-S-(1)	CZAO-CI-(1)
Total Loaded Metal Content (g/ft^3)	21.5	57.9	38.7

The structures of the washcoated monoliths are imaged with SEM and shown in Figures 4.3, 4.4 and 4.5 for CZO-CI+AO-(1), CZAO-S-(1) and CZAO-CI-(1) monolithic catalysts respectively. During the coating process, washcoating slurry containing the catalyst deposits on the walls of the monolith cells. With the washcoat deposition, a layer is formed and as the washcoat amount increases, the corners of the cells are filled more. As a result, the square shaped cells of the monolith become circular. When the SEM images of the catalysts are compared, it is seen that the cells of the CZAO-S-(1) monolithic catalyst are more circular and similar to metal content value, this is also a consequence of higher washcoat amount. For the CZO-CI+AO-(1) and CZAO-CI-(1) monolithic catalysts, thinner layers are observed on the walls of monolith cells. These layers are not enough to fill the corners of the cells so the square shape of the cells are almost maintained. The washcoat amount should not be too high since the catalyst layers should not block the cells and should leave a space for gas flow. SEM images show that there is not any blockage of cells for all catalysts and they are convenient to be exposed to reaction gas flow.

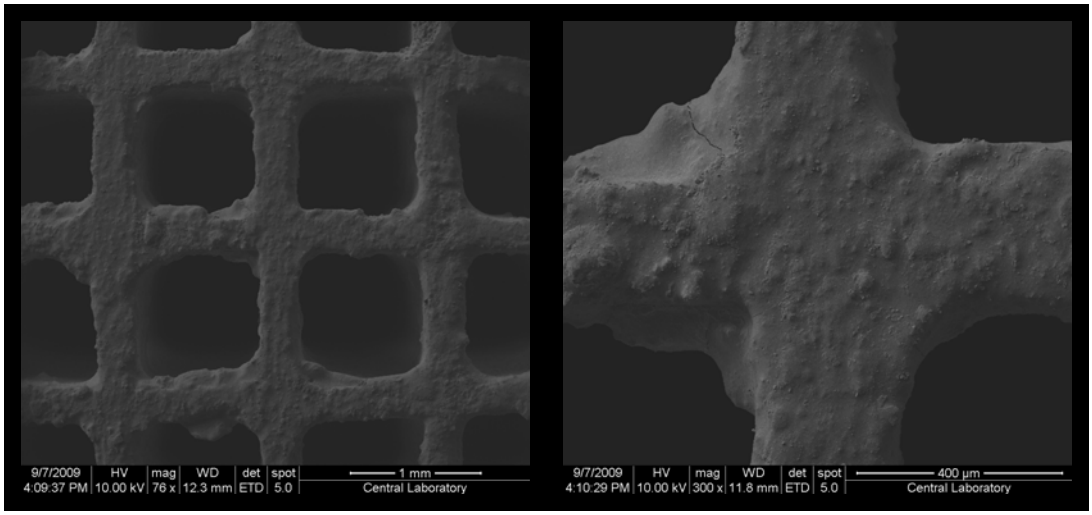

Figure 4. 3 SEM Images of CZO-CI+AO-(1) Monolithic Catalyst

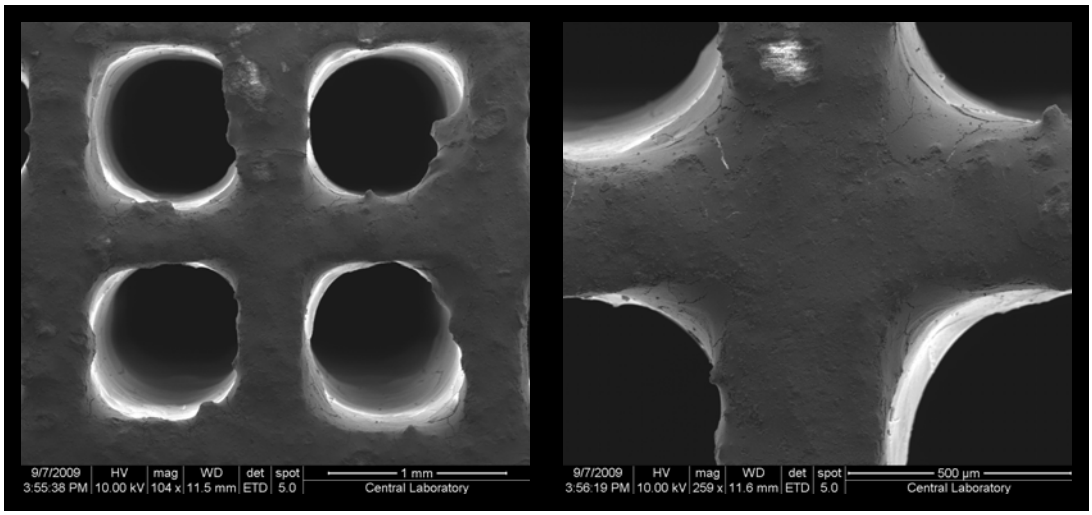

Figure 4. 4 SEM Images of CZAO-S-(1) Monolithic Catalyst

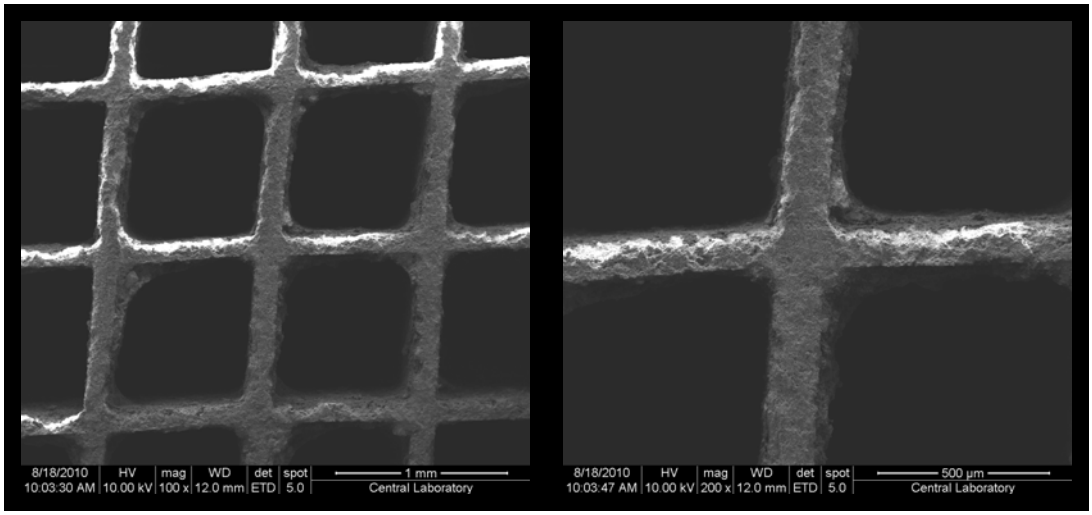

Figure 4. 5 SEM Images of CZAO-CI-(1) Monolithic Catalyst

4.2.2 Catalytic Activity Tests

The resistance of monolithic catalysts against SO_2 exposure during the catalytic activity tests are determined by comparison of the four tests that the catalysts are subjected to. The fresh catalytic activities of the monolithic catalysts are determined during Test 1 with the simulated exhaust gas which does not contain SO_2. The simulated exhaust gas including 20 ppm SO_2 is used during Test 2 and Test 3. The change in the catalytic activities of the catalysts during Test 2 and Test 3 with respect to catalytic activities during Test 1 established the effect of exposure to SO_2. In order to determine the permanency of this effect, one more test, Test 4, is performed with the same conditions as Test 1, that is using simulated exhaust gas without SO_2. Before going into details of the results of these tests, in order to explain what kinds of data are obtained during the catalytic activity tests in general, the catalytic activity data of CZO-CI+AO-(1) monolithic catalyst during Test 1 is given in details below as an example.

Catalytic activities of the monolithic catalysts for species of CO, NO, C_3H_6, C_3H_8, H_2 and O_2 are evaluated according to their conversion versus temperature behaviors. The light-off temperature (T50) is the main evaluation parameter of catalytic activity of catalysts for the corresponding species. The other important parameters are the maximum conversion and the corresponding temperature (Tmax). Together with the highest conversion, lowest T50 value indicates higher catalytic activity. The catalytic activity data in Table 4.5 and the corresponding conversion vs. temperature graphs in Figures 4.6, 4.7, 4.8, 4.9, 4.10 and 4.11 are belong to CZO-CI+AO-(1) monolithic catalyst during Test 1. When the T50 values, in Table 4.5, during the heating and cooling steps are compared, it is seen that during the cooling step lower T50 values are achieved with the same maximum conversions attained during the heating step. During the cooling step, the maximum conversions are also achieved at lower temperatures than the heating step. This situation can be visualized more explicitly from the shift between the heating and cooling activity curves of the species given in Figures 4.6, 4.7, 4.8, 4.9, 4.10 and 4.11. The activity curves for the cooling step shifts toward left, through lower temperatures. Probably during the heating step, the catalyst is reduced and resulted in improvement of the activity during the cooling step. Di Monte et al. (1998) reported that reductive pretreatment enhances the conversion of NO significantly and lowers the light-off temperatures for CO and HCs. In addition, as can be seen from the figures below, during the heating step, some oscillations are observed due to the inability of the oven to increase the temperature linearly at low temperatures. On the other hand, during the cooling step smoother “S” shape curves are obtained. For the reasons discussed above, the catalytic activity data during the cooling steps are taken into consideration for the evaluation of the catalytic activities of catalysts.

Table 4. 5 Catalytic Activity Data of CZO-CI+AO-(1) Monolithic Catalyst During Test 1

Species	Heating			Cooling		
	T50 (C)	Maximum Conversion (%)	Tmax (C)	T50 (C)	Maximum Conversion (%)	Tmax (C)
CO	219	100	490	202	100	462
NO	486	96	587	251	96	508
C_3H_6	392	100	459	202	100	427
C_3H_8	536	100	597	263	100	551
H_2	150	100	246	162	100	243
O_2	220	90	587	197	92	440

The CZO-CI+AO-(1) monolithic catalyst can convert the mentioned species almost 100%. The light-off behavior for conversions of CO, C_3H_6, H_2 and O_2 have a typical “S” curve shapes. On the other hand, the conversions of NO and C_3H_8 increase slowly as the temperature increases. Automotive exhaust gases composed of up to 200 different hydrocarbon species including paraffins, olefins, aromatics and oxygenates. An active catalyst can reduce olefins easily than paraffins (Schuetzle et al.,1994). So C_3H_6 as an olefin is easily converted by the CZO-CI+AO-(1) monolithic catalyst, whereas C_3H_8 is converted with difficulty since it is a paraffin. Oscillations of O_2 between the reducing and oxidizing conditions performed during the test reflect as oscillations in the catalytic activity curves of O_2.

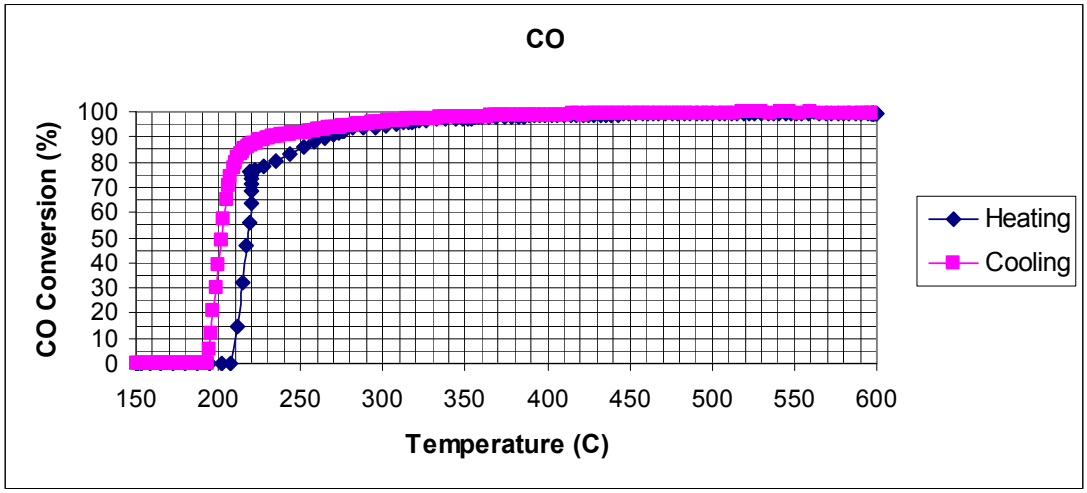

Figure 4. 6 CO Catalytic Activity of CZO-CI+AO-(1) Monolithic Catalyst During Test 1

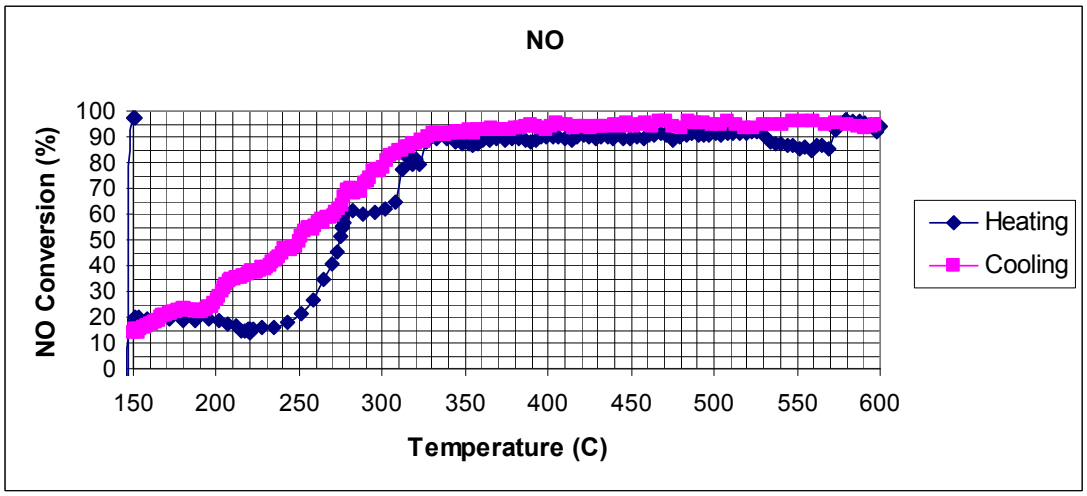

Figure 4. 7 NO Catalytic Activity of CZO-CI+AO-(1) Monolithic Catalyst During Test 1

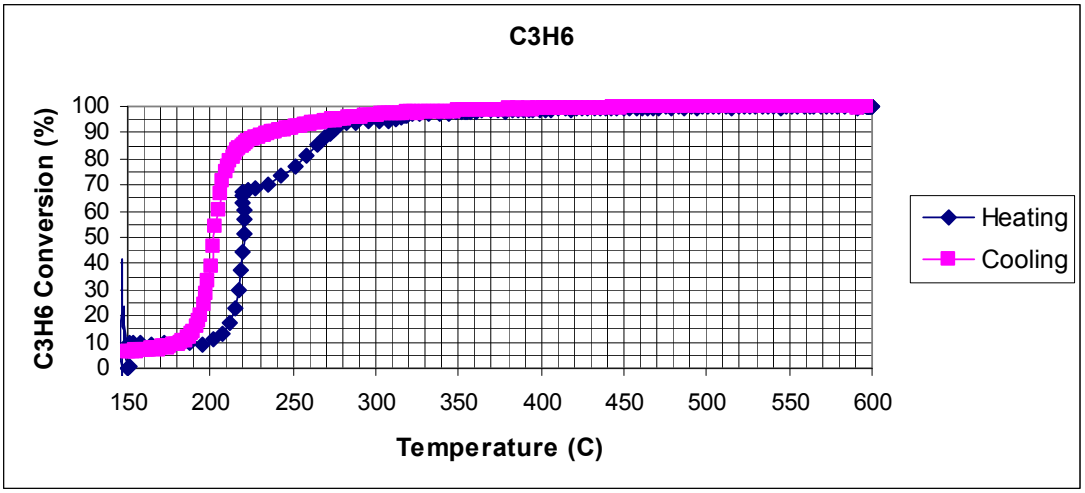

Figure 4. 8 C_3H_6 Catalytic Activity of CZO-CI+AO-(1) Monolithic Catalyst During Test 1

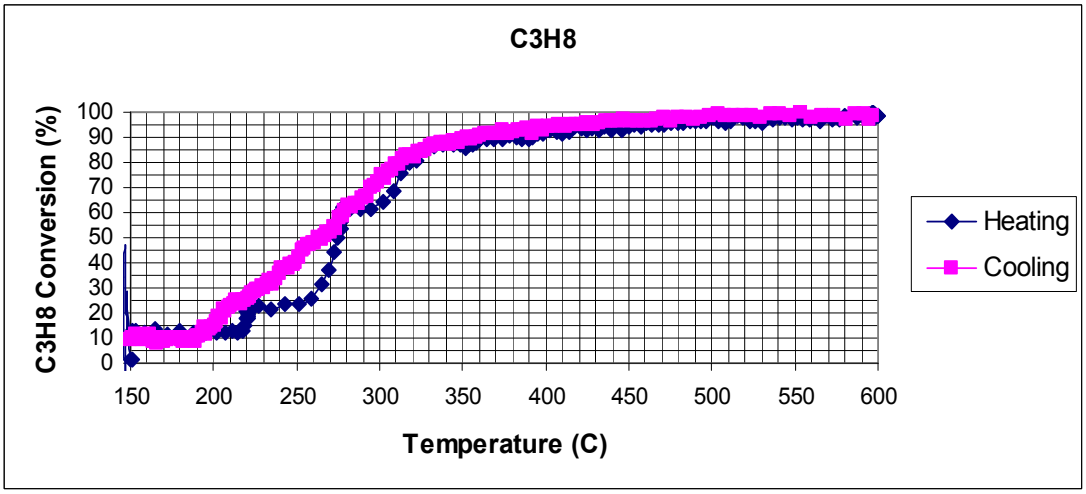

Figure 4. 9 C_3H_8 Catalytic Activity of CZO-CI+AO-(1) Monolithic Catalyst During Test 1

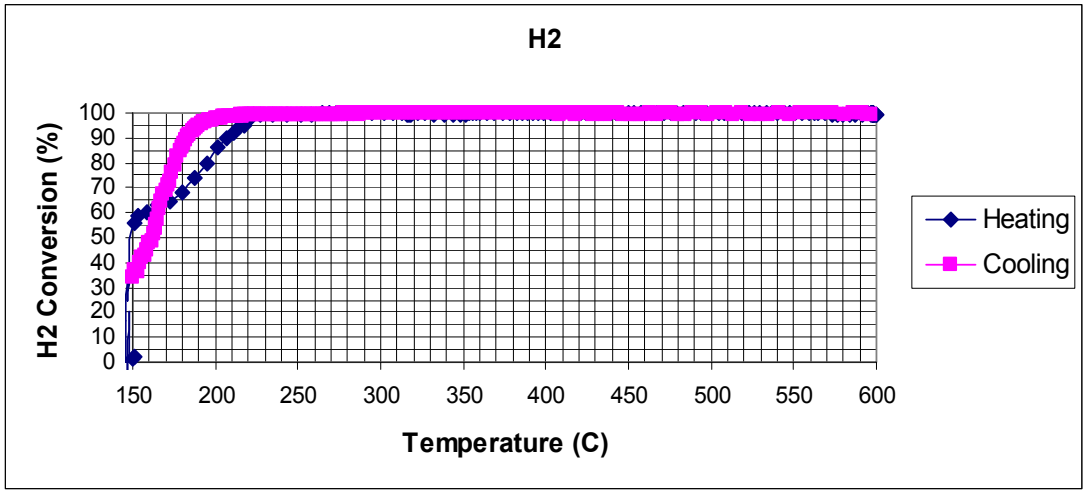

Figure 4. 10 H_2 Catalytic Activity of CZO-CI+AO-(1) Monolithic Catalyst During Test 1

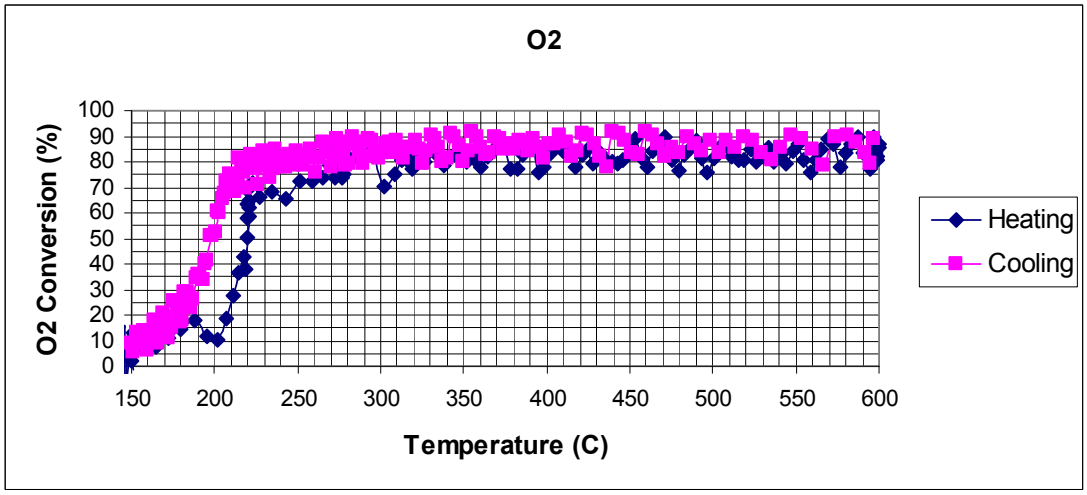

Figure 4. 11 O_2 Catalytic Activity of CZO-CI+AO-(1) Monolithic Catalyst During Test 1

Catalytic activity is specific for each monolithic catalyst, even if the washcoated catalyst is the same. Catalytic activity depends on the bulk structure as a whole and differences in homogeneity of the washcoated catalyst, amount of washcoat, total metal content of the monolithic catalysts and many other properties result in the differences in catalytic activities. Besides, a monolithic catalyst will not show the same catalytic performance when the tests are repeated, since the fresh nature of the catalyst is altered. For these reasons, the catalytic activity tests are performed once and the catalytic activity data from these tests related to specific monolithic catalysts are evaluated and compared with each other. The necessity of this approach is exemplified by the comparison of the catalytic activity data of two samples of monolithic commercial catalyst. The commercial catalyst contains Pd and Rh metals with a Pd/Rh ratio of 6.5 and the nominal total metal content is 30 g/ft^3. Commercial catalyst is preferred for this exemplification, since its catalytic activity is proved commercially and it is 200 fold bigger in volume than laboratory scale monoliths, so the samples of commercial catalyst can be assumed to be washcoated more homogeneously and more identical. The monolith samples with the same dimensions of laboratory scale monoliths are cut out from the same slice of bulk commercial monolith and named as COM-M1 and COM-M2. Activity tests are performed at same conditions, with simulated exhaust gas including 20 ppm SO_2. The catalytic activity data of two pieces are given in Table 4.6 and the conversion vs. temperature curves for each species are combined in Figures 4.12, 4.13, 4.14, 4.15, 4.16 and 4.17.

Table 4. 6 Catalytic Activity Data of COM-M1 and COM-M2 Monolithic Catalysts

Species	COM-M1			COM-M2		
	T50 (C)	Maximum Conversion (%)	Tmax (C)	T50 (C)	Maximum Conversion (%)	Tmax (C)
CO	205	100	413	226	100	481
NO	205	93	383	231	86	493
C_3H_6	202	100	383	223	100	421
C_3H_8	258	100	591	286	98	597
H_2	*	100	354	171	100	295
O_2	188	100	347	218	99	539

* At 150ºC the conversion of H_2 is 54.1%.

These comparisons show that although the two monolithic samples are almost identical to each other, there is a comparable difference in catalytic activities. Especially, there are 20 to 30 ºC differences in T50 data as can be seen in Table 4.6. The difference in catalytic activities for all the species are also obvious from the conversion vs. temperature curves below. However, the characteristics of the catalytic activity curves are very similar to each other. This result indicates that the reliability of the catalytic activity tests that enables the catalysts to show the same characteristics in catalytic activity.

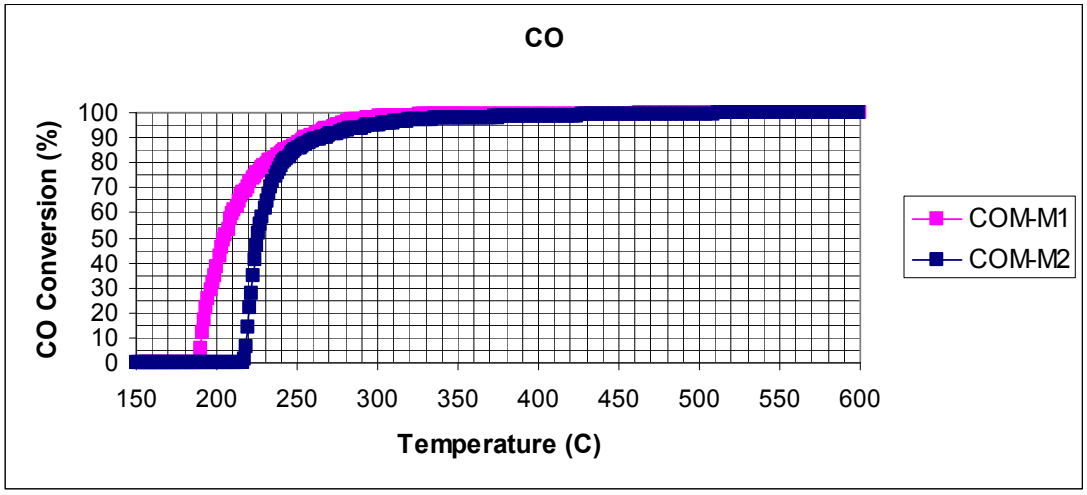

Figure 4. 12 CO Catalytic Activities of COM-M1 and COM-M2 Monolithic Catalysts

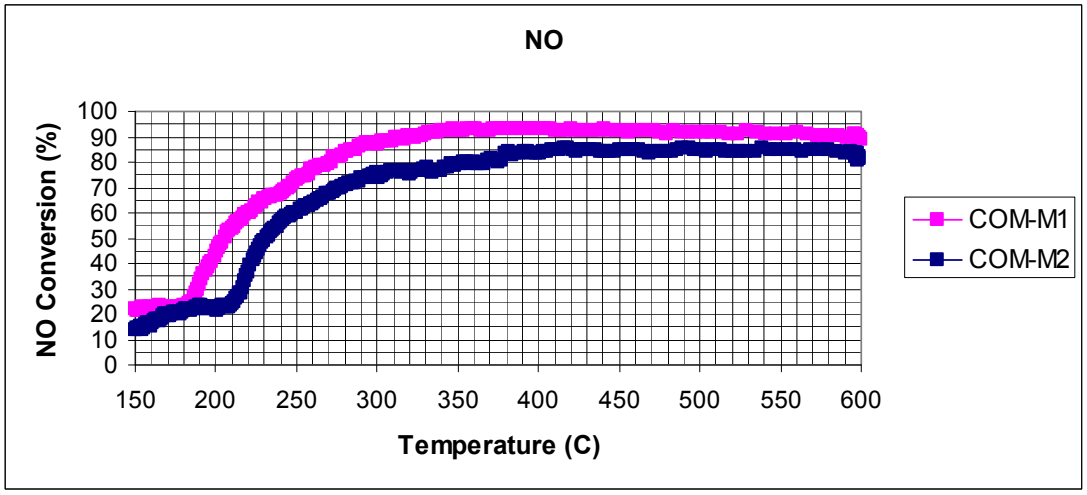

Figure 4. 13 NO Catalytic Activities of COM-M1 and COM-M2 Monolithic Catalysts

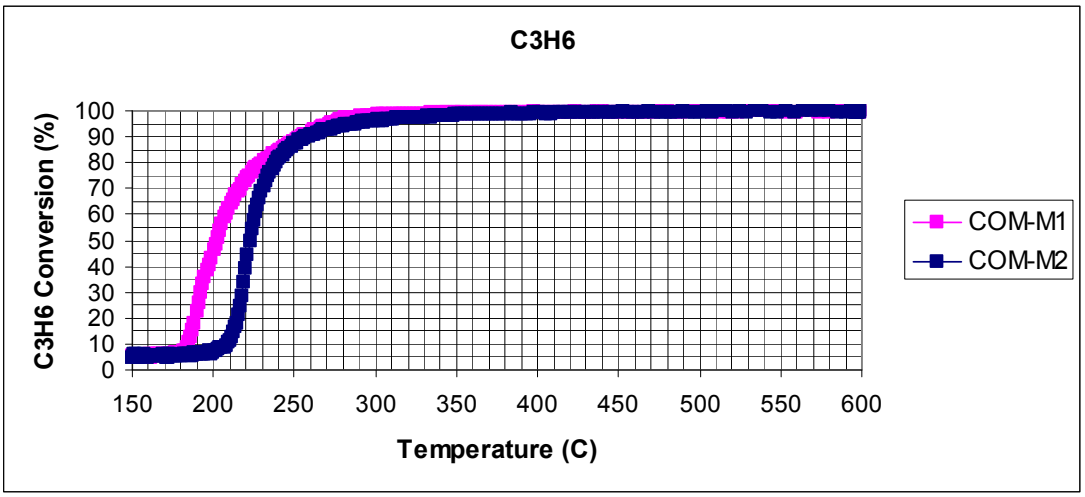

Figure 4. 14 C_3H_6 Catalytic Activities of COM-M1 and COM-M2 Monolithic Catalysts

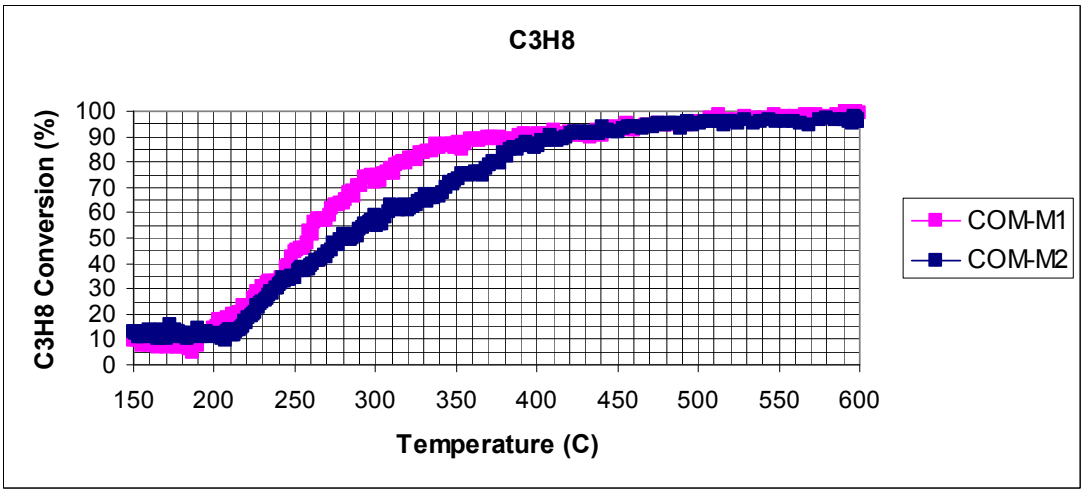

Figure 4. 15 C_3H_8 Catalytic Activities of COM-M1 and COM-M2 Monolithic Catalysts

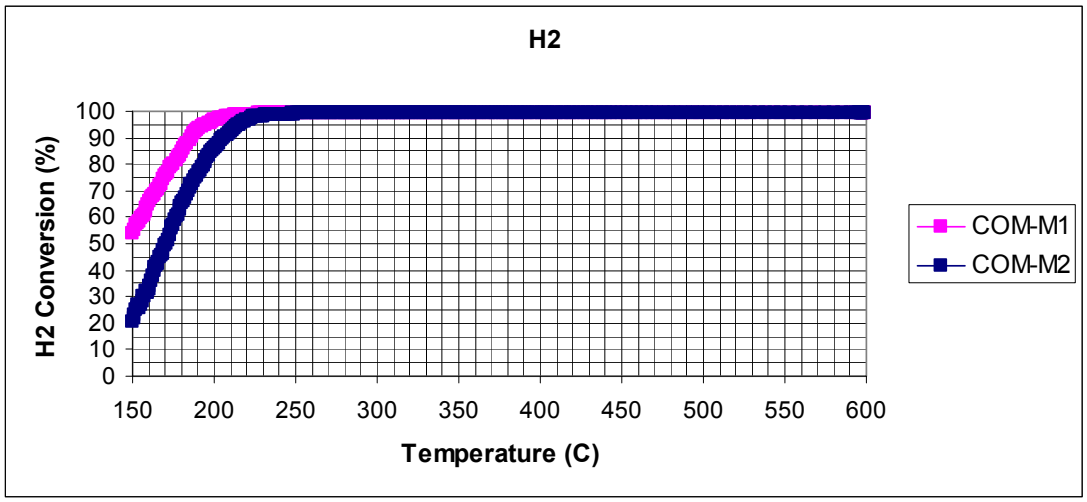

Figure 4. 16 H_2 Catalytic Activities of COM-M1 and COM-M2 Monolithic Catalysts

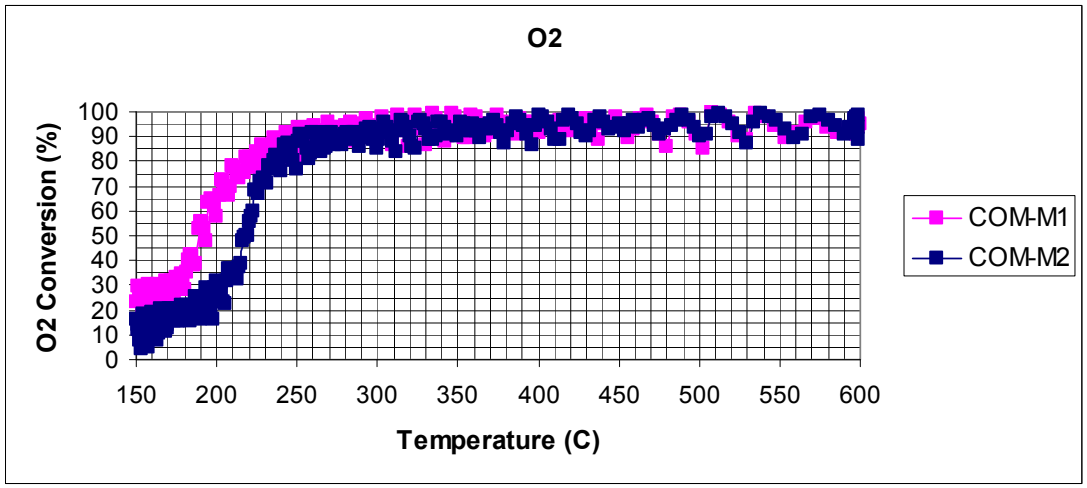

Figure 4. 17 O_2 Catalytic Activities of COM-M1 and COM-M2 Monolithic Catalysts

In order to evaluate the effect of four tests that the monolithic catalysts are subjected, the catalytic activity data of CZO-CI+AO-(1) monolithic catalyst for CO are plotted together in Figure 4.18 as an example. The monolithic

catalyst loses its activity during Tests 2 and 3 with shifted curves to right, through higher temperatures than the curve of Test 1. This behavior reveals the exposure to SO_2 with high temperature causes a decrease in catalytic performance. To determine the permanency of this effect, the first test is repeated and it is seen that the absence of SO_2 improves the catalytic performance. However this improvement is not enough to achieve the same catalytic performance as during the Test 1.

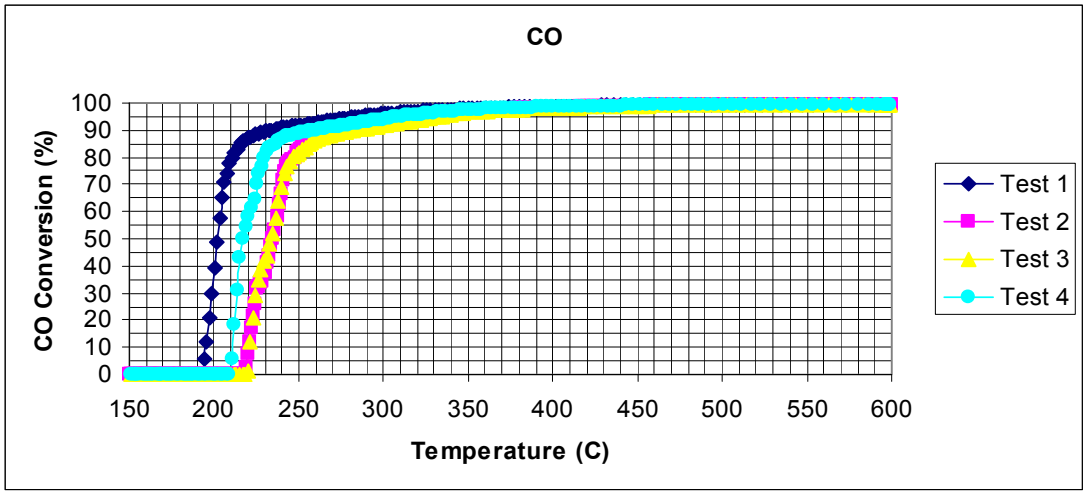

Figure 4. 18 CO Catalytic Activity of CZO-CI+AO-(1) Monolithic Catalyst During Tests 1, 2, 3 & 4

In order to determine the net effect, the CO catalytic data of same catalyst during Test 1 and Test 4 are plotted in Figure 4.19, as an example. The shift of the catalytic activity curve during Test 4 through higher temperatures shows the loss in catalytic performance. Also the same result can be drawn from the T50 values. The T50 value during Test 4 is higher than the T50 value during Test 1, which indicates the catalytic performance loss. Catalytic activity plots of all tested catalysts for all species are given in Appendix D.

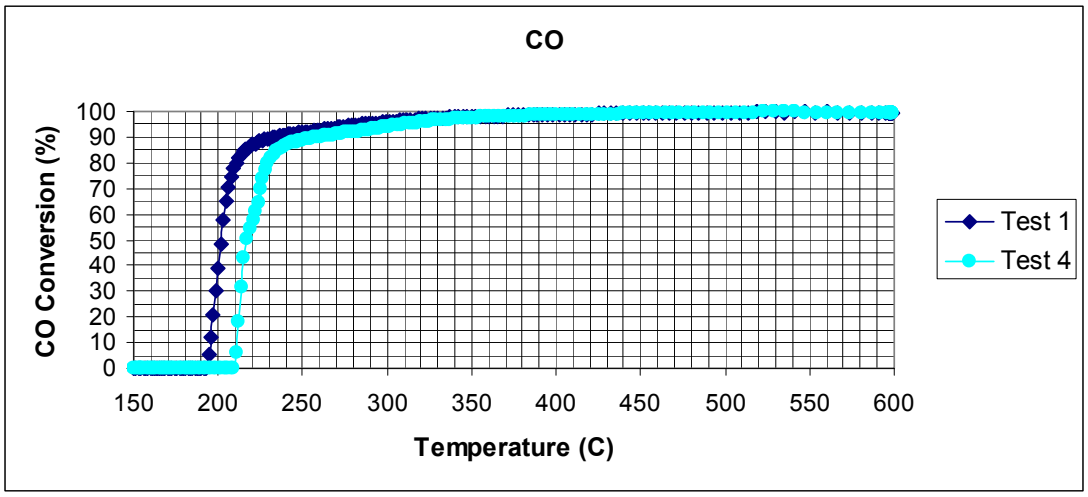

Figure 4. 19 CO Catalytic Activity of CZO-CI+AO-(1) Monolithic Catalyst During Tests 1 & 4

The T50 values, maximum conversion and corresponding temperature values achieved by CZO-CI+AO-(1) monolithic catalyst during Tests 1 and 4 are given in Table 4.7. Although the achieved maximum conversions are similar for the two tests, T50 and Tmax values differ each other. The difference between the T50 values of Test 4 and Test 1 can be represented as in Equation 4.1

$$\Delta T50 = T50(Test\,4) - T50(Test\,1) \tag{4.1}$$

The ΔT50 values for CZO-CI+AO-(1) monolithic catalyst is visualized in Figure 4.20 according to each species. Positive ΔT50 values for CO, C_3H_6, H_2 and O_2 indicate that the light-off temperatures are higher during Test 4 than Test 1 and the catalytic activity for the conversion of these species is decreased. On the other hand, negative ΔT50 values for NO and C_3H_8 indicate that the light-off temperatures are lower during Test 4 than Test 1

and there is an improvement in the catalytic activity for these species. The small improvement in T50 value for C_3H_8 as 1ºC can be accepted as constant T50. The same discussions are also valid for Tmax values, so comparison of T50 values generally represent the catalytic behavior during the tests.

Table 4. 7 Catalytic Activity Data of Monolithic CZO-CI+AO-(1) Catalyst During Tests 1 & 4

Species	Test 1			Test 4		
	T50 (C)	Maximum Conversion (%)	Tmax (C)	T50 (C)	Maximum Conversion (%)	Tmax (C)
CO	202	100	462	217	100	473
NO	251	96	509	239	96	506
C_3H_6	202	100	427	218	100	441
C_3H_8	263	100	551	262	100	521
H_2	162	100	242	185	100	326
O_2	197	92	440	213	91	465

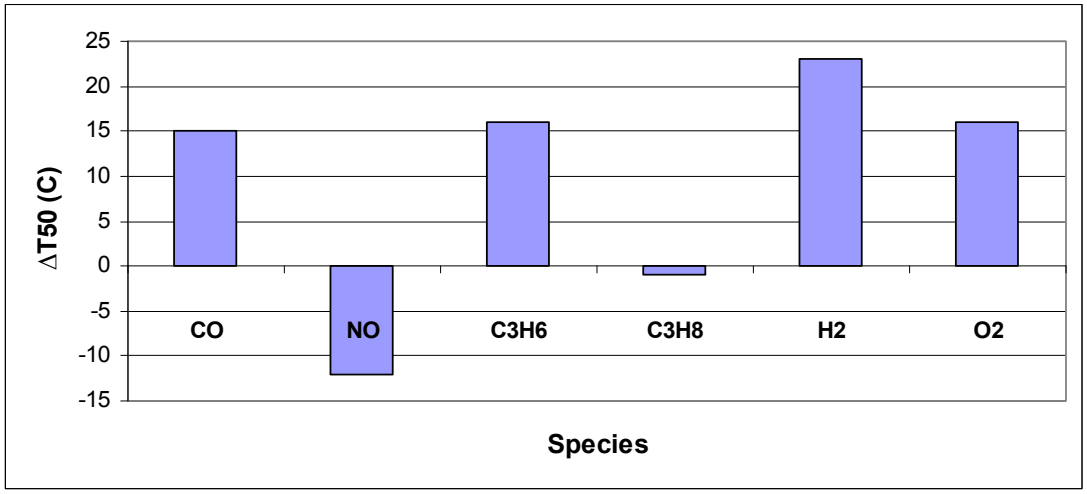

Figure 4. 20 Change of T50 Data of CZO-CI+AO-(1) Monolithic Catalyst During Tests 1 & 4

The CZAO-S-(1) monolithic catalyst also loses its catalytic activity for CO, C_3H_6, H_2 and O_2 but resulting in much higher differences in T50 values as can be seen from Table 4.8 and Figure 4.21. The conversion of NO can not even reach to 50% for both tests but there is an increase in achieved maximum conversion which indicates an improvement in catalytic activity for this species. However this increased maximum conversion is achieved at much higher temperatures. During Test 1 and Test 4, the same maximum conversions are achieved for the other species. There is also an improvement in the catalytic activity for the C_3H_8, resulting 64 ºC of lower T50 value than the T50 value of Test 1.

Table 4. 8 Catalytic Activity Data of CZAO-S-(1) Monolithic Catalyst During Tests 1 & 4

Species	Test 1			Test 4		
	T50 (C)	**Maximum Conversion (%)**	**Tmax (C)**	**T50 (C)**	**Maximum Conversion (%)**	**Tmax (C)**
CO	169	100	387	278	100	404
NO	-	37	184	-	46	447
C_3H_6	185	100	359	273	100	391
C_3H_8	403	100	589	339	100	594
H_2	174	100	270	234	100	282
O_2	172	96	493	273	97	574

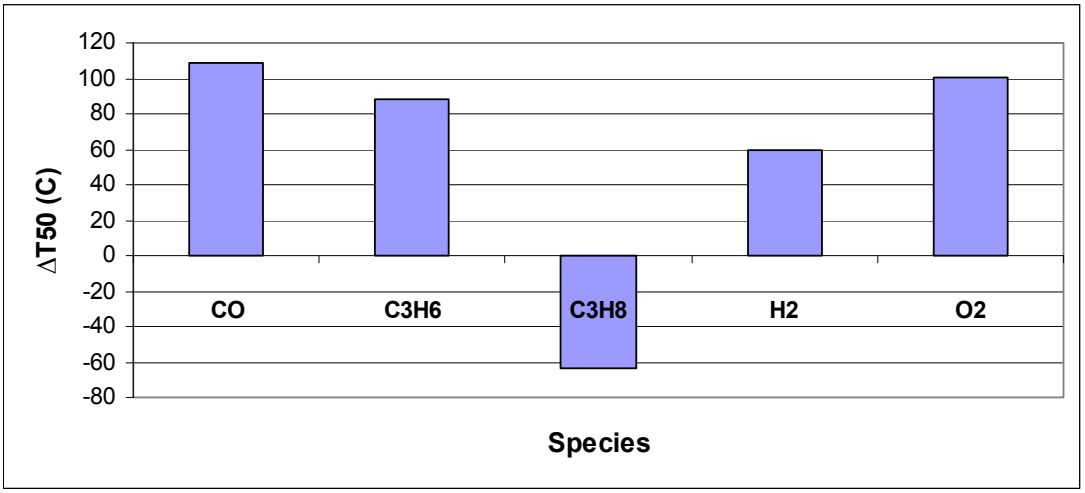

Figure 4. 21 Change of T50 Data of CZAO-S-(1) Monolithic Catalyst During Tests 1 & 4

The catalytic activity data of CZAO-CI-(1) monolithic catalyst in Table 4.9 and the ΔT50 values in Figure 4.22 show that having the same maximum conversions for each species for the two tests, CZAO-CI-(1) monolithic catalyst loses its catalytic activity for CO, NO, C_3H_6, H_2 and O_2. This catalyst also exhibits a little improvement in the catalytic activity for C_3H_8.

Table 4. 9 Catalytic Activity Data of CZAO-CI-(1) Monolithic Catalyst During Tests 1 & 4

Species	Test 1			Test 4		
	T50 (C)	Maximum Conversion (%)	Tmax (C)	T50 (C)	Maximum Conversion (%)	Tmax (C)
CO	218	100	326	251	100	440
NO	219	100	477	243	100	456
C_3H_6	217	100	278	244	100	307
C_3H_8	281	100	521	276	100	577
H_2	151	100	268	178	100	247
O_2	213	91	521	241	95	458

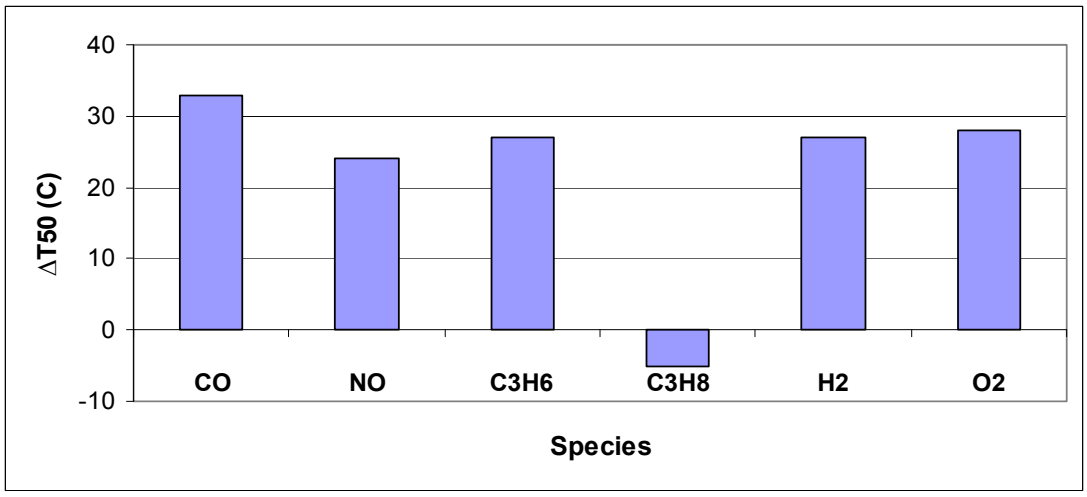

Figure 4. 22 Change of T50 Data of CZAO-CI-(1) Monolithic Catalyst During Tests 1 & 4

When the three catalyst are compared according to their catalytic activity performances during the Test 1, although CZAO-S-(1) monolithic catalyst contains highest total metal as 57.9 g/ft^3, it exhibits the lower catalytic performance with lowest T50 values. The CZAO-CI-(1) monolithic catalyst with total metal content of 38.7 g/ft3, have lower T50 values than CZAO-S-(1) catalyst. For the NO, the CZAO-S-(1) monolithic catalyst can not even reach to 50% conversion. It is generally expected that higher amounts of metals in a catalyst should exhibit higher catalytic performance. For the CZAO-S-(1) and CZAO-CI-(1) catalysts, this situation is not valid and the difference in catalytic performance points out the difference in the metal loading process. It is obvious that even if the total metal content is lower, the impregnation of metals on the support material improves the catalytic performance rather than addition of metals directly into the sol of support material. On the other hand CZO-CI+AO-(1) monolithic catalyst with lowest total metal content of 21.5 g/ft^3 exhibits the lowest T50 values for CO, C_3H_6 and C_3H_8. As a result, CZO-CI+AO-(1) monolithic catalyst with half of the total metal content of CZAO-CI-(1) monolithic catalyst shows higher catalytic performance in

general, which proves that the use of CZO support material for the metals and the mixing of this catalyst with alumina result in highest catalytic performance.

The change in T50 data of all catalysts during Test 1 and Test 4 are compared in Figure 4.23. After the four tests that the catalysts are subjected, a permanent loss of catalytic performance of all three catalysts occurred for CO, C_3H_6, H_2 and O_2. The CZAO-S-(1) monolithic catalyst has the highest level of catalytic performance loss, whereas the CZO-CI+AO-(1) monolithic catalyst has the lowest level of catalytic performance loss for these species. If we do not take the low catalytic activity of CZAO-S-(1) monolithic catalyst for NO into consideration, only CZAO-CI-(1) monolithic catalyst loses its catalytic activity for NO. On the other hand, the CZO-CI+AO-(1) monolithic catalyst shows better catalytic activity for NO during the Test 4 than the catalytic activity during the Test 1. The little improvement in catalytic activity of CZO-CI+AO-(1) and CZAO-CI-(1) monolithic catalysts for C_3H_8 can be considered as negligible and it can be concluded that these catalysts do not lose their catalytic activity for C_3H_8 throughout the tests. However, CZAO-S-(1) monolithic catalyst exhibits a 64 ºC of improvement in the T50 value for C_3H_8 which indicates an appreciable increase in catalytic activity for C_3H_8.

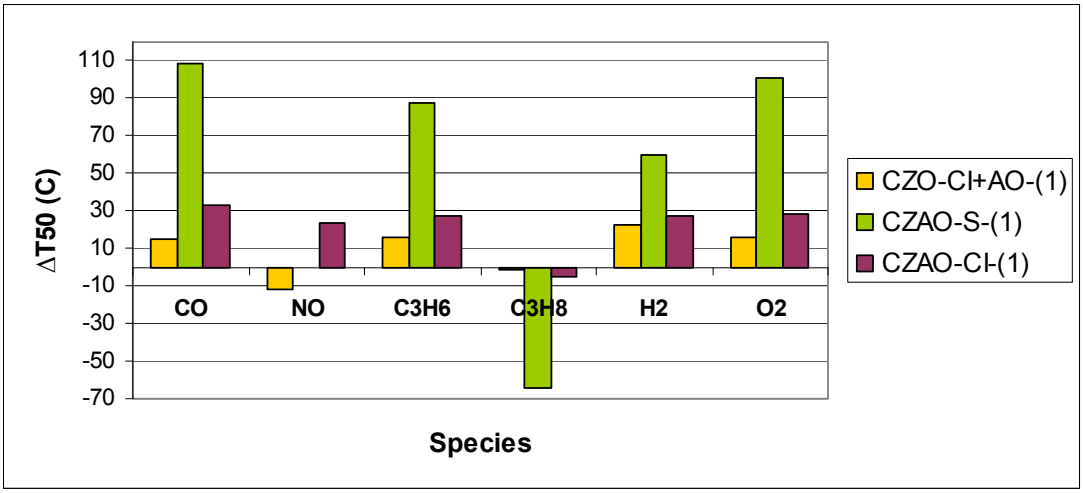

Figure 4. 23 Change of T50 Data of First Set of Monolithic Catalyst During Tests 1 & 4

In three way catalysts, Rh is used for NOx reduction, whereas Pd is used for CO and hydrocarbon oxidation reactions (Ulla, 2003). Shinjoh et al. (1989) determined that the Pd is catalytically more active than the Rh for propylene oxidation.

In his study, Cornelius (2001) states that Rh is much more resistant to sulphur than Pd. When the sulphur in the feed is removed, Rh can recover the lost activity rapidly but Pd can not. Torbati (2009) explains that the high sensitivity of Pd against sulphur is caused from the migration of sulphur into bulk Pd. Cornelius (2001) also give information of the promoting effect of sulphur on propane oxidation.

Under the light of these information, since the Pd is responsible of conversion of CO and C_3H_6 and it is highly sensitive to sulphur, the poisoning of Pd by sulphur can be responsible for the loss of catalytic activities for CO and C_3H_6. On the other hand, the improvement in the catalytic activity of CZO-CI+AO-

(1) monolithic catalyst for NO arises from the activity of Rh which is more resistant to sulphur than Pd. The conservation or improvement of catalytic activity for C_3H_8 can be explained as the promoted oxidation of C_3H_8 by sulphur.

A sample monolithic commercial catalyst (COM-M3) with the same dimensions of laboratory scale monoliths, is subjected to similar catalytic activity test procedures. The catalytic activity data of COM-M3 during Test 1 and Test 4 are given in Table 4.10 and the change in T50 data is illustrated in Figure 4.24. The T50 values are worsen during the Test 4 for all species comparing the T50 values during Test 1.

Table 4. 10 Catalytic Activity Data of COM-M3 Monolithic Catalyst During Tests 1 & 4

Species	Test 1			Test 4		
	T50 (C)	**Maximum Conversion (%)**	**Tmax (C)**	**T50 (C)**	**Maximum Conversion (%)**	**Tmax (C)**
CO	164	100	286	232	100	285
NO	*	67	213	230	69	276
C_3H_6	162	100	208	229	100	295
C_3H_8	286	95	598	327	100	598
H_2	**	100	161	181	100	232
O_2	160	93	573	231	91	550

* At 150ºC the conversion of NO is 52%.
** At 150ºC the conversion of H_2 is 89%.

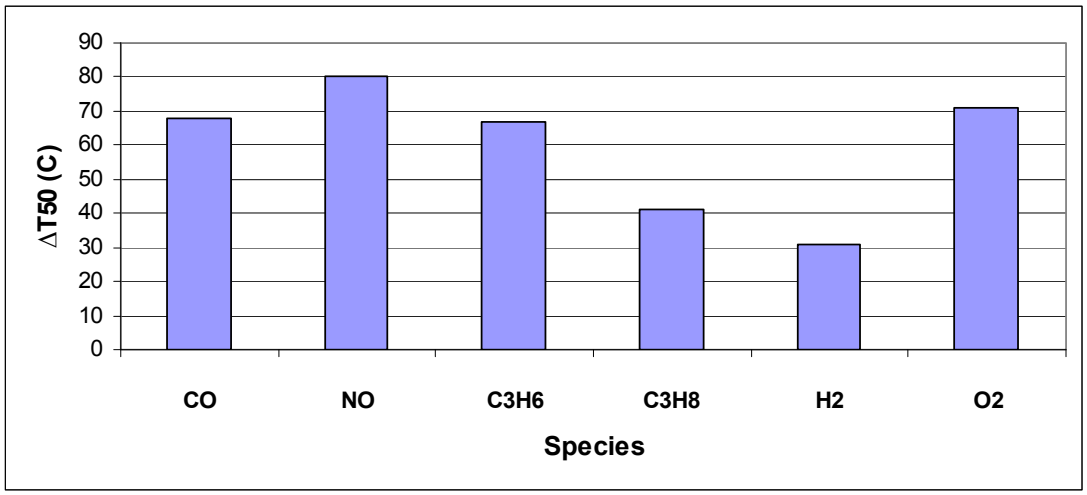

Figure 4. 24 Change of T50 Data of COM-M3 Monolithic Catalyst During Tests 1 & 4

Among the first set of catalysts the CZO-CI+AO-(1) and CZAO-CI-(1) monolithic catalysts, which show resistance against sulphur, are decided to be compared with the commercial catalyst. The comparison of change in T50 values in Figure 4.25 exhibits the level of resistances of the catalyst against exposure to simulated exhaust gases including sulphur. The CZO-CI+AO-(1) and CZAO-CI-(1) monolithic catalysts do not lose their catalytic activity as much as commercial catalyst. Especially the CZO-CI+AO-(1) monolithic catalyst has lower total metal content than the commercial catalyst and the catalytic activity of this catalyst can be accepted better than the commercial catalyst regarding the resistance against exposure to simulated exhaust gases including SO_2. In consequence of these studies, CZO-CI+AO-(1) and CZAO-CI-(1) monolithic catalysts are found promising and decided to be studied further.

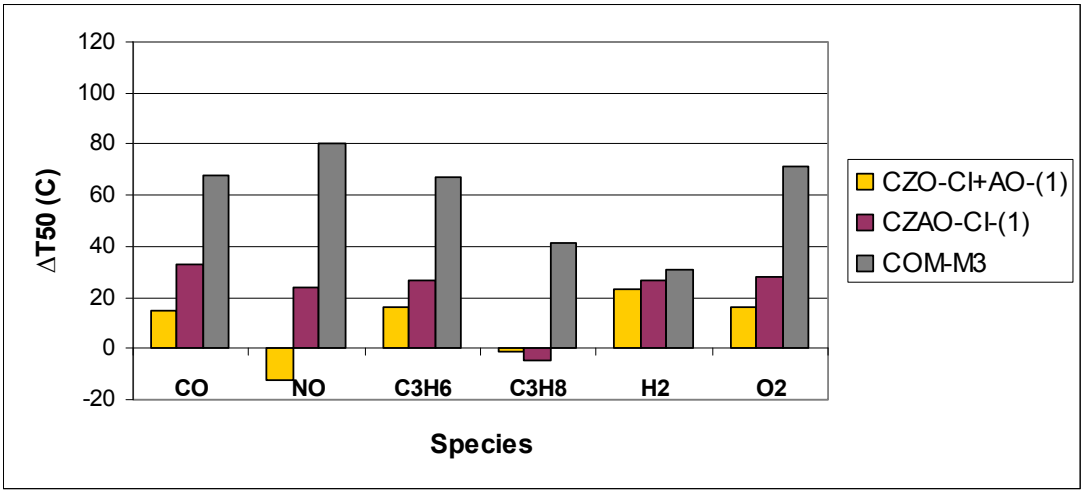

Figure 4. 25 Change of T50 Data of CZO-CI+AO-(1), CZAO-CI-(1) & COM-M3 Monolithic Catalysts During Tests 1 & 4

CHAPTER 5

EFFECT OF THERMAL AGING

5.1 Catalysts

The CZAO-CI-(1) and CZO-CI+AO-(1) monolithic catalysts that are studied as first set of catalysts to determine the effect of SO_2 exposure during activity tests, are synthesized again to perform thermal aging tests. While washcoating the newly synthesized catalysts, pseudoboehmite is added in the slurry as binder material and the washcoating process is repeated twice with drying and calcination steps in between. These catalysts are indicated with (2) after their names as CZAO-CI-(2) and CZO-CI+AO-(2). In Addition to these two catalysts, CZO-SI+AO-(2) catalyst is synthesized. The difference of CZO-SI+AO-(2) catalyst from the CZO-CI+AO-(2) catalyst is that the Rh and Pd metals are impregnated on separate CZO support materials and mixed afterwards. Different monoliths coated with the same catalyst, to be subjected to thermal aging procedures at 900 ºC and 1000 ºC separately, are indicated as M1 and M2.

5.2 Fresh Catalysts

The powder and monolithic catalysts are named as fresh before subjected to thermal aging. Characterizations of the slurries of the powder catalysts are considered to be more informative rather than the characterizations of the

powder catalysts, since the slurries exhibit the final properties of the catalyst, washcoated on the monoliths. For this purpose, slurries of the catalysts are dried and calcined at same conditions with the washcoated monoliths and characterized as powder. The metal contents, BET surface areas and the particle sizes of the powdered slurries are determined while they are fresh. Besides, pieces of the monolithic catalysts are imaged by SEM as fresh.

5.2.1 Catalyst Characterizations

The metal contents of the powdered slurries are analyzed by ICP-MS and the metal contents of the powder slurries are given in Table 5.1. The Rh and Pd content of the slurries are around the targeted values of 0.1% for Rh and 0.65% for Pd. The differences between the actual and targeted contents of metals can be resulted from the same reasons discussed in Chapter 4.

Table 5. 1 Metal Contents of Powdered Slurries of Catalysts

Catalyst	CZAO-CI-(2)	CZO-CI+AO-(2)	CZO-SI+AO-(2)
Rh	0.073±0.001	0.077±0.001	0.075±0.001
Pd	0.581±0.005	0.633±0.006	0.671±0.002

Table 5.2 shows the BET surface areas of the powdered slurries. As expected, the powdered slurry of CZAO-CI-(2) catalyst with the CZAO support material has the highest surface area. Since the CZO-CI+AO-(2) and CZO-SI+AO-(2) catalysts are synthesized through similar treatments, the surface area of powdered slurries of these samples are close to each other.

Table 5. 2 BET Surface Areas of Powdered Slurries of Catalysts

Catalyst	CZAO-CI-(2)	CZO-CI+AO-(2)	CZO-SI+AO-(2)
BET Surface Area (m^2/g)	155.1	95.95	99.72

The particle sizes of the CZO and CZAO support materials in the powdered slurries are estimated using the XRD data and Scherrer Equation (Cullity & Stock, 2001). The corresponding XRD diffractograms and the use of Scherrer Equation are given in Appendix E. The estimated particle sizes, shown in Table 5.3, are consistent with the surface areas of the samples. The powdered slurry for the CZAO-CI-(2) catalyst have the support material with the smallest particle size and highest surface area. On the other hand, the particle size for the CZO-CI+AO-(2) and CZO-SI+AO-(2) catalysts are higher, resulting in lower surface areas. For these catalysts, like the surface areas, the particle sizes are almost the same with each other.

Table 5. 3 Particle Sizes of Support Materials in the Powdered Slurries of Catalysts

Catalyst	CZAO-CI-(2)	CZO-CI+AO-(2)	CZO-SI+AO-(2)
Particle Size (nm)	17	33	34

The total metal contents of the monolithic catalysts which are catalytically tested are given in Table 5.4. Considering the metal contents of the slurries are not much different form each other, the low total metal content of the monolithic catalysts washcoated with the slurry of CZAO-CI-(2) results from the low amount of washcoat. On the contrary, the total metal content of the monolithic catalysts washcoated with the slurries of CZO-CI+AO-(2) and

CZO-SI+AO-(2) catalysts are close to each other and much higher than the one for CZAO-CI-(2) catalyst. These results also demonstrate the difference between the support materials of CZAO and CZO.

Table 5. 4 Total Metal Contents of Catalysts

Catalyst	Total Metal Content (g/ft^3)
CZAO-CI-(2)	32.48
CZO-CI+AO-(2)-M1	56.92
CZO-CI+AO-(2)-M2	53.95
CZO-SI+AO-(2)-M1	54.97
CZO-SI+AO-(2)-M2	57.33

The SEM image of the CZAO-CI-(2) monolithic catalyst in Figure 5.1 supports the lower amount of washcoat. The amount of washcoat layer on the walls of the monolith cells and the deposits at the corners of the cells are so low that the shapes of the cells are still very close to square.

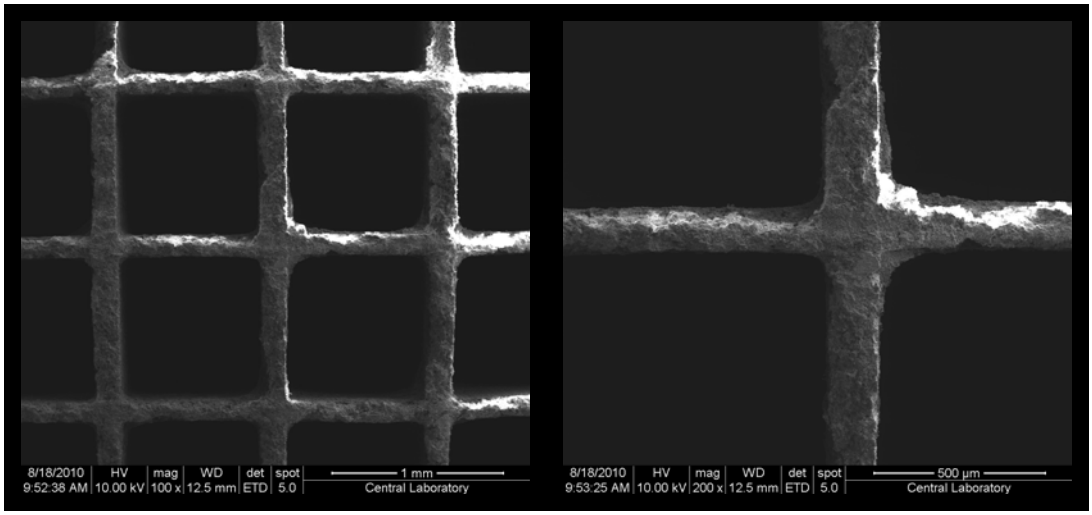

Figure 5. 1 SEM Images of CZAO-CI-(2) Monolithic Catalyst

Higher amounts of washcoat can be recognized from the SEM images of monolithic catalysts of CZO-CI+AO-(2) and CZO-SI+AO-(2) catalysts in Figures 5.2 and 5.3. For both monolithic catalysts the space of the cells are rounded with the deposition of washcoat. Especially the washcoat layer on the cell walls can be easily seen from the SEM image of monolithic catalyst of CZO-CI+AO-(2)-M1 catalyst in Figure 5.2. In general, all the monolithic catalysts do not have any blockage of the monolith cells to prevent the gas flow.

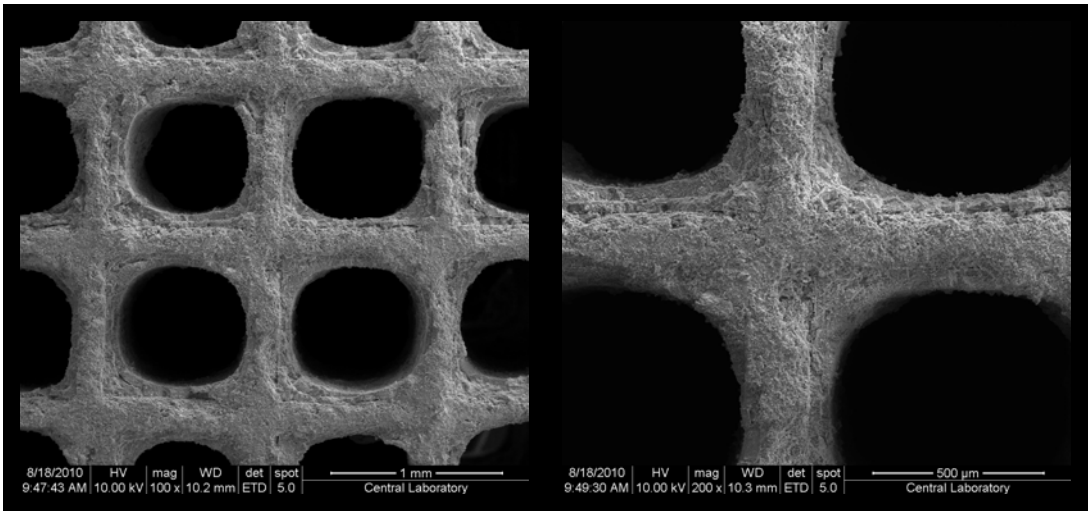

Figure 5. 2 SEM Images of CZO-CI+AO-(2)-M1 Monolithic Catalyst

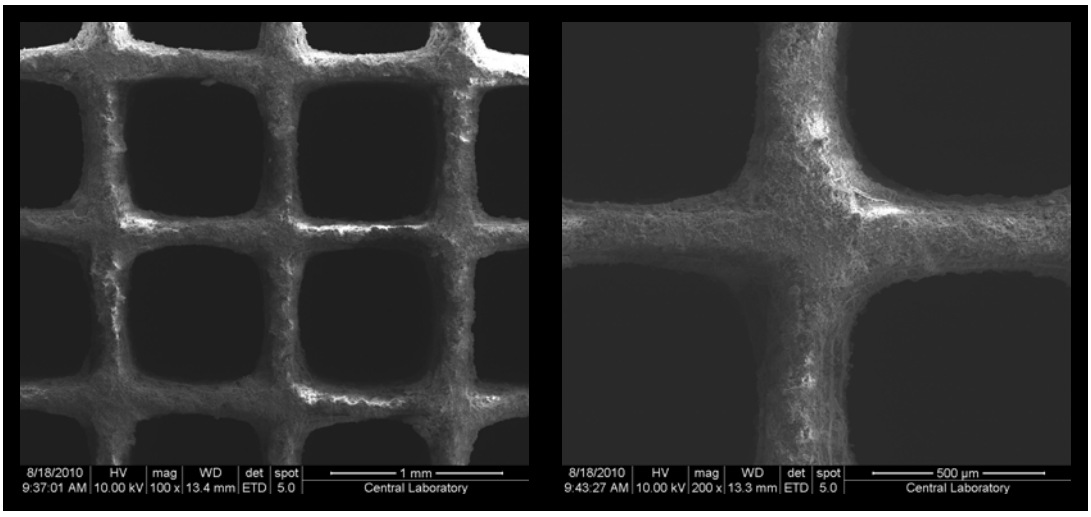

Figure 5. 3 SEM Images of CZO-SI+AO-(2)-M1 Monolithic Catalyst

Strong adherence of the coated catalyst is needed on the monolith in order not to lose the catalyst during operation. The weight loss of the monolithic catalysts after the adherence test in ultrasound bath, given in Table 5.5, show that the CZAO-CI-(2) monolithic catalyst loses the highest weight percent which is 7.66%. The lower adherence ability of the CZAO-CI-(2)

catalyst is consistent with the lower washcoat amount. On the other hand, the CZO-CI+AO-(2) and CZO-SI+AO-(2) monolithic catalysts lose about half of this value which are 4.03% and 3.98% respectively. The adherence of the CZO-CI+AO-(2) and CZO-SI+AO-(2) catalyst are stronger than the sample commercial catalyst (COM-M4) which resulted in 5.89% of weight loss after the same test.

Table 5. 5 Weight Loss of Monolithic Catalysts after Adherence Test

	CZAO-CI-(2)	**CZO-CI+AO-(2)**	**CZO-SI+AO-(2)**	**COM-M4**
Weight Loss (%)	7.66	4.03	3.98	5.89

5.3 Thermally Aged Catalysts

The powdered slurries of the catalysts which are characterized as fresh are subjected to thermal aging procedures at 900 ºC and 1000 ºC. In order to determine the change in surface area and particle size after aging, powders are characterized with BET and XRD analyses. The monolithic catalysts are also aged at high temperature. The catalytic activities of the monolithic catalysts while fresh and aged are compared to determine the effect of high temperature aging.

5.3.1 Catalyst Characterizations

In Table 5.6, the surface areas of the fresh and aged powdered slurries are compared and it is observed that the surface area decreases as the aging temperature increases. This decrease is higher than half of the surface area while the powders are fresh. The powdered slurry of fresh CZAO-CI-(2) catalyst with the highest surface area, again have the highest surface areas after aging at both 900 ºC and 1000 ºC. The levels of decrease in surface area are quite similar for the CZO-CI+AO-(2) and CZO-SI+AO-(2) catalysts, which also have close surface areas while fresh.

Table 5. 6 BET Surface Areas of Fresh and Aged Powdered Slurries of Catalysts

	BET Surface Area (m^2/g)		
Catalyst	**CZAO-CI-(2)**	**CZO-CI+AO-(2)**	**CZO-SI+AO-(2)**
Fresh	155.1	95.95	99.72
Aged at 900 ºC	90.34	52.37	50.87
Aged at 1000 ºC	68.54	35.52	33.18

The reverse situation applies for the estimated particle sizes. As seen in Table 5.7, the particle sizes of the CZO and CZAO support materials in the powders of the slurries, increases with increasing temperature, supporting the decreasing surface areas. The increase in particle size for CZAO-CI-(2) catalyst is not as much as it is for the CZO-CI+AO-(2) and CZO-SI+AO-(2) catalysts. Even after aging at 1000 ºC the particle size for the CZAO-CI-(2) catalyst is lower than that are for the CZO-CI+AO-(2) and CZO-SI+AO-(2) catalysts. The level of increase in particle size for the CZO-CI+AO-(2)

catalyst is higher than it is for the CZO-SI+AO-(2) catalyst, even if the particle sizes for the two fresh samples are similar to each other.

Table 5. 7 Particle Sizes of Support Materials in the Fresh and Aged Powdered Slurries of Catalysts

	Particle Size (nm)		
Catalyst	**CZAO-CI-(2)**	**CZO-CI+AO-(2)**	**CZO-SI+AO-(2)**
Fresh	17	33	34
Aged at 900 ºC	21	100	80
Aged at 1000 ºC	23	186	135

5.4 Catalytic Activity Tests

The monolithic catalysts that will be subjected to aging procedures are tested as fresh monolithic catalysts first. The monolithic catalysts of CZAO-CI-(2), CZO-CI+AO-(2)-M1 and CZO-SI+AO-(2)-M1, are later aged at 900ºC whereas the monolithic catalysts of CZO-CI+AO-(2)-M2 and CZO-SI+AO-(2)-M2 are aged at 1000ºC.

To determine the level of aging, the differences of T50 values during the cooling steps of tests for the aged and fresh catalysts are sketched as ΔT50 for each species.

When the catalytic activity data of the fresh monolithic catalysts are compared using the data in Tables 5.8, 5.9 and 5.10, catalytic activity of monolithic CZAO-CI-(2) catalyst for all the species is found to be lower than the catalytic activity of the other monolithic catalysts. This lower catalytic

activity can be related with the lower total metal content of the monolithic catalyst.

The CZO-CI+AO-(2)-M1 monolithic catalyst is catalytically more active than the CZO-SI+AO-(2)-M1 monolithic catalyst as fresh. In addition the total metal content of the CZO-CI+AO-(2)-M1 monolithic catalyst is slightly higher than that of CZO-SI+AO-(2)-M1 catalyst. So the better catalytic activity of the CZO-CI+AO-(2)-M1 monolithic catalyst can be related to its higher total metal content while fresh.

As a result, the total metal contents of the catalysts seem to be responsible for the differences in fresh catalytic activities. In order to make the difference in catalytic activities more explicit, aging procedures are applied to monolithic catalysts.

Table 5.8 and Figure 5.4 show that the CZAO-CI-(2) monolithic catalyst can achieve the same T50 values for CO, NO and C_3H_6 after aging at 900 ºC with 0 ºC of difference in T50 value. There is a small improvement in the T50 values for C_3H_8 and H_2, whereas there is a small degradation for O_2. However these small variations can be also accepted as negligible and the catalyst can be regarded as it performs the same catalytic activity as it is fresh.

Table 5. 8 Catalytic Activity Data of CZAO-CI-(2) Monolithic Catalyst

Species	Fresh			Aged (900 ºC)		
	T50 (C)	Maximum Conversion (%)	Tmax (C)	T50 (C)	Maximum Conversion (%)	Tmax (C)
CO	263	100	376	263	100	417
NO	265	90	392	265	91	425
C_3H_6	256	100	281	256	100	283
C_3H_8	275	100	542	273	100	513
H_2	189	100	446	186	99	393
O_2	251	100	333	253	100	377

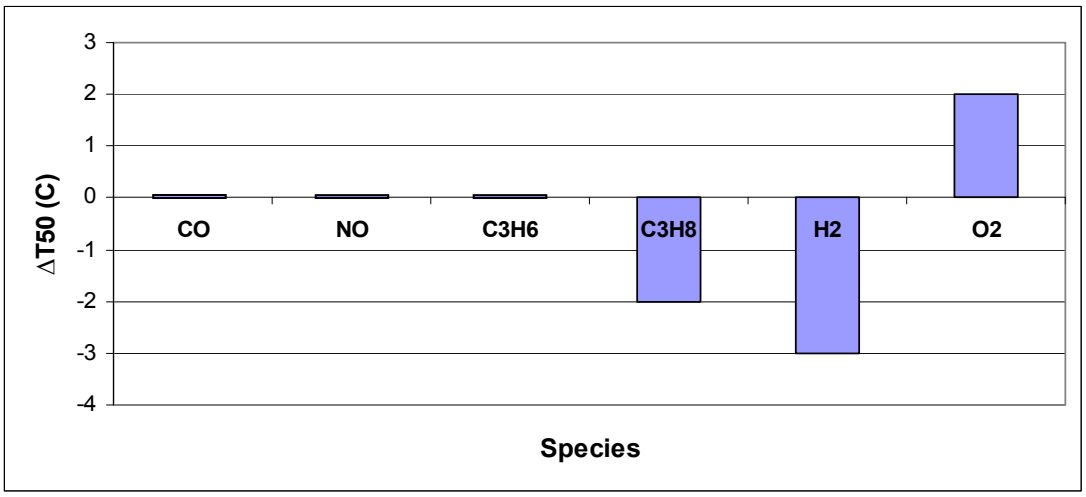

Figure 5. 4 Change of T50 Data of CZAO-CI-(2) Catalyst after Aging at 900 ºC

The difference in the catalytic activity can also be revealed from the light-off behavior. The light-off curves of the fresh and aged CZAO-CI-(2) monolithic catalyst for CO are plotted together in Figure 5.5 as an example. The curves seems exactly the same showing that the catalyst performs the same catalytic activity for CO, after aging. The similar plots for the comparison of

catalytic activities of all the monolithic catalysts while fresh and aged are given in Appendix D for all species.

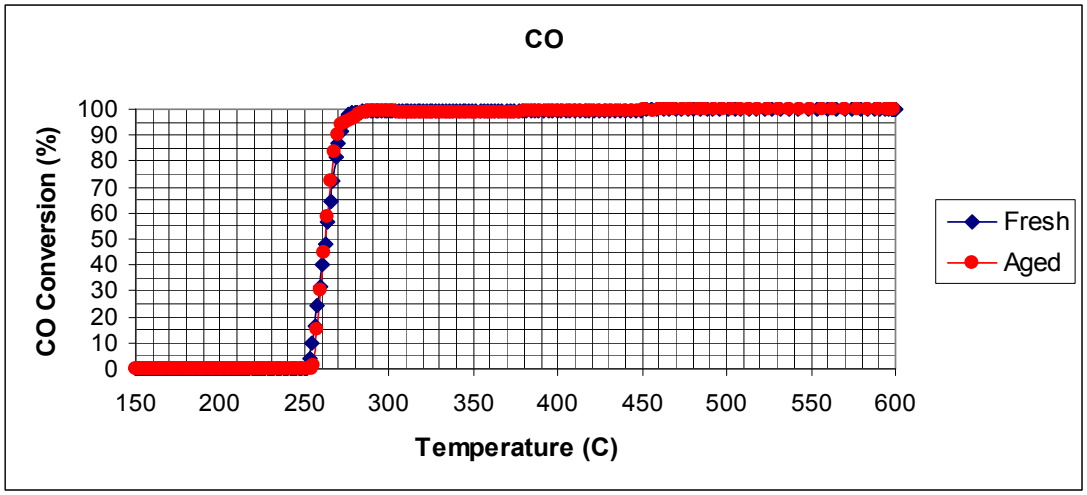

Figure 5. 5 CO Catalytic Activity of Fresh and Aged (900 ºC) CZAO-CI-(2) Monolithic Catalyst

The catalytic activity data of CZO-CI+AO-(2)-M1 monolithic catalyst in Table 5.9 and ΔT50 values Figure 5.6, reveal that this catalyst loses its catalytic activity for all the species and achieves 50% conversions at higher temperatures than it is fresh. The smallest increase in T50 is observed for C_3H_8.

Table 5. 9 Catalytic Activity Data of CZO-CI+AO-(2)-M1 Monolithic Catalyst

Species	Fresh			Aged (900 ºC)		
	T50 (C)	Maximum Conversion (%)	Tmax (C)	T50 (C)	Maximum Conversion (%)	Tmax (C)
CO	218	100	423	256	100	424
NO	217	96	543	267	91	403
C_3H_6	215	100	252	252	100	293
C_3H_8	254	100	597	278	100	563
H_2	168	99	272	199	100	597
O_2	211	100	379	246	100	296

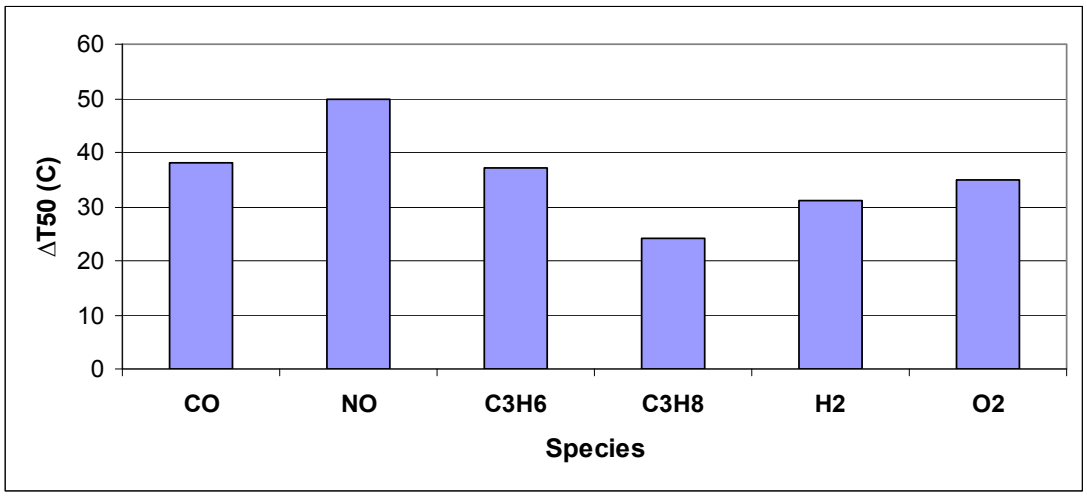

Figure 5. 6 Change of T50 Data of CZO-CI+AO-(2)-M1 Catalyst after Aging at 900 ºC

On the contrary of the previous catalysts, the catalytic activity of the CZO-SI+AO-(2)-M1 monolithic catalyst improves after aging for all the species, as can be seen in Table 5.10 and Figure 5.7. Especially for the NO and C_3H_8, it gains an appreciable increase in catalytic activity.

Table 5. 10 Catalytic Activity Data of CZO-SI+AO-(2)-M1 Monolithic Catalyst

Species	Fresh			Aged (900 ºC)		
	T50 (C)	Maximum Conversion (%)	Tmax (C)	T50 (C)	Maximum Conversion (%)	Tmax (C)
CO	239	100	411	233	99	528
NO	255	90	379	233	94	589
C_3H_6	234	100	331	230	100	334
C_3H_8	268	100	588	256	100	598
H_2	191	100	592	181	99	370
O_2	229	100	343	227	100	357

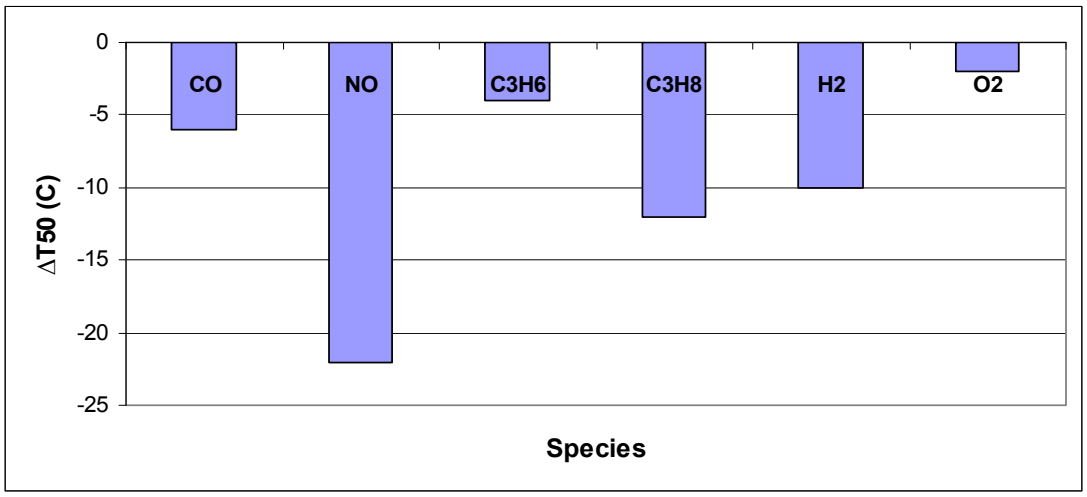

Figure 5. 7 Change of T50 Data of CZO-SI+AO-(2)-M1 Catalyst after Aging at 900 ºC

The change in T50 data of second set of catalysts after aging at 900 ºC are compared in Figure 5.8. The CZO-SI+AO-(2)-M1 monolithic catalyst shows the lowest resistance against thermal aging at 900 ºC. The CZAO-CI-(2) monolithic catalyst shows almost the same catalytic activity as fresh and aged. The CZO-SI+AO-(2)-M1 monolithic catalyst shows the highest

resistance to thermal aging at 900 ºC and shows improved activity after aging.

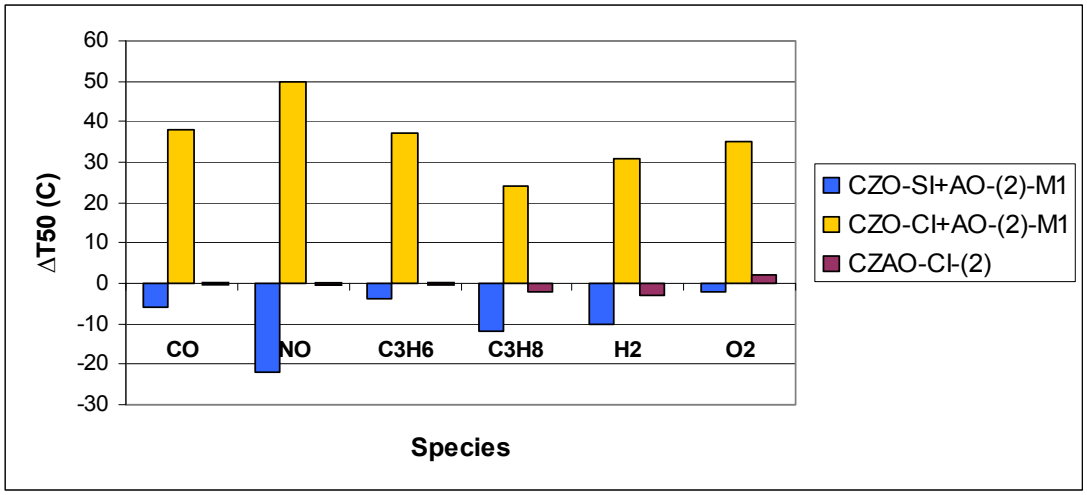

Figure 5. 8 Change of T50 Data of Second Set of Catalyst after Aging at 900 ºC

High temperature ageing results the deactivation of the catalyst, however the improvement in the catalytic activity of the monolithic catalysts washcoated with CZO-SI+AO-(2) catalyst after thermal aging is the opposite of this phenomena. A similar surprising result is also discovered by Haneda et al. (2010) with 0.4 wt% Rh loaded CeO_2-ZrO_2 catalyst with only Ce/Zr ratio of 76/24. In this study, the catalyst is aged at 1000 ºC for 25 h with reaction gas containing NO, C_3H_6, O_2 and H_2O diluted with He and oscillating between stoichiometric and lean conditions. The catalytic activity of the catalyst for NO-C_3H_6-O_2 reaction was measured before and after aging treatment and it is found that the activity for NO reduction and C_3H_6 oxidation was increased after high temperature aging with respect to fresh catalyst. They found that this enhancement in the catalytic activity resulted from the reduced surface of

Rh at high temperature and alteration of the surface properties of the CeO_2-ZrO_2 preventing the formation of formate species which poisons the active sites of the catalyst.

Remembering that the prepared support material of CZO have the chemical structure of $Ce_{0.8}Zr_{0.2}O_2$ and the Rh metal impregnated on CZO support material separately from Rh, CZO-SI+AO-(2) catalyst shows the similar behavior of improved catalytic activity after high temperature aging.

The resistance of CZAO-CI-(2) monolithic catalyst against thermal aging is attributed to a different reason than that of CZO-SI+AO-(2) monolithic catalyst, since the CZAO-CI-(2) catalyst contains Pd and Rh metals as impregnated together like the CZO-CI+AO-(2) catalyst. So the source of improvement should be searched by comparing the CZAO-CI-(2) catalyst with the CZO-CI+AO-(2) catalyst. The difference between the two catalysts is the support material. The CZAO support material has higher surface area than the CZO support material and this higher surface area result in higher dispersion of metals with the same loading. So highly dispersed metals are more resistant to sintering at high temperatures.

A sample monolith of commercial catalyst named as COM-M5 is subjected to same aging procedures and activity tests. The catalytic activity data of commercial sample in Table 5.11, show that after aging at 900 ºC, the commercial catalyst loses its activity for all species with higher T50 and Tmax values. The catalytic activity loss is visualized in Figure 5.9 with positive ΔT50 values for all species.

Table 5. 11 Catalytic Activity Data of COM-M5 Catalyst

Species	Fresh			Aged (900 ºC)		
	T50 (C)	Maximum Conversion (%)	Tmax (C)	T50 (C)	Maximum Conversion (%)	Tmax (C)
CO	217	100	288	269	100	456
NO	224	91	408	291	91	497
C_3H_6	214	100	283	263	100	355
C_3H_8	279	99	598	309	100	598
H_2	157	100	220	213	100	280
O_2	207	100	344	255	100	388

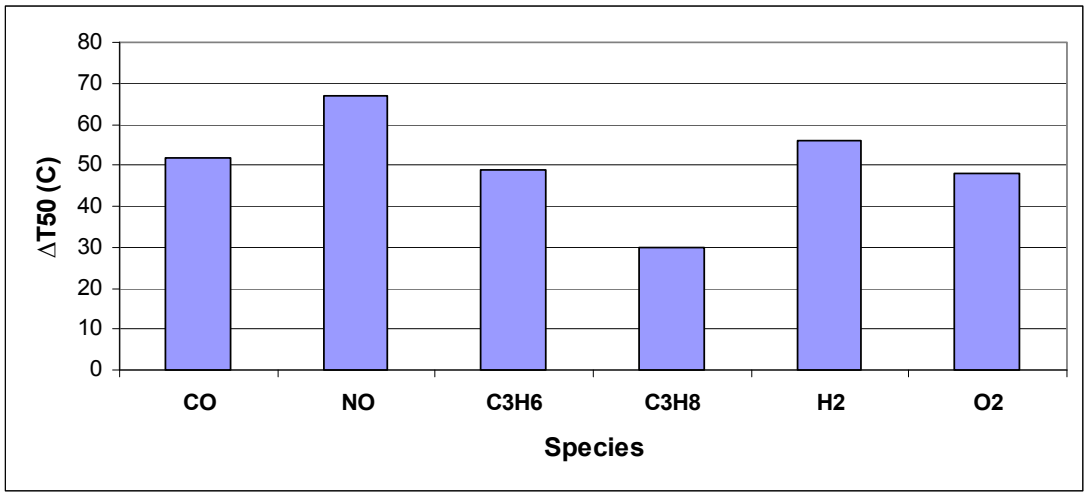

Figure 5. 9 Change of T50 Data of COM-M5 Catalyst after Aging at 900 ºC

The CZO-SI+AO-(2)-M1 monolithic catalyst, which is the best monolithic catalyst showing high resistance against thermal aging is compared with the catalytic activity data of COM-M5 monolithic catalyst both as change in T50 values and as light-off behavior in Figures 5.10 and 5.11 respectively. The comparison in Figure 5.10 displays the big difference between the two catalysts considering the thermal resistance.

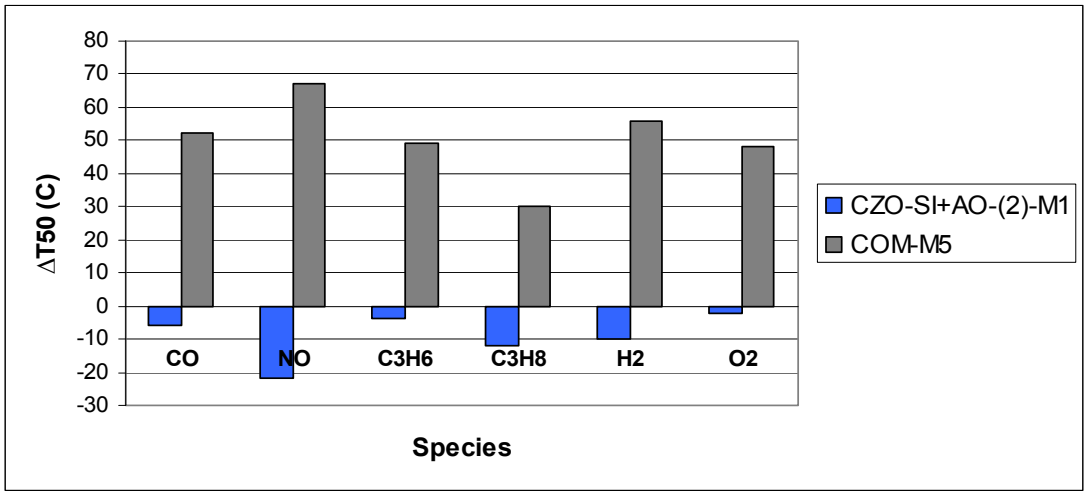

Figure 5. 10 Change of T50 Data of CZO-SI+AO-(2)-M1 and COM-M5 Catalysts after Aging at 900 ºC

Light-off behaviors of the two catalysts in Figure 5.11 reveal that although the commercial catalyst shows better catalytic activity when it is fresh with lower conversion temperatures, its catalytic activity is worse than the CZO-SI+AO-(2)-M1 monolithic catalyst after aging. The behavior for the catalytic activity loss of commercial catalyst is rather similar to the behavior of CZO-CI+AO-(2)-M1 monolithic catalyst. This similarity evokes the existence of the metals together. Probably the commercial catalyst also contains the metals together and shows no improvement in the catalytic activity after aging like the CZO-SI+AO-(2)-M1 monolithic catalyst.

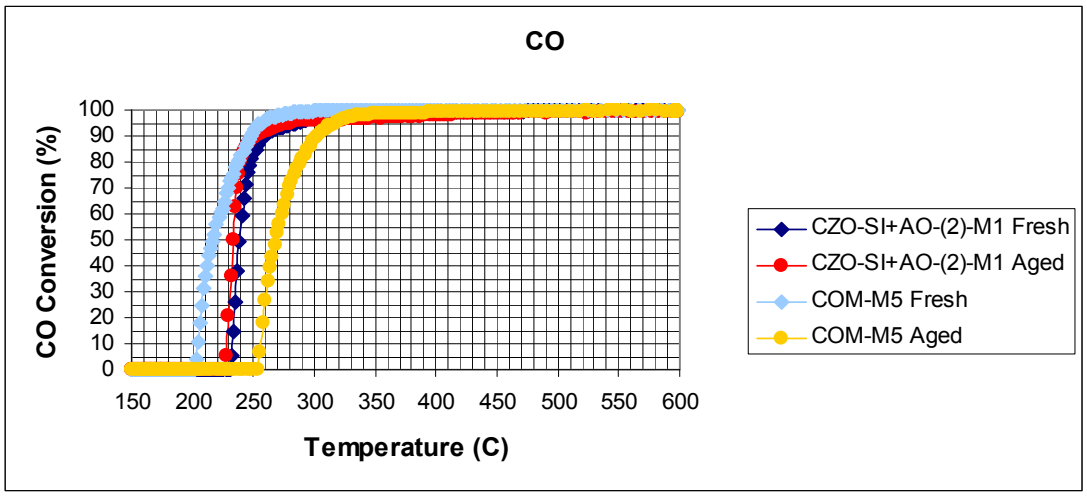

Figure 5. 11 Catalytic Activity Data of Fresh and Aged (900 ºC) CZO-SI+AO-(2)-M1 and COM-M5 Monolithic Catalysts

Two other monoliths washcoated with CZO-CI+AO-(2) and CZO-SI+AO-(2) catalysts are subjected to severe aging at 1000 ºC. When the fresh catalytic activities of these catalysts in Table 5.12 and Table 5.13 are compared, it is seen that the catalytic activities are again related to their total metal contents. The CZO-SI+AO-(2)-M2 monolithic catalyst with higher amount of total metal content than CZO-CI+AO-(2)-M2 monolithic catalyst, shows higher catalytic performance.

After aging at 1000 ºC, CZO-CI+AO-(2)-M2 monolithic catalyst loses its catalytic activity for all species and results in change in T50 values in Figure 5.12. Compared to ΔT50 values of CZO-CI+AO-(2)-M1 monolithic catalyst after aging at 900 ºC (Figure 5.6), CZO-CI+AO-(2)-M2 monolithic catalyst have lower ΔT50 values after aging at 1000 ºC contrary to expectations, except C_3H_8. The difference in T50 value for C_3H_8 was two fold higher than it is obtained for aging at 900 ºC.

Table 5. 12 Catalytic Activity Data of CZO-CI+AO-(2)-M2 Catalyst

Species	Fresh			Aged (1000 ºC)		
	T50 (C)	Maximum Conversion (%)	Tmax (C)	T50 (C)	Maximum Conversion (%)	Tmax (C)
CO	229	100	440	257	99	598
NO	224	93	409	254	93	476
C_3H_6	223	100	331	253	100	291
C_3H_8	231	100	581	282	100	598
H_2	177	100	230	204	100	240
O_2	217	100	336	241	100	312

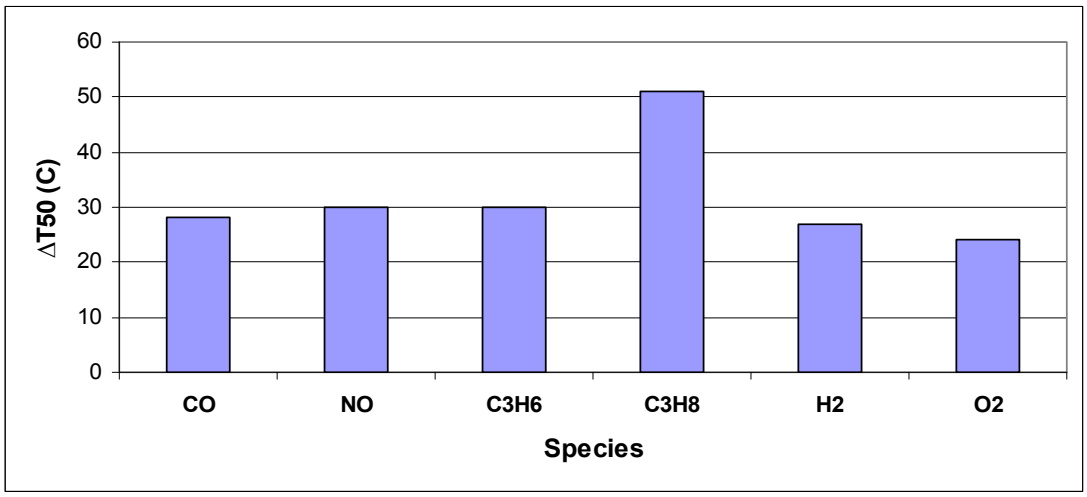

Figure 5. 12 Change of T50 Data of CZO-CI+AO-(2)-M2 Catalyst after Aging at 1000 ºC

As seen in Table 5.13 and Figure 5.13, like the CZO-CI+AO-(2)-M2 monolithic catalyst, after aging at 1000 ºC the CZO-SI+AO-(2)-M2 monolithic catalyst also shows better catalytic activity than the fresh one, compared to CZO-SI+AO-(2)-M1 monolithic catalyst which is aged at 900 ºC, except for C_3H_8 and H_2. The T50 value for C_3H_8 species is 67 ºC higher than T50 value for the fresh monolith.

Table 5. 13 Catalytic Activity Data of CZO-SI+AO-(2)-M2 Catalyst

Species	Fresh			Aged (1000 ºC)		
	T50 (C)	Maximum Conversion (%)	Tmax (C)	T50 (C)	Maximum Conversion (%)	Tmax (C)
CO	222	100	406	203	94	597
NO	218	96	495	196	68	272
C_3H_6	218	100	276	202	100	325
C_3H_8	243	100	595	310	100	597
H_2	173	100	216	186	99	256
O_2	213	100	300	198	100	350

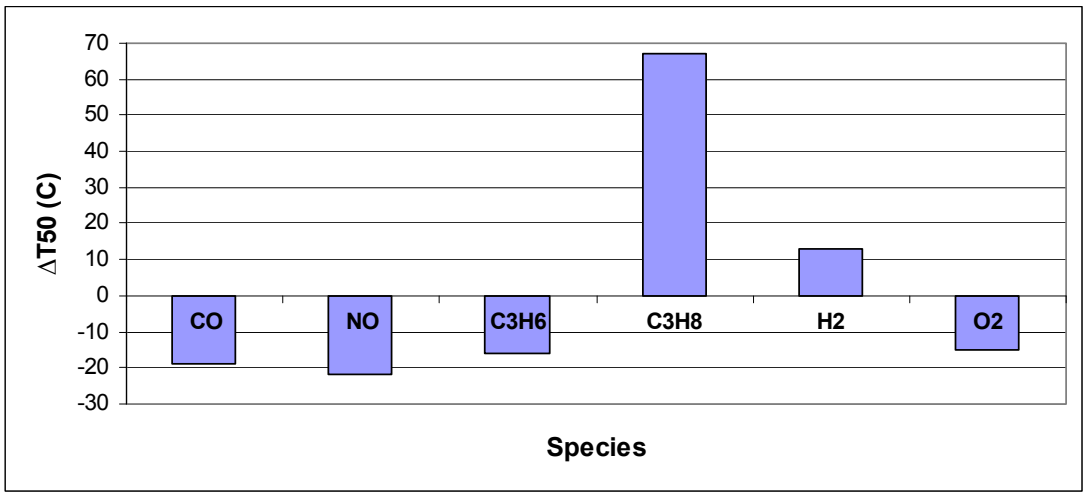

Figure 5. 13 Change of T50 Data of CZO-SI+AO-(2)-M2 Catalyst after Aging at 1000 ºC

The data in Figures 5.12 and 5.13 are combined in Figure 5.14, to see the difference in level of aging more clearly. Except the increase in T50 value for C_3H_8, the CZO-SI+AO-(2)-M2 monolithic catalyst seems more resistant to thermal aging at 1000 ºC. The aging at 1000 ºC reveals the difference between the catalytic activities of two catalysts after aging more than the case after aging at 900 ºC. Regarding CZO-SI+AO-(2)-M2 monolithic

catalyst, as discussed above, the improvement in the catalytic activity for NO and C_3H_6 is related to existence of Rh separately from Pd. On the other hand, the Pd is responsible for the conversions of C_3H_8 and H_2 and any special activation is not observed for Pd. Aging of Pd results in loss of catalytic activity for C_3H_8 and H_2.

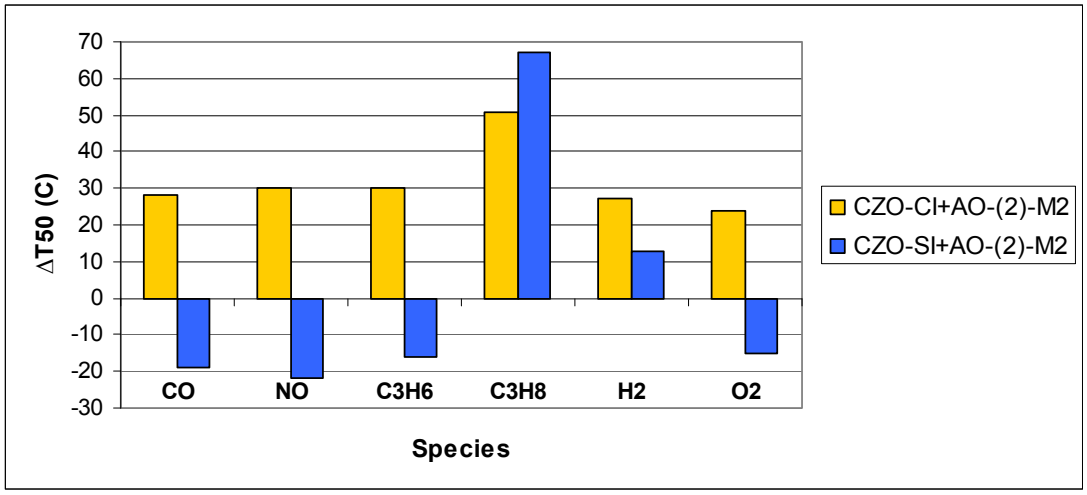

Figure 5. 14 Change of T50 Data of CZO-CI+AO-(2)-M2 and CZO-SI+AO-(2)-M2 Catalysts after Aging at 1000 ºC

In order the compare the resistance of CZO-SI+AO-(2)-M2 monolithic catalyst against thermal aging, a sample of commercial catalyst (COM-M6) is subjected to same aging procedure at 1000 ºC and the catalytic activity data and the ΔT50 values are given in Table 5.14 and Figure 5.15 respectively. This data show that after aging at 1000 ºC, light-off temperatures of commercial catalyst for all species increase enormously.

Table 5. 14 Catalytic Activity Data of COM-M6 Catalyst

Species	Fresh			Aged (1000 ºC)		
	T50 (C)	Maximum Conversion (%)	Tmax (C)	T50 (C)	Maximum Conversion (%)	Tmax (C)
CO	198	100	297	272	98	598
NO	196	98	467	284	86	509
C_3H_6	195	100	292	265	100	414
C_3H_8	236	100	598	323	100	597
H_2	*	100	197	200	100	559
O_2	183	100	285	248	100	503

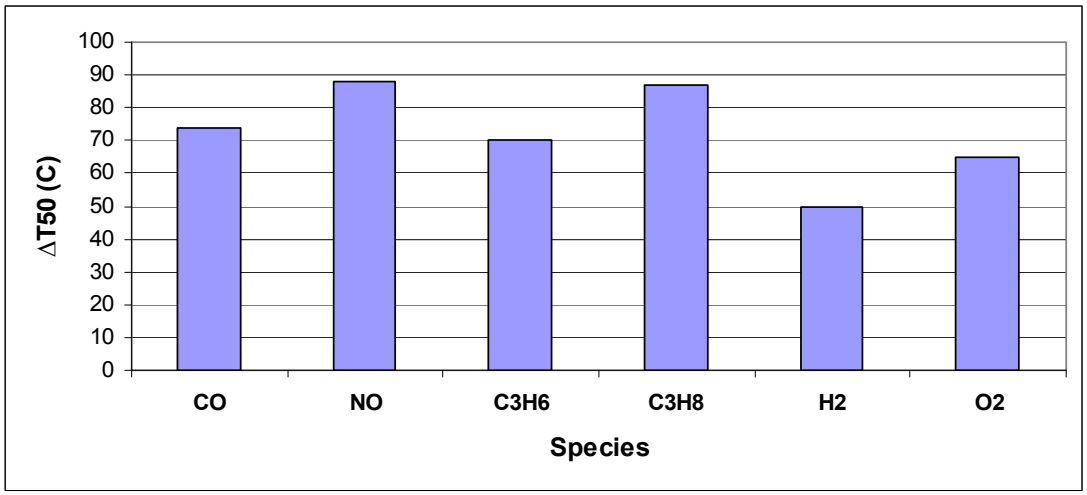

Figure 5. 15 Change of T50 Data of COM-M6 Catalyst after Aging at 1000 ºC

Figures 5.16 and 5.17 show that, the CZO-SI+AO-(2)-M2 monolithic catalyst can resist thermal aging at 1000 ºC far better than commercial catalyst. Even if the fresh catalytic activity of the commercial catalyst is better than the CZO-SI+AO-(2)-M2 monolithic catalyst, the catalytic activity of the CZO-SI+AO-(2)-M2 monolithic catalyst after aging is almost equivalent to the fresh catalytic activity of the commercial catalyst.

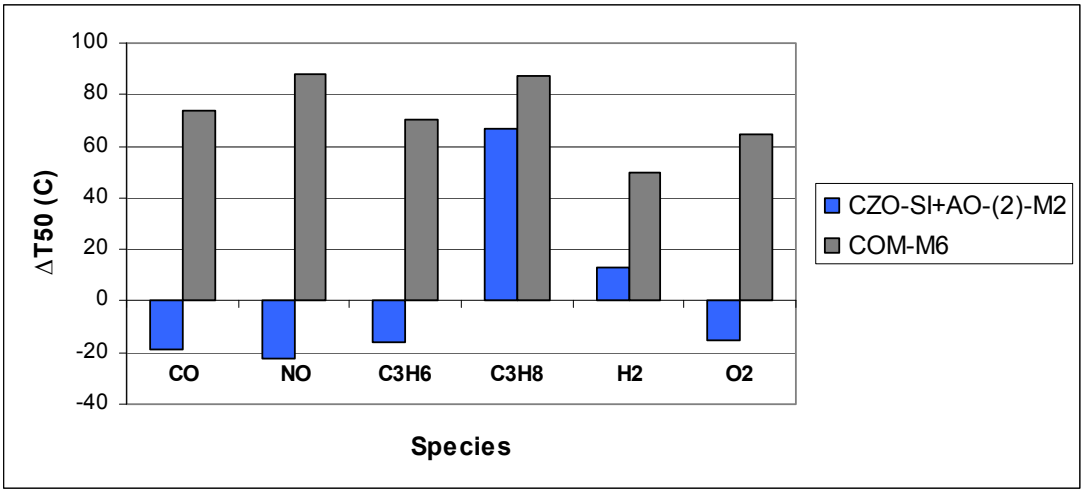

Figure 5. 16 Change of T50 Data of CZO-SI+AO-(2)-M2 and COM-M6 Catalysts after Aging at 1000 ºC

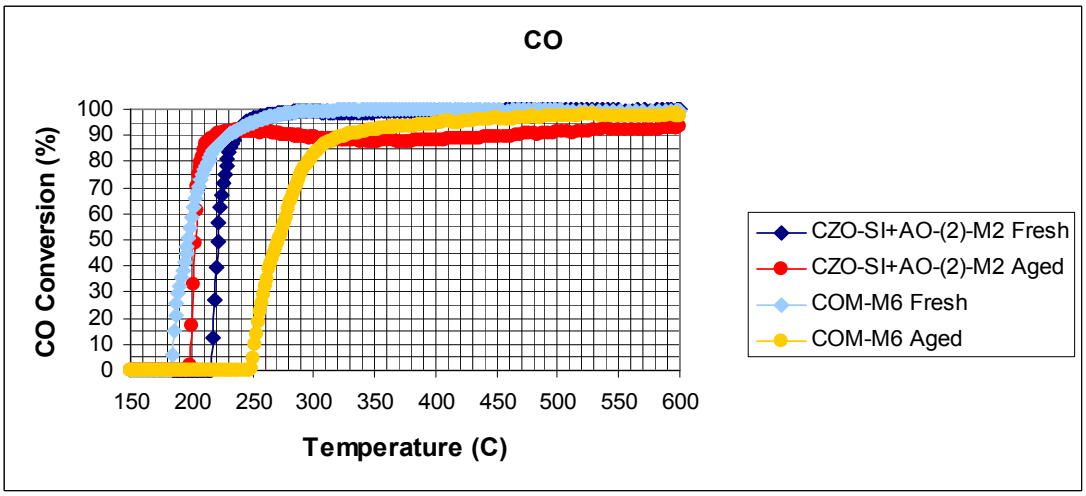

Figure 5. 17 Catalytic Activity Data of Fresh and Aged (1000 ºC) CZO-SI+AO-(2)-M2 and COM-M6 Monolithic Catalysts

CHAPTER 6

CONCLUSIONS

Mixed oxides of $Ce_{0.8}Zr_{0.2}O_2$ and $Ce_{0.68}Zr_{0.32}O_2$ are synthesized by co-precipitation and sol-gel techniques respectively for the use as a support material of three way catalyst.

Sol-gel technique resulted in higher surface area mixed oxides. After metal loading, the surface area of the catalyst was still higher than the surface area of metal loaded mixed oxides synthesized by co-precipitation technique.

The catalysts are prepared to have nominally 0.65 wt% Pd and 0.1 wt% Rh metals with a Pd/Rh ratio of 6.5. Slurries of the metal loaded catalysts are used to washcoat the cordierite monoliths to obtain monolithic catalysts. Monolithic catalysts are tested in dynamic test system for determination of catalytic activity.

During the heating and cooling steps of the catalytic activity tests of monolithic catalysts, similar maximum conversions are achieved. However during the cooling step, the temperatures are lower for the same conversions, pointing out the improved activity. This improvement in the activity is related with the reduction of the catalyst during the heating step. Therefore, for the evaluation of the catalytic activity of all catalysts, the activity data during the cooling step are considered.

During the catalytic activity tests, generally, catalysts can easily convert CO, C_3H_6, H_2 and O_2 and display typical “S” curved conversion vs. temperature

curves. On the other hand, the catalysts can convert NO and C_3H_8 more difficultly and the conversions increase more slowly as the temperature increases.

The effect of SO_2 exposure on catalytic activity is studied on a set of catalysts, first set of catalysts, during a series of test procedures. These catalysts are CZO-CI+AO-(1), CZAO-S-(1) and CZAO-CI-(1). The CZO-CI+AO-(1) catalyst is prepared by co-impregnating CZO support material with Rh and Pd, and then mixing with AO. On the other hand, CZAO-S-(1) catalyst is prepared by adding the metals into the sol of CZAO support material, whereas the CZAO-CI-(1) catalyst is prepared by co-impregnating CZAO support material. Monolithic catalysts are first tested as fresh, with simulated exhaust gas without SO_2. Then they are subjected to two other tests with simulated exhaust gas including 20 ppm SO_2 and finally tested again similarly as the first test, with simulated exhaust gas without SO_2. When the catalytic activities of the monolithic catalysts during the four tests are compared, it is observed that, with respect to the first test, the catalysts generally lose their catalytic performance during the second and third tests with exposure to SO_2. In addition to this, with the absence of SO_2 in the reaction gas mixture during the last test, catalysts can recover their catalytic performance to some extent.

After the treatment with simulated exhaust gases including SO_2 the CZO-CI+AO-(1) monolithic catalyst converted NO and C_3H_8 at lower light-off temperatures, whereas the light-off temperatures for other species increased. The improvement in the catalytic activity for C_3H_8 was negligible. The CZAO-S-(1) monolithic catalyst could not reach 50% conversion of NO even while fresh. After the treatment, the catalyst lost the catalytic activity for CO, C_3H_6, H_2 and O_2, and could reach the 50% conversions at much higher temperatures. However like the CZO-CI+AO-(1) monolithic catalyst, CZAO-

S-(1) monolithic catalyst also showed enhanced activity for C_3H_8 with 64 ºC lower light-off temperature. The CZAO-CI-(1) monolithic catalyst also lost its catalytic performance except for the little enhancement in C_3H_8. When the commercial catalyst is subjected to same treatments, it is found to lose its catalytic activity for all species much more than the prepared monolithic catalysts.

The loss of catalytic activity for CO and C_3H_6 is considered to be resulted from the sulphur poisoning of Pd. On the other hand, enhanced catalytic activity for NO is related to high resistance of Rh to sulphur poisoning, whereas the enhanced catalytic activity for C_3H_8 is related to the promoting effect of sulphur for C_3H_8 oxidation.

The effect of thermal aging is studied on another set of catalysts, second set of catalysts. CZAO-CI-(1) and CZO-CI+AO-(1) catalysts are synthesized again and included in the second set as CZAO-CI-(2) and CZO-CI+AO-(2) catalysts. In addition this set includes the CZO-SI+AO-(2) catalyst, which is prepared by the impregnation of Rh and Pd metals on separate CZO support materials and mixing the impregnated support materials with AO . Monolithic catalysts are aged at 900 ºC and 1000 ºC in dry air atmosphere. The catalytic activities of the fresh and aged monolithic catalysts are compared.

The adherence ability of the second set of catalysts is determined by subjecting the monolithic catalysts to ultrasound test. The results show that the monolithic CZAO-CI-(2) catalyst loses two times more weight than the monolithic CZO-CI+AO-(2) and CZO-SI+AO-(2) catalysts. In addition, the CZAO-CI-(2) catalyst shows lower adherence on cordierite monolith. On the other hand, CZO-CI+AO-(2) and CZO-CI+AO-(2) catalysts show higher adherence than commercial catalyst.

Powdered slurries of the catalysts are also subjected to aging procedures and characterized by BET and XRD. With increasing aging temperature, particle sizes of CZO and CZAO support materials in the samples, estimated using XRD data, are increased and surface area of the powders are decreased.

After aging at 900 ºC, the CZAO-CI-(2) monolithic catalyst did not lose its catalytic performance and achieved similar light-off temperatures as it is fresh. On the other hand, compared to catalytic activity while fresh, CZO-CI+AO-(2)-M1 monolithic catalyst could reach 50% conversions for all species at higher light-off temperatures and could not show resistance against aging. Surprisingly, the CZO-SI+AO-(2)-M1 catalyst was highly resistant to thermal aging and no increase in light-off temperatures is observed after aging treatment. In fact, this catalyst showed improved activity for NO and C_3H_8 after aging treatment.

The CZO-CI+AO-(2)-M2 monolithic catalyst, aged at 1000 ºC, also lost its catalytic performance for all the species, with the highest loss in activity for C_3H_8. On the other hand, the CZO-SI+AO-(2)-M2 monolithic catalyst showed improved activity after aging at 1000 ºC, except for C_3H_8 and H_2 conversions. The increase in the light-off temperature for C_3H_8 was even higher than it is for the aged CZO-SI+AO-(2)-M2 monolithic catalyst.

After aging at both 900 ºC and 1000 ºC, the commercial catalyst lost its catalytic activity for all species. The CZO-SI+AO-(2)-M2 monolithic catalyst is found more resistant to thermal aging than the commercial catalyst.

The high resistance of the CZO-SI+AO-(2) monolithic catalysts against high temperature aging is related to the composition of the mixed oxide support material and the impregnation of the Rh metal separately from Pd metal.

Thus the use of CZO-SI+AO-(2) monolithic catalyst is found as a promising invention for use as a three way catalyst in automotive technology.

REFERENCES

Addiego, W.P. et al. High surface area washcoated substrate and method for producing same. US Patent 5212130. 18 May 1993.

Agrafiotis, C., Tsetsekou, A., Stournaras, C. J., Julbe, A., Dalmazio, L., Guizard, C. et al. (2001). Evaluation of sol–gel methods for the synthesis of doped-ceria environmental catalysis systems Part II. Catalytic activity and resistance to thermal aging. Applied Catalysis B: Environmental, 34, 149 - 159.

Beck, D.D., Sommers, J.W., DiMaggio, C.L. (1994). Impact of sulfur on model palladium-only catalysts under simulated three-way operation. Applied Catalysis B: Environmental, 3, 205 – 227.

Ciambelli, P., Sannino, D., Palma, V., & Russo, P. (2003). Experimental methods for activity measurements in environmental catalysis. Catalysis Today, 77, 347 - 358.

Cooper, B.J., Evans, W.D.J., & Harrison, B. (1987). Aspects of automotive catalyst preparation, performance and durability. In A. Crucq & A. Frennet (Eds.), Catalysis and pollution control, Studies in surface science and catalysis, Vol.30 (pp. 117-141). Amsterdam: Elsevier.

Cornelius, S.J. (2001). Modelling and control of automotive catalysts. (Doctoral dissertation). Retrieved from http://www-control.eng.cam.ac.uk/Engines/files/cat_model_thesis.pdf

Cullity, B. P., & Stock, S.R. (2001). Elements of X-ray Diffraction (3rd. Ed.). New York: Prentice Hall.

Di Monte, R., Fornasiero, P., Graziani, M., & Kaspar, J. (1998). Oxygen storage and catalytic NO removal promoted by CeO2 -containing mixed oxides. Journal of Alloys and Compounds, 275–277, 877–885.

Di Monte, R., & Kaspar, J. (2005). Heterogeneous environmental catalysis – a gentle art: CeO2–ZrO2 mixed oxides as a case history. Catalysis Today, 100, 27 – 35.

Di Monte, R., Kaspar, J., Fornasiero, P., Graziani, M., Paze, C., & Gubitosa, G. (2002). NO reduction by CO over Pd/Ce0.6Zr0.4O2 - Al2O3 catalysts: in situ FT-IR studies of NO and CO adsorption. Inorganica Chimica Acta, 334, 318 - 326.

Farrauto, R. J., & Heck, R. M. (1999). Catalytic converters: state of the art and perspectives. Catalysis Today, 51, 351 - 360.

Fogler, H. S. (2006). Elements of chemical reaction engineering (4th. Ed.). Massachusetts: Prentice Hall.

Fornasiero, P., Di Monte, R., Montini, T., Kaspar, J., & Graziani, M. (2000). Thermal stability and oxygen storage capacity of noble metal/ceria-zirconia catalysts for the automotive converters with the on-board-diagnostics (OBD). Studies in Surface Science and Catalysis, 130, 1355 - 1360.

Fornasiero, P., Montini, T., Graziani, M., Zilio, S., & Succi, M. (2008). Development of functionalized Fe–Al–Cr alloy fibers as innovative catalytic oxidation devices. Catalysis Today, 137, 475 - 482.

Gas Correction Factors. Retrieved December 24, 2008 from Teledyne Hastings Instruments Web Site: http://www.teledyne-hi.com/tech-papers/GasDataTables.xls

Gennari, F.C., Montini, T., Fornasiero, P., & Gamboa, J.J.A. (2008). Reduction behavior of nanoparticles of Ce0.8Zr0.2O2 produced by different approaches. Int J Hydrogen Energy, doi:10.1016/j.ijhydene.2007.12.006.

Germani, G., Alphonse, P., Courty, M., Schuurman, Y., & Mirodatos, C. (2005). Platinum/ceria/alumina catalysts on microstructures for carbon monoxide conversion. Catalysis Today, 110, 114 – 120.

Gonzales – Velasco, J.R., Gutierrez-Ortiz, M.A., Marc, J.L., Gonzales-Marcos, M.P., & Blanchard, G. (2001). Selectivity of high surface area Ce0.68Zr0.32O2 for the new generation of TWC under environments with different redox character. Applied Catalysis B: Environmental, 33, 303 – 314.

Graham, J. H., & Vedrine, J. C. (2003). Heterogeneous Catalyst Preparation. In M. Baerns (Ed.), Basic principles in applied catalysis (pp. 215-258). Berlin: Springer.

Granados, M. L., Galisteo, F. C., Mariscal, R., Alifanti, M., Gurbani, A., Fierro, J. L. G. et al. (2006). Modification of a three-way catalyst washcoat by

aging: A study along the longitudinal axis. Applied Surface Science, 252, 8442 - 8450.

Granados, M.L., Larese, C., Galisteo, F.C., Mariscal, R., Fierro, J.L.G., & Fernandez – Ruiz, R. et al. (2005). Effect of mileage on the deactivation of vehicle-aged three-way catalysts. Catalysis Today, 107 – 108, 77 – 85.

Haneda, M., Houshito, O., Sato, T., Takagi, H., Shinoda, K., & Nakahara, Y. et al. (2010). Improved activity of Rh/CeO –ZrO three-way catalyst by high-temperature ageing. Catalysis Communications, 11, 317 – 321.

Kaspar, J., & Fornasiero, P. (2003). Nanostructured materials for advanced automotive de-pollution catalysts. Journal of Solid State Chemistry, 171, 19 – 29.

Kaspar, J., Fornasiero, P., Balducci, G., Di Monte, R., Hickey, N., & Sergo, V. (2003b). Effect of ZrO2 content on textural and structural properties of CeO2-ZrO2 solid solutions made by citrate complexation route. Inorganica Chimica Acta, 349, 217 – 226.

Kaspar, J., Fornasiero, P., & Hickey, N. (2003a). Automotive catalytic converters: current status and some perspectives. Catalysis Today, 77, 419 - 449.

Lachman, I.M. et al. Process for removal of hydrocarbons carbon manoxide, and oxides of nitrogen from oxygen-containing waste gas using molecular sieve-palladium-platinum catalyst on a substrate. US Patent 5292991. 8 Mar. 1994.

Larese, C., Galisteo, F.C., Granados, M.L., Mariscal, R., Fierro, J.L.G., & Lambrou, P.S. et al. (2004). Effects of the CePO4 on the oxygen storage and release properties of CeO2 and Ce0.8Zr0.2O2 solid solution. Journal of Catalysis, 226, 443 – 456.

Lambrou, P. S., Christou, S. Y., Fotopoulos, A. P., Foti, F. K., Angelidis, T. N., & Efstathiou, A. M. (2005). The effects of the use of weak organic acids on the improvement of oxygen storage and release properties of aged commercial three-way catalysts. Applied Catalysis B: Environmental, 59, 1 – 11.

Nguefack, M., Popa, A.F., Rossignol, S., & Kappenstein, C. (2003). Preparation of alumina through a sol–gel process. Synthesis, characterization, thermal evolution and model of intermediate boehmite. Phys. Chem., 5, 4279–4289.

Nijhuis, T.A., Beers, A.E.W., Vergunst, T., Hoek, I., Kapteijn, F., & Moulijn, J.A. (2001). Preparation of monolithic catalysts. Catalysis Reviews, 43, 4, 345 – 380.

Noh, J., Yang, O., Kim, D. H., & Woo, S. I. (1999). Characteristics of the Pd-only three-way catalysts prepared by sol–gel method. Catalysis Today, 53, 575 – 582.

Perry, R. H., & Green, D. W. (1997). Perry's chemical engineers' handbook (7th. Ed.). New York: Mc Graw Hill.

Rossignol, G., Gerard, F., & Duprez, D. (1999a). Effect of the preparation method on the properties of zirconia–ceria materials. Journal of Materials Chemistry, 9, 1615 – 1620.

Rossignol, G., Madier, Y., & Duprez, D. (1999b). Preparation of zirconia–ceria materials by soft chemistry. Catalysis Today, 50, 261 – 270.

Schuetzle, D., Siegl, W.O., Jensen, T.E., Dearth, M.A., Kaiser, E.W., & Gorse, R. et al. (1994). The relationship between gasoline composition and vehicle hydrocarbon emissions: A review of current studies and future research needs. Environmental Health Perspectives, 102, 4, 3 – 12.

Shinjoh, H., Muraki, H., & Fujitani, Y. (1989). Periodic operation effects in propane and propylene oxidation over noble metal catalysts. Applied Catalysis, 49, 2, 195 – 204.

Shinjoh, H., Tanabe, T., Yokota, K., & Sugiura, M. (2004). Comparative NOx reduction behavior of Pt, Pd, and Rh supported catalysts in simulated exhaust gases as a function of oxygen concentration.Topics in Catalysis, 30/31, 319 – 324.

Suopanki, A., Polvinen, R., Valden, M., & Harkonen, M. (2005). Rh oxide reducibility and catalytic activity of model Pt–Rh catalysts. Catalysis Today, 100, 327 – 330.

Tanaka, H., Mizuno, N., & Misono, M. (2003). Catalytic activity and structural stability of La0.9Ce0.1Co1−xFexO3 perovskite catalysts for automotive emissions control. Applied Catalysis A: General, 244, 371 – 382.

Torbati, R. (2009). Advanced catalytic systems for the partial oxidation of hydrocarbons: Improving sulphur tolerance of Rh based catalysts (Doctoral dissertation). Retrieved from http://www.fedoa.unina.it/3845/

Ulla, L. (2003). Deactivation correlations of Pd/Rh three way catalysts designed for Euro IV emission limits. Effects of ageing atmosphere, temperature and time (Academic dissertation). University of Oulu, Oulu.

Wang, J. A., Chen, L. F., Valenzuela, M. A., Montoya, A., Salmones, J., & Angel, P. D. (2004). Rietveld refinement and activity of CO oxidation over Pd/Ce0.8Zr0.2O2 catalyst prepared via a surfactant-assisted route. Applied Surface Science, 230, 34 – 43.

Yamazaki, K., Takahashi, N., Shinjoh, H., & Sugiura, M. (2004). The performance of NOx storage-reduction catalyst containing Fe-compound after thermal aging. Applied Catalysis B: Environmental, 53, 1 – 12.

Yao, M. H., Baird, R. J., Kunz, F. W., & Hoosty, T. E. (1997). An XRD and TEM investigation of the structure of alumina-supported ceria–zirconia. Journal of Catalysis, 166, 67 – 74.

Yingying, G., Shengsheng, F., Jinlin, L., Xiangkui, G., & Manjuan, W. (2007). Preparation of mesoporous Ce0.5Zr0.5O2 mixed oxide by hydrothermal templating method. Journal of Rare Earths, 25, 710 – 714.

Yucai, H. (2006). Hydrothermal synthesis of nano Ce-Zr-Y oxide solid solution for automotive three way catalyst. J. Am. Ceram. Soc., 89 [9], 2949 - 2951. doi:10.1111/j.1551-2916.2006.01130.x

Zahir, M.H., Ikuhara, Y.H., Fujisaki, S., Sato, K., Nagano, T., & Iwamoto, Y. (2007). Preparation and characterization of mesoporous ceria-zirconia-alumina nanocomposite with high hydrothermal stability. Journal of Materials Research, 22, 3201 – 3209.

Zoarob, Z.K. (1991). Transient modeling of diffusivity for monolithic catalyst by using pulse testing technique (Master's thesis). METU, Ankara, Türkiye.

APPENDIX A

CATALYST PREPARATION

A.1 Preparation of Ceria – Zirconia Mixed Oxide

- 86.46 g of $CeN_3O_9.6H_2O$ and 16.72 g of $N_2O_7Zr.aq$ are dissolved in 1 L of deionized water. The mixture is stirred for 30 min.
- 333 mL of H_2O_2 is added into the mixture and stirred for 1 h.
- The mixture is added dropwise into 250 mL NH_4OH solution and kept for 12 h.
- The product is filtered with $CH_3CHOHCH_3$ and refluxed in 250 mL $CH_3CHOHCH_3$ for 6 h.
- The refluxed product is dried at 150 ºC for 12 h.
- The powder sample is grounded and calcined in an oven under dry air at 550 ºC for 1 h.

A.2 Preparation of Ceria – Zirconia – Alumina Mixed Oxide

- 126.97 g $Al(OC_4H_9)_3$ is hydrolysed with 900 mL of deionized water at 85 ºC under vigorous stirring for 1 h.
- The mixture is cooled to 60 ºC and 2243 µL HNO_3 solution is added.
- The mixture is heated again to 85 ºC and refluxed for 12 h.
- 27.41 g of $CeN_3O_9.6H_2O$ and 21.21 g of $N_2O_7Zr.aq$ are dissolved in 250 mL of deionized water and added into the refluxed sol.

- The resulting gel product is dried at 150 ºC for 48 h.
- The powder sample is grounded and calcined in an oven under dry air at 600 ºC for 3 h with a heating rate of 1 ºC/min.

A.3 Preparation of Pseudoboehmite

- 24 g of $Al(OC_4H_9)_3$ is hydrolysed with 175 mL of deionized water at 60 ºC under vigorous stirring for 2 h.
- 0.8 mL of HCl is added into the mixture.
- The mixture is heated to 80 ºC and stirred vigorously for 1 h.
- The resulting gel product is dried at 150 ºC for 48 h.
- The powder sample is grounded and calcined in an oven under dry air at 300 ºC for 5 h with a heating rate of 5 ºC/min.

A.4 Addition of Metals

Addition of metals by impregnation technique:

- For 1 g of support material 0.01 g of $Rh(NO_3)_3$ and 0.217 g of $PdCl_2$ solution is weighted.
- For 1 g of Ceria – Zirconia Mixed Oxide as support material metal precursor or solution is dissolved in 633 µL of deionized water.
- For 1 g of Ceria – Zirconia – Alumina Mixed Oxide as support material metal precursor or solution is dissolved in 840 µL of deionized water.
- The mixture is rotated in rotary vacuum evaporator for 15 min. without vacuum and heating.

- The support material is added into the mixture and rotated in water bath at 80 ºC under vacuum to evaporate the liquid.
- The product is dried at 150 ºC for 12 h.
- The powder sample is grounded and calcined in an oven under dry air at 550 ºC for 1 h.

Addition of metals in sol:

- For 1 g of Ceria – Zirconia – Alumina Mixed Oxide support material 0.01 g of $Rh(NO_3)_3$ and 0.217 g of $PdCl_2$ solution is weighted and dissolved in 40 mL of deionized water.
- Aqueous solution of metals is added into the refluxed sol and stirred for 30 min.
- The resulting gel product is dried at 150 ºC for 48 h.
- The powder sample is grounded and calcined in an oven under dry air at 600 ºC for 3 h with a heating rate of 1 ºC/min.

A.5 Preparation of Washcoating Slurry

Preparation of washcoating slurry with ceria-zirconia mixed oxide:

- 10 g of impregnated ceria-zirconia mixed oxide, 23.5 g of γ-Al_2O_3 and 2.57 g of pseudoboehmite is mixed with 54 mL of deionized water in a 250 mL HDPE mortar.
- 3 mm alumina mills are added occupying 33V% of the mixture.
- The mixture is ball-milled for 30 min at 275 rpm.
- 2378 µL HNO_3 solution is added into the slurry and ball-milled again for 3 h at 275 rpm.

Preparation of washcoating slurry with ceria - zirconia –alumina mixed oxide:

- 36 g of metals added ceria-zirconia-alumina mixed oxide and 2.14 g of pseudoboehmite is mixed with 57 mL of deionized water in a 250 mL HDPE mortar.
- 3 mm alumina mills are added occupying 33V% of the mixture.
- The mixture is ball-milled for 30 min at 275 rpm.
- 2515 µL HNO_3 solution is added into the slurry and ball-milled again for 3 h at 275 rpm.

APPENDIX B

CATALYTIC ACTIVITY TEST

B.1 Total Simulated Exhaust Gas Flow Rate

For selected gas hourly space velocity (GHSV) of 50,000 h^{-1}, the necessary total gas flow rate is calculated using equation B.1 (Fogler, 2006).

$$GHSV = \frac{\nu_0}{V_{eff}} \tag{B.1}$$

Effective volume of a monolith, 2.2 cm in diameter and 1.3 cm in height with open frontal flow area of 0.69% (Kaspar et al., 2003) is calculated as;

$$V_{eff} = \left(\pi \times \left(\frac{(2.2\,cm)^2}{4} \right) \times (1.3\,cm) \right) \times (0.69) = 3.4\,cm^3$$

The gas flow rate is calculated as 2841.5 mL/min from Equation B.1 for the selected GHSV and calculated effective volume.

$$50.000\,h^{-1} = \frac{\nu_0 (L/h)}{(3.4\,cm^3) \times (1L/1000\,cm^3)}$$

$$\nu_0 = 170.5\,L/h$$

$$\nu_0 = (170.5\,L/h) \times (1000\,mL/1L) \times (1h/60\,\text{min}) = 2841.5\,mL/\text{min}$$

B.2 Exhaust Gas Composition

The desired gas mixture composition of simulated exhaust composition is given in Table B.1 as “ppm” and “%”. The oxygen composition is determined as to have the stoichiometric number of 1.0.

Table B. 1 Desired Simulated Exhaust Gas Mixture Composition

Species	Gas Mixture Composition (ppm)	Gas Mixture Composition (%)
C_3H_6	375	0.0375
C_3H_8	125	0.0125
CO	10000	1.00
H_2	2300	0.23
CO_2	100000	10.00
NO	1500	0.15
SO_2	20	0.002
O_2	7700	0.77
N_2	Balance	Balance

The oxygen composition for the stoichiometric number S of 1.0, as defined below, is calculated as 0.77%.

$$S = \frac{2[O_2]+[NO]}{[H_2]+[CO]+9[C_3H_6]+10[C_3H_8]}$$

$$1.0 = \frac{2[O_2]+[0.15]}{[0.23]+[1.00]+9[0.0375]+10[0.0125]}$$

$$[O_2] = 0.77\%$$

For the exhaust gas composition, five different gas cylinders are used. The first cylinder contains C_3H_6, C_3H_8, CO, H_2 and CO_2 as mixture. In order to

have the desired exhaust gas composition, the compositions of these species are determined as given in Table B.2. The actual cylinder composition is used to recalculate the exhaust gas composition. All the compositions of five cylinders are given in Table B.3.

Table B. 2 Composition of Cylinder 1

Species	Desired		Actual
	Gas Mixture Composition (%)	Cylinder Composition (%)	Cylinder Composition (%)
C_3H_6	0.0375	0.3324	0.33
C_3H_8	0.0125	0.1108	0.11
CO	1.00	8.8652	8.87
H_2	0.23	2.039	2.04
CO_2	10.00	88.6525	88.65

Table B. 3 Actual Cylinder Compositions

Cylinder	Species	Cylinder Composition (%)	Cylinder Composition (ppm)
1	C_3H_6	0.33	3300
	C_3H_8	0.11	1100
	CO	8.87	88700
	H_2	2.04	20400
	CO_2	88.65	886500
2	NO	50	500000
	N_2	50	500000
3	SO_2	0.01	100
	N_2	99.99	999900
4	O_2	99.5	995000
5	N_2	99.998	999980

According to the actual cylinder compositions, flow rate from each cylinder is calculated as exemplified below. In order to have oxygen oscillation around

the stoichiometric number of 1.0, an additional oxygen flow of 10.5 mL/min is used with a frequency of 1 Hz. As a result the exhaust gas composition is oscillated between the reducing and oxidizing conditions satisfying the average stoichiometric condition. All the flow rates are given in Table B.4.

$$Flow\,Rate = \frac{\nu_0\,(mL/\min)\times\left(Gas\,Mixture\,Composition\,(\%)\right)}{\left(Cylinder\,Composition\,(\%)\right)}$$

$$NO\,Mixture\,Flow\,Rate = \frac{2841.5(mL/\min)\times\left(0.00150\right)}{\left(0.0050\right)} = 8.52\,mL/\min$$

Table B. 4 Flow rates for Reducing, Stoichiometric and Oxidizing Conditions

Cylinder	Flow Rate (mL/min)		
	Reducing	**Stoichiometric**	**Oxidizing**
1	320.52	320.52	320.52
2	8.52	8.52	8.52
3	568.30	568.30	568.30
4	16.67	21.92	27.17
5	1638.09	1638.09	1638.09
water	284.15	284.15	284.15
Total	2836.25	2841.50	2846.75

According to the flow rates given above the gas composition of the simulated exhaust gas for three conditions used in the catalytic activity tests are given in Table B.5.

Table B. 5 Simulated Gas Mixture Compositions for Reducing, Stoichiometric and Oxidizing Conditions

Species	Gas Mixture Composition (%)		
	Reducing	**Stoichiometric**	**Oxidizing**
C_3H_6	0.037	0.037	0.037
C_3H_8	0.012	0.012	0.012
CO	1.002	1.001	0.999
H_2	0.231	0.230	0.230
CO_2	10.018	10.000	9.981
NO	0.150	0.150	0.150
SO_2	0.002	0.002	0.002
O_2	0.585	0.767	0.949
N_2	57.754	57.648	57.541

For three different conditions, the oxygen composition and the stoichiometric number changes as given in Table B.6.

Table B. 6 O_2 Concentration and Stoichiometric Number for Reducing, Stoichiometric and Oxidizing Conditions

	Reducing	**Stoichiometric**	**Oxidizing**
O2 (%)	0.585	0.767	0.950
S	0.78	1.0	1.21

B.3 Simulated Exhaust Gas Water Content

The saturation temperature of the water vapor for the 1638.105 ml of N_2 as carrier gas is calculated using Antoine Equation (Equation B.2) (Perry & Green, 1997) with P^{sat} in torr and T in ºC. For water, this equation is valid between the temperatures of 1-100 ºC with the constants below.

$$\log P^{sat} = A - \frac{B}{C+T} \tag{B.2}$$

$$T = \frac{B}{A - \log P^{sat}} - C$$

Where;

$A = 8.07131$

$B = 1730.63$

$C = 233.426$

In the calculations, the atmosphere pressure is accepted as 1 atm. The fraction of the necessary flow rate of the water vapor and the total flow rate with N_2 gas is assumed as the partial pressure of the water.

$$\frac{H_2O}{N_2 + H_2O} = \frac{284.15}{1638.105 + 284.15} = 0.1478$$

$$P^{sat} = (1atm) \times 0.1478 = 0.1478\,atm$$

$$P^{sat} = (0.1478\,atm) \times \frac{760\,torr}{1\,atm} = 112.344\,torr$$

Using the estimated saturation pressure and the constants, the saturation pressure is found as 54 ºC.

$$T = \frac{1730.63}{8.07131 - \log(112.344)} - 233.426$$

$$T = 54°C$$

B.4 Analysis of Catalytic Activity Test Data

The data from CO analyzer is obtained as the concentration of CO with ppm unit. The conversion of CO is directly calculated using Equation B.3 (Fogler, 2006).

$$X = \frac{C_{A0} - C_A}{C_{A0}} \times 100\% \tag{B.3}$$

As an example, taking the initial concentration as 9999 ppm, which is the highest value that CO analyzer can read, and an instant concentration of 281 ppm, the conversion is found as 97.19% from Equation B.3.

$$X = \frac{C_{A0} - C_A}{C_{A0}} = \frac{9999 - 281}{9999} \times 100\% = 97.19\%$$

The data from MS need to be converted to concentration values using the specific calibration equations for each species. To give an example, an initial MS data of 6.70E-08 and an instant data of 4.05E-08 for NO are taken. Initial and instant concentrations are calculated from the corresponding calibration equation.

$$NO\ Calibration\ Equation: y = (4E+10)x - 517.59$$

$$C_{A0} = (4E+10) \times (6.70E-08) - 517.59 = 2160\ ppm$$

$$C_A = (4E+10) \times (4.05E-08) - 517.59 = 1100\ ppm$$

Using Equation B.3, the conversion is calculated as 49.10%.

$$X = \frac{C_{A0} - C_A}{C_{A0}} = \frac{2160 - 1100}{2160} \times 100\% = 49.10\%$$

APPENDIX C

CALIBRATIONS

C.1 Mass Flow Controller Calibrations

All the MFCs are calibrated with nitrogen gas and a gas correction factor is used for each gas mixture in the cylinders. The gas correction factors in Table C.1 are obtained from the homepage of Teledyne for 200 series of MFCs (Gas Correction Factors, 2008). The gas correction factor of the mixture in Cylinder 1 is taken as 0.743 which is the factor for CO_2 existing in maximum concentration. For the gas mixture in Cylinder 2, the average of the gas correction factors of NO and N_2 is used. The gas correction factor for Cylinder 4 is 0.981 for pure oxygen. The gas correction factor of 1.0 for nitrogen is taken for Cylinder 5 and Cylinder 3. Calibration data for MFCs are given in following Tables C.2, C.3, C.4, C.5 and C.6 and Figures C.1, C.2, C.3, C.4 and C.5.

Table C. 1 Composition of Cylinders and Gas Correction Factors

Cylinder	MFC	Species	Cylinder Composition (%)	Gas Correction Factor
1	MFC1	C_3H_6	0.33	0.743
		C_3H_8	0.11	
		CO	8.87	
		H_2	2.04	
		CO_2	88.65	
2	MFC2	NO	50	0.98975
		N_2	50	
3	MFC3	SO_2	0.01	1
		N_2	99.99	
4	MFC4	O_2	99.5	0.981
5	MFC5	N_2	99.998	1

Table C. 2 Calibration Data for MFC1

Set Flow Rate (ml/min)	Calibration Volume (mL)	Measured Time (sec)	Measured Time (min)	Measured Nitrogen Flow Rate (ml/min)	Corrected Gas Flow Rate (ml/min)
150	30	7.06	0.118	254.958	189.433
200	30	5.35	0.089	336.449	249.981
250	30	4.32	0.072	416.667	309.583
300	30	3.51	0.059	512.821	381.026
350	30	2.97	0.050	606.061	450.303
400	30	2.56	0.043	703.125	522.422
450	30	2.25	0.038	800.000	594.400
500	30	1.98	0.033	909.091	675.455
550	30	1.8	0.030	1000.000	743.000
600	30	1.66	0.028	1084.337	805.663

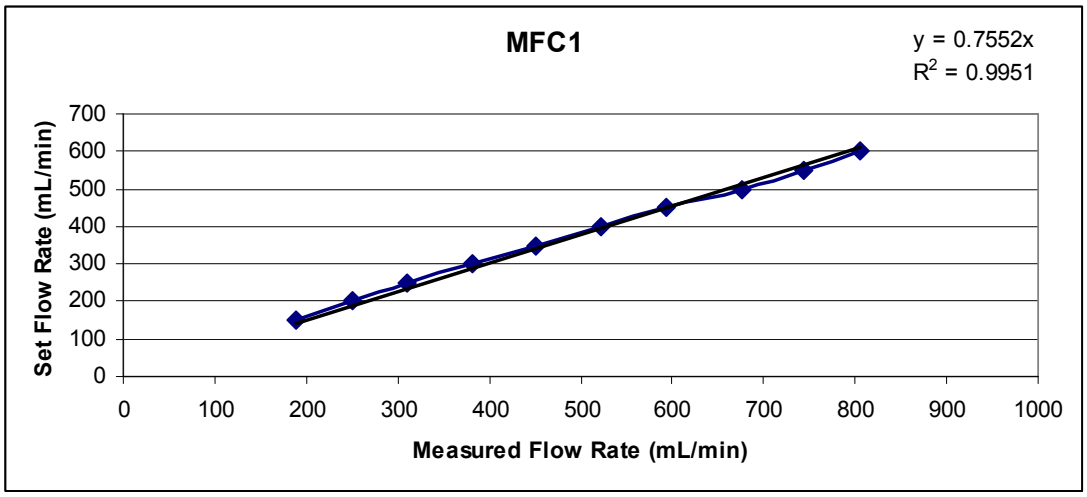

Figure C. 1 Calibration Graph for MFC1

Table C. 3 Calibration Data for MFC2

Set Flow Rate (ml/min)	Calibration Volume (mL)	Measured Time (sec)	Measured Time (min)	Measured Nitrogen Flow Rate (ml/min)	Corrected Gas Flow Rate (ml/min)
5	10	88.33	1.472	6.793	6.723
10	10	45.22	0.754	13.268	13.132
15	10	30.28	0.505	19.815	19.612
20	10	22.77	0.380	26.350	26.080
25	10	18.31	0.305	32.769	32.433
30	10	15.3	0.255	39.216	38.814
35	10	13.09	0.218	45.837	45.367
40	10	11.43	0.191	52.493	51.955
45	10	10.17	0.170	58.997	58.392

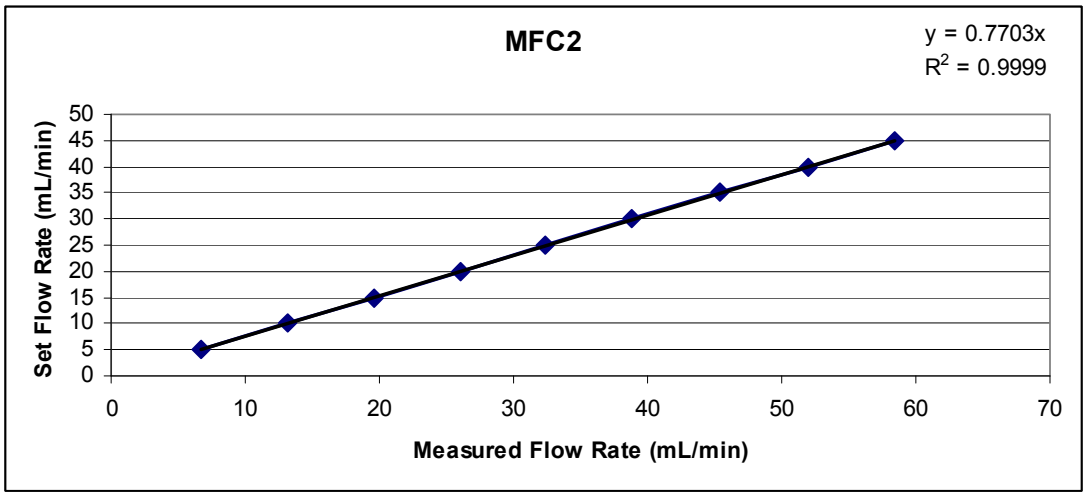

Figure C. 2 Calibration Graph for MFC2

Table C. 4 Calibration Data for MFC3

Set Flow Rate (ml/min)	Calibration Volume (mL)	Measured Time (sec)	Measured Time (min)	Measured Nitrogen Flow Rate (ml/min)
250	30	5.8	0.097	310.345
500	30	2.74	0.046	656.934
750	30	1.71	0.029	1052.632

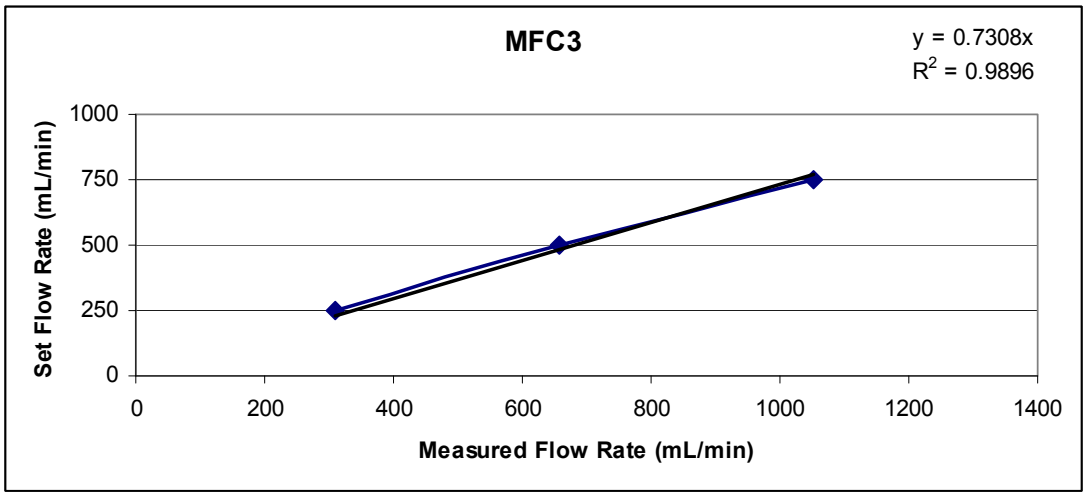

Figure C. 3 Calibration Graph for MFC3

Table C. 5 Calibration Data for MFC4

Set Flow Rate (ml/min)	Calibration Volume (mL)	Measured Time (sec)	Measured Time (min)	Measured Nitrogen Flow Rate (ml/min)	Corrected Gas Flow Rate (ml/min)
10	10	46.57	0.776	12.884	12.639
15	10	30.87	0.515	19.436	19.067
20	10	23.13	0.386	25.940	25.447
25	10	18.54	0.309	32.362	31.748
30	10	15.48	0.258	38.760	38.023
35	10	13.14	0.219	45.662	44.795
40	10	11.74	0.196	51.107	50.136

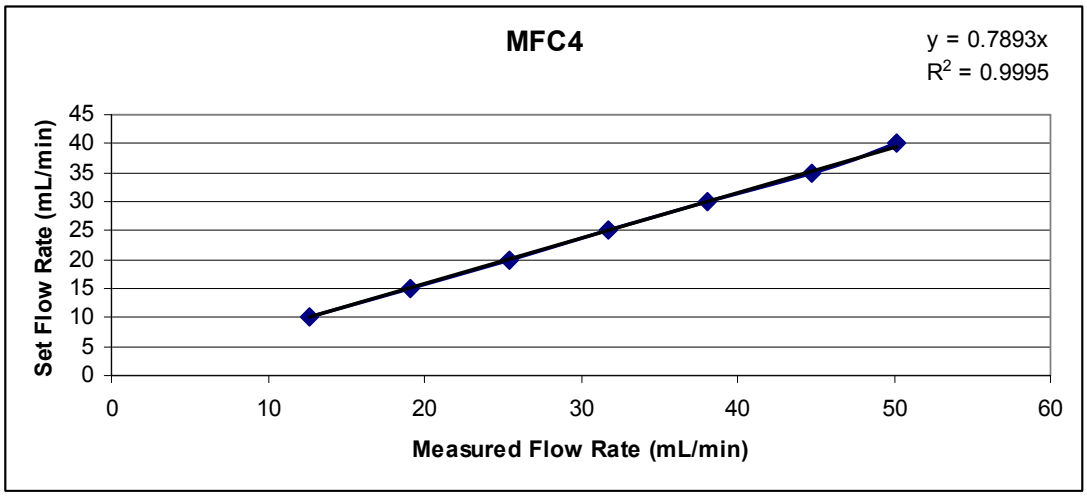

Figure C. 4 Calibration Graph for MFC4

Table C. 6 Calibration Data for MFC5

Set Flow Rate (ml/min)	Calibration Volume (mL)	Measured Time (sec)	Measured Time (min)	Measured Nitrogen Flow Rate (ml/min)
250	30	5.85	0.098	307.692
500	30	2.74	0.046	656.934
750	30	1.71	0.029	1052.632
1000	30	1.21	0.020	1487.603
1250	30	0.94	0.016	1914.894

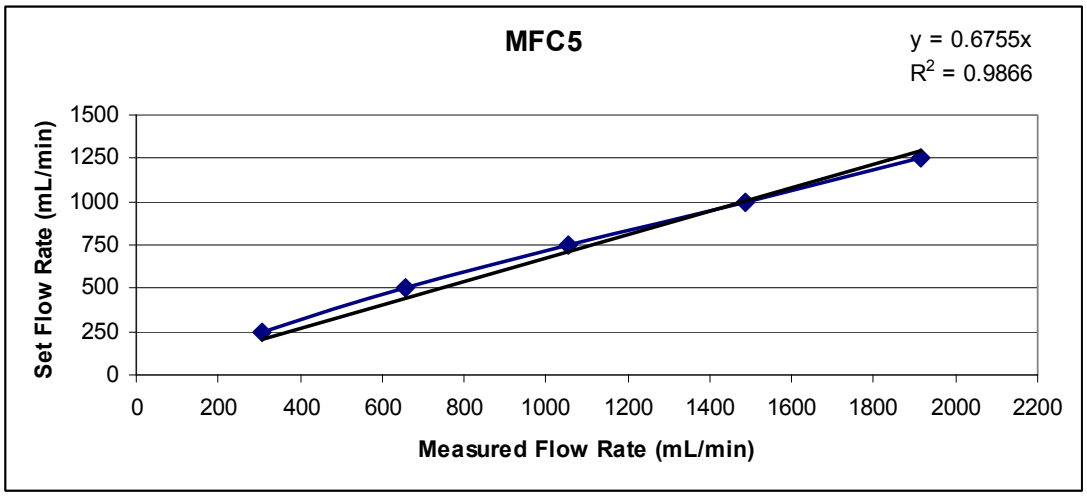

Figure C. 5 Calibration Graph for MFC5

The slope of the calibration graphs of the MFCs are taken as the calibration constants, given in Table C.7. These constants are used to determine the calibrated flow rate values of the theoretical flow rates of the gases from MFCs.

Table C. 7 Calibration Constants of MFCs

MFC	Calibration Constant
1	0.7552
2	0.7703
3	0.7308
4	0.7893
5	0.6755

Multiplying the theoretical flow rates with the calibration constants, the flow rates to be set for each cylinder are found as given in Table C.8 for the stoichiometric condition.

Table C. 8 Theoretical and Calibrated Flow Rates of Gases from Cylinders

Cylinder	Theoretical Flow Rate (mL/min)	Calibrated Flow Rate (mL/min)
1	320.52	241.99
2	8.52	6.56
3	568.30	414.86
4	21.92	17.29
5	1638.09	1105.71

C.2 Mass Spectrometer Calibrations

MS calibration data and graphs for C_3H_6, C_3H_8, H_2, NO and N_2 are given below for three different calibrations used in the analysis of the catalytic activity test data.

C.2.1 Mass Spectrometer Calibration-1

Table C. 9 MS Calibration-1 Data for C_3H_6

C_3H_6	
Concentration (ppm)	**MS Signal**
0	1.37E-10
24024	3.94E-09
48047	7.47E-09
72071	1.09E-08
96094	1.42E-08
120118	1.72E-08

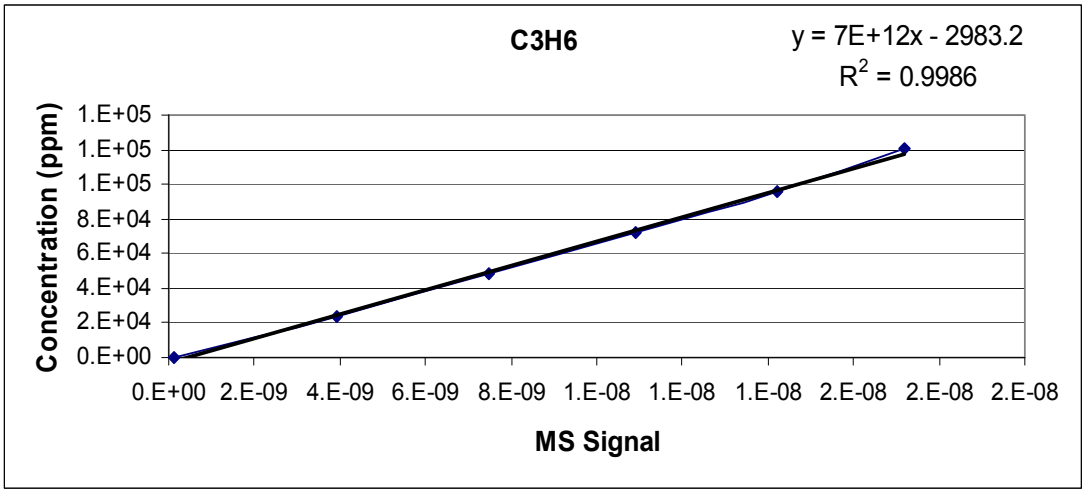

Figure C. 6 MS Calibration-1 Graph for C_3H_6

Table C. 10 MS Calibration-1 Data for C_3H_8

C_3H_8	
Concentration (ppm)	**MS Signal**
0	2.21E-09
24024	4.17E-09
48047	6.00E-09
72071	8.16E-09
96094	1.01E-08
120118	1.20E-08

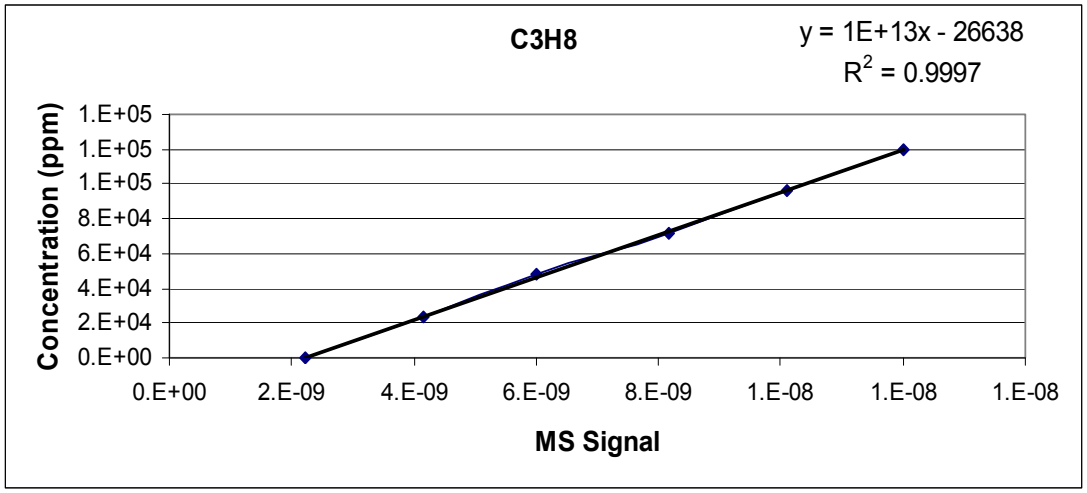

Figure C. 7 MS Calibration-1 Graph for C_3H_8

Table C. 11 MS Calibration-1 Data for H_2

H_2	
Concentration (ppm)	**MS Signal**
0	2.44E-09
24024	1.23E-08
48047	2.20E-08
72071	3.13E-08
96094	3.98E-08
120118	4.85E-08

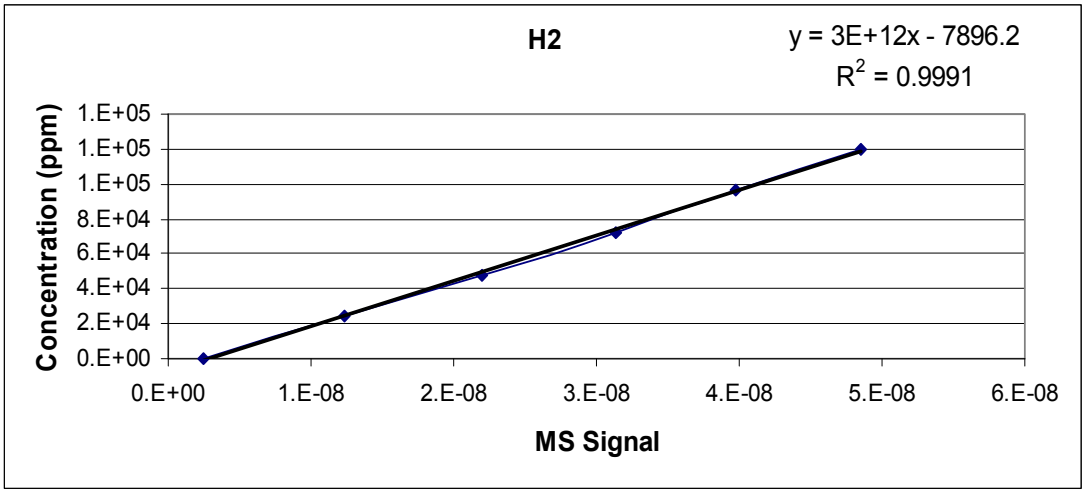

Figure C. 8 MS Calibration-1 Graph for H_2

Table C. 12 MS Calibration-1 Data for NO

NO	
Concentration (ppm)	**MS Signal**
0	2.78E-08
360	3.82E-08
720	5.14E-08
1080	6.48E-08
1440	7.80E-08
1800	9.13E-08

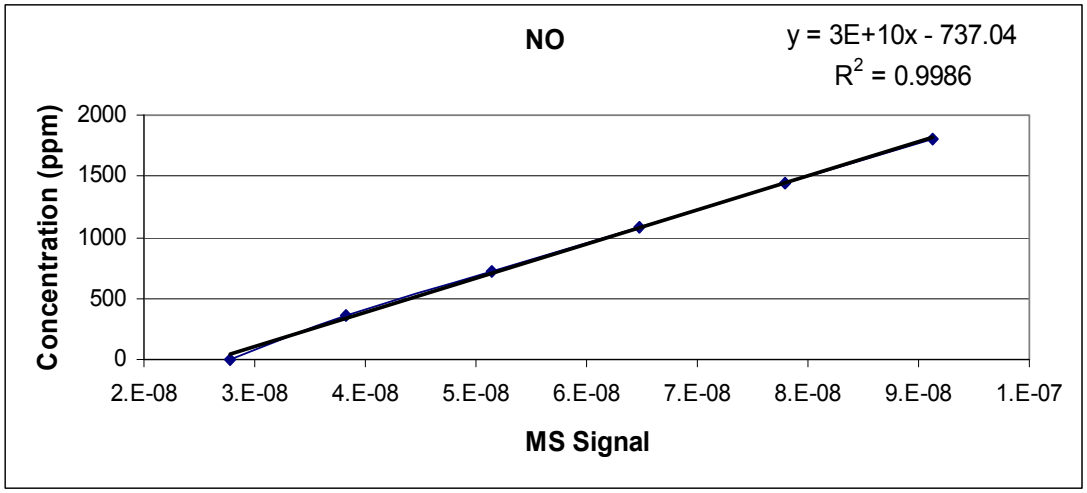

Figure C. 9 MS Calibration-1 Graph for NO

Table C. 13 MS Calibration-1 Data for O_2

O2	
Concentration (ppm)	**MS Signal**
0	1.70E-07
1842	2.21E-07
3684	2.70E-07
5527	3.30E-07
7369	3.70E-07
9211	4.20E-07

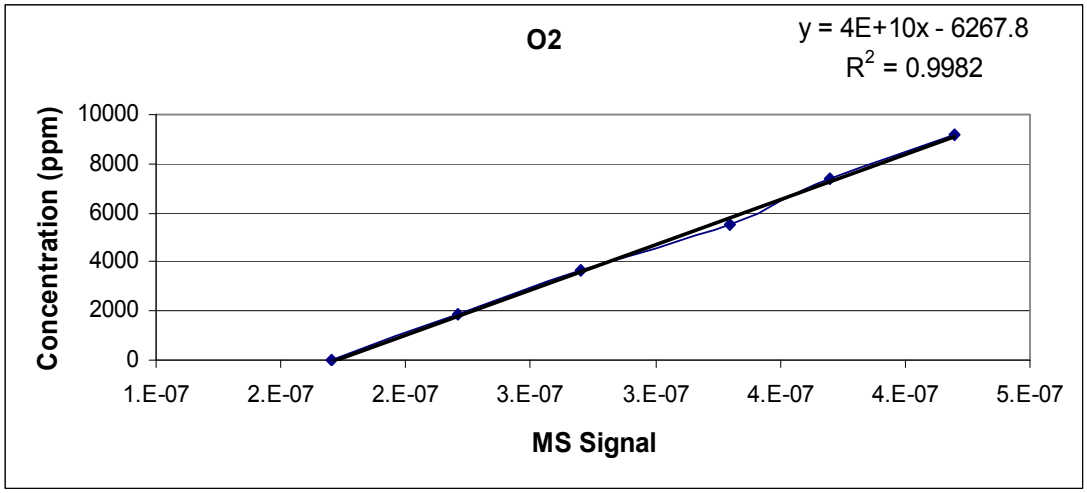

Figure C. 10 MS Calibration-1 Graph for O_2

Table C. 14 Calibration Equations for MS Calibration-1

Species	Calibration Equation
C_3H_6	7E+12x – 2983.2
C_3H_8	1E+13x – 26638
H_2	3E+12x – 7896.2
NO	3E+10x – 737.04
O_2	4E+10x – 6267.8

C.2.2 Mass Spectrometer Calibration-2

Table C. 15 MS Calibration-2 Data for C_3H_6

C_3H_6	
Concentration (ppm)	**MS Signal**
0	4.78E-12
89	3.32E-09
179	6.40E-09
268	9.20E-09
358	1.17E-08
447	1.40E-08

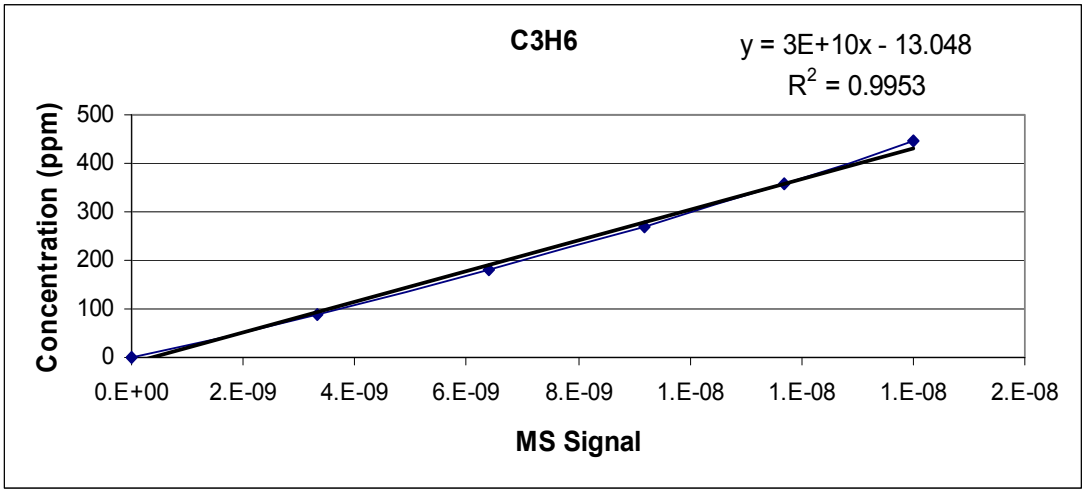

Figure C. 11 MS Calibration-2 Graph for C_3H_6

Table C. 16 MS Calibration-2 Data for C_3H_8

C_3H_8	
Concentration (ppm)	**MS Signal**
0	2.43E-09
30	3.58E-09
60	5.30E-09
89	6.90E-09
119	8.30E-09
149	9.70E-09

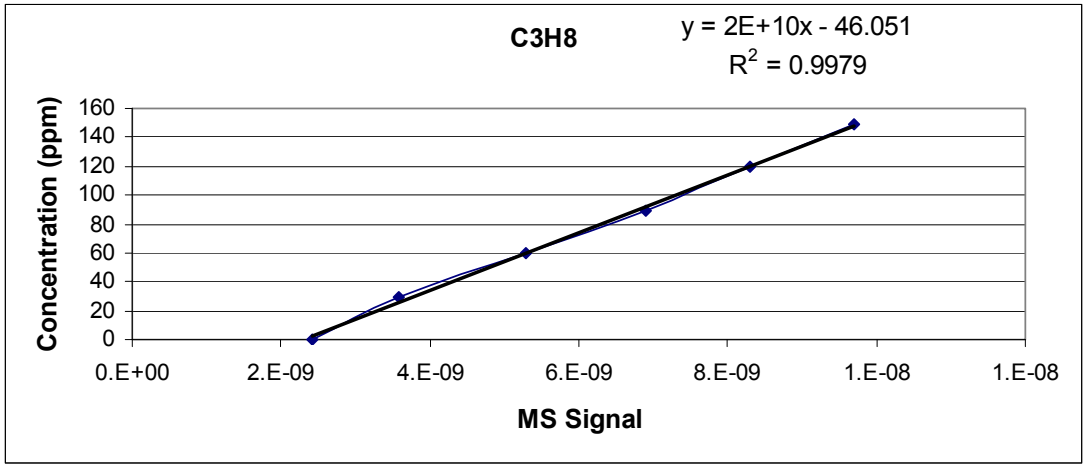

Figure C. 12 MS Calibration-2 Graph for C_3H_8

Table C. 17 MS Calibration-2 Data for H_2

H_2	
Concentration (ppm)	**MS Signal**
0	2.53E-09
553	1.25E-08
1106	2.20E-08
1658	3.10E-08
2211	3.93E-08
2764	4.80E-08

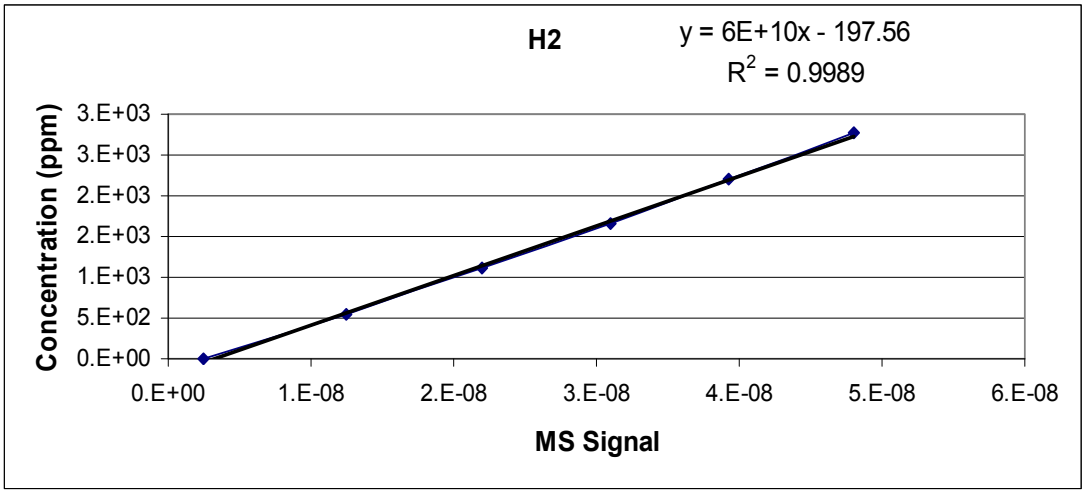

Figure C. 13 MS Calibration-2 Graph for H_2

Table C. 18 MS Calibration-2 Data for NO

NO	
Concentration (ppm)	**MS Signal**
0	1.45E-08
360	2.26E-08
720	3.30E-08
1080	4.30E-08
1440	5.38E-08
1800	6.12E-08

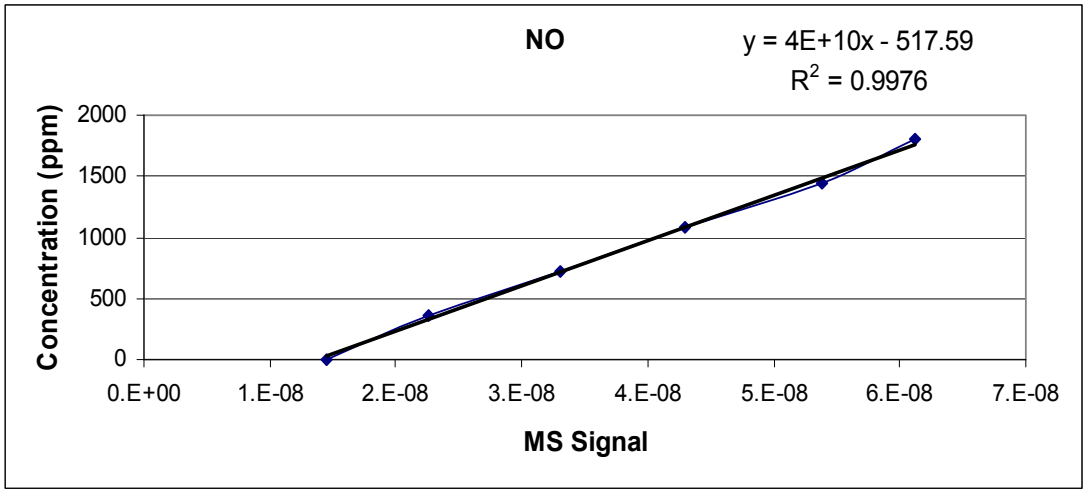

Figure C. 14 MS Calibration-2 Graph for NO

Table C. 19 MS Calibration-2 Data for O_2

O2	
Concentration (ppm)	**MS Signal**
0	3.00E-08
1842	6.00E-08
3684	1.00E-07
5526	1.40E-07
7369	1.80E-07
9211	2.20E-07

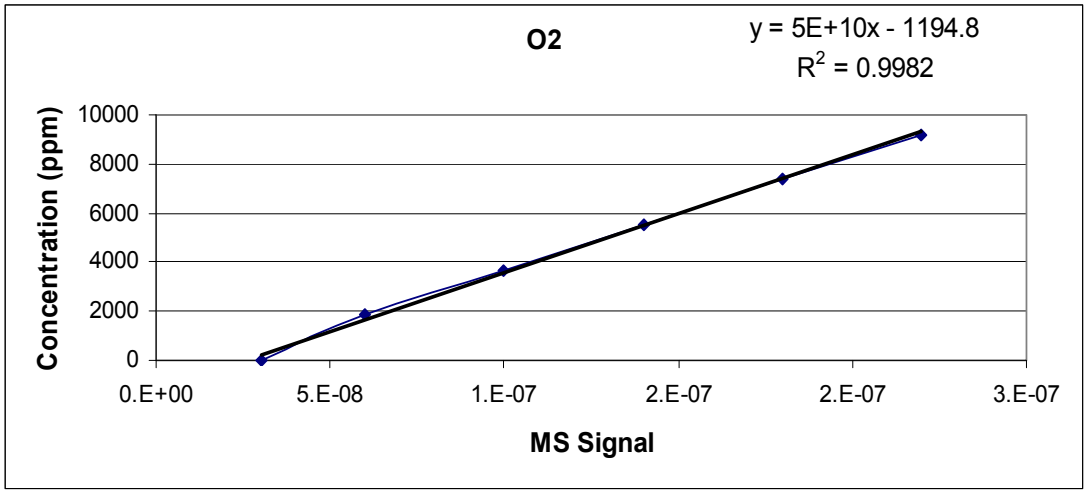

Figure C. 15 MS Calibration-2 Graph for O_2

Table C. 20 Calibration Equations for MS Calibration-2

Species	Calibration Equation
C_3H_6	3E+10x – 13.048
C_3H_8	2E+10x – 46.051
H_2	6E+10x – 197.56
NO	4E+10x – 517.59
O_2	5E+10x – 1194.8

C.2.3 Mass Spectrometer Calibration-3

Table C. 21 MS Calibration-3 Data for C_3H_6

C_3H_6	
Concentration (ppm)	**MS Signal**
0	3.06E-10
89	3.64E-09
179	6.84E-09
268	9.66E-09
358	1.22E-08
447	1.46E-08

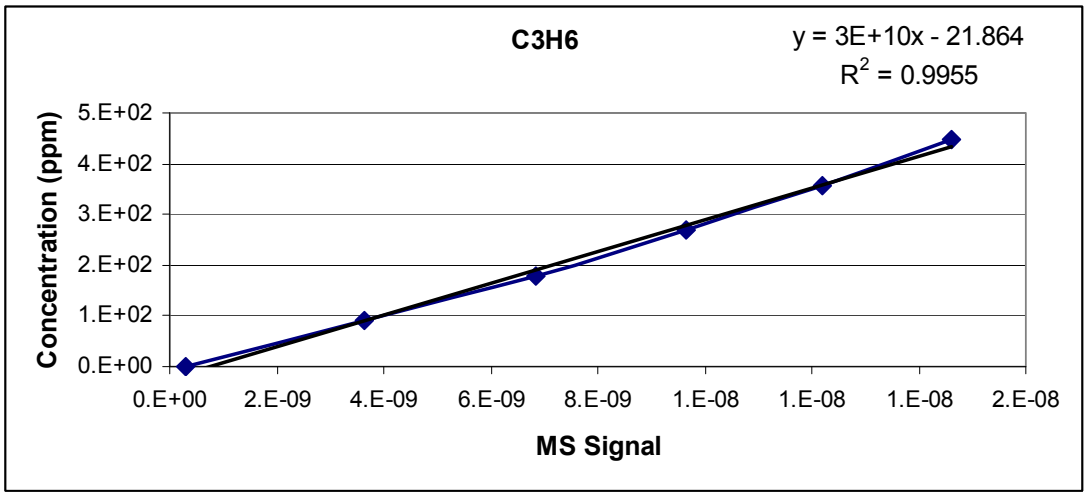

Figure C. 16 MS Calibration-3 Graph for C_3H_6

Table C. 22 MS Calibration-3 Data for C_3H_8

C_3H_8	
Concentration (ppm)	**MS Signal**
0	3.14E-09
30	5.00E-09
60	6.80E-09
89	8.17E-09
119	9.55E-09
149	1.07E-08

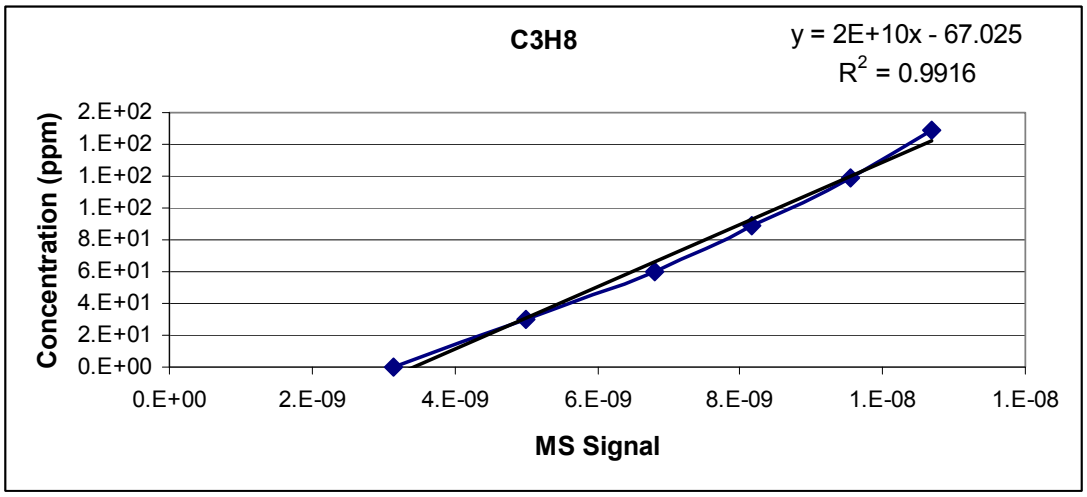

Figure C. 17 MS Calibration-3 Graph for C_3H_8

Table C. 23 MS Calibration-3 Data for H_2

H_2	
Concentration (ppm)	**MS Signal**
0	2.80E-09
553	9.40E-09
1106	1.58E-08
1658	2.22E-08
2211	2.84E-08
2764	3.46E-08

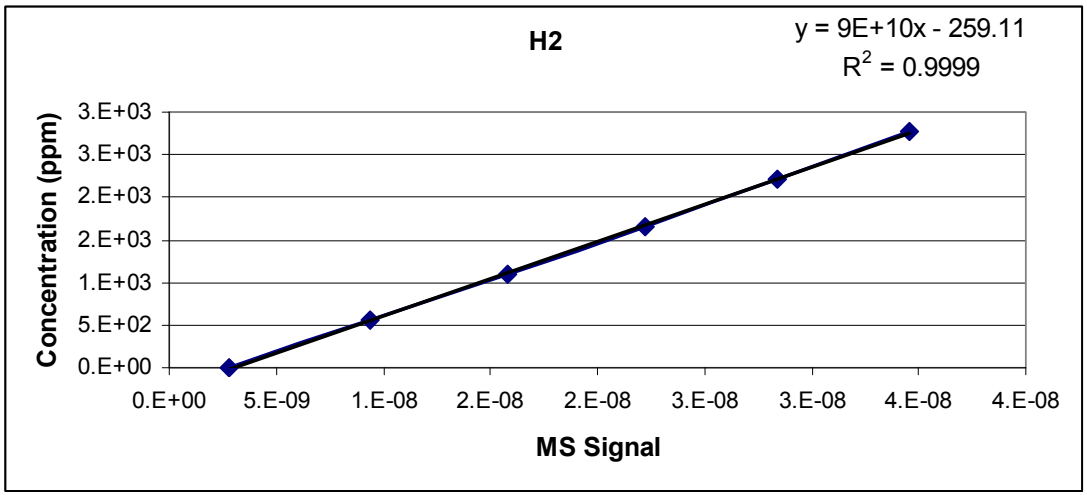

Figure C. 18 MS Calibration-3 Graph for H_2

Table C. 24 MS Calibration-3 Data for NO

NO	
Concentration (ppm)	**MS Signal**
0	1.34E-08
360	2.12E-08
720	3.14E-08
1080	4.23E-08
1440	5.20E-08
1800	6.20E-08

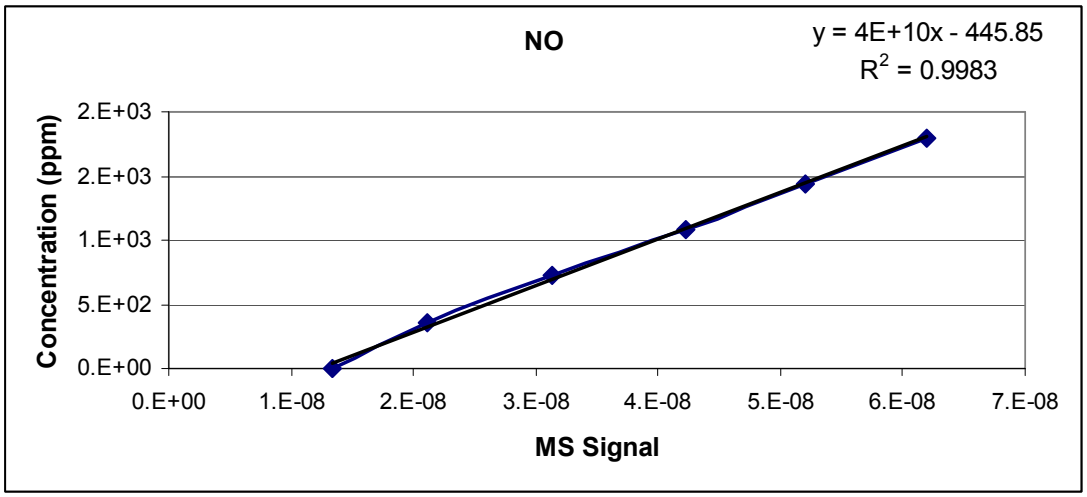

Figure C. 19 MS Calibration-3 Graph for NO

Table C. 25 MS Calibration-3 Data for O_2

O2	
Concentration (ppm)	**MS Signal**
0	2.80E-08
1842	6.20E-08
3684	1.00E-07
5526	1.33E-07
7369	1.75E-07
9211	2.08E-07

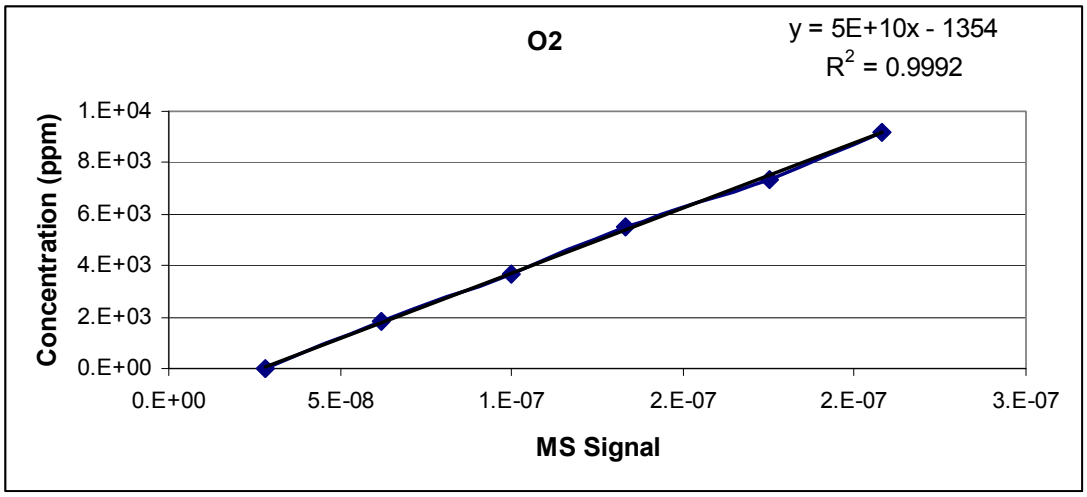

Figure C. 20 MS Calibration-3 Graph for O_2

Table C. 26 Calibration Equations for MS Calibration-3

Species	Calibration Equation
C_3H_6	3E+10x – 21.864
C_3H_8	2E+10x – 67.025
H_2	9E+10x – 259.11
NO	4E+10x – 445.85
O_2	5E+10x – 1354

APPENDIX D

CATALYTIC ACTIVITY TEST RESULTS

D.1 Results of Catalytic Activity Tests to Determine the Effect of Exposure to SO_2 during Catalytic Activity Tests

D.1.1 CZO-CI+AO-(1) Monolithic Catalyst

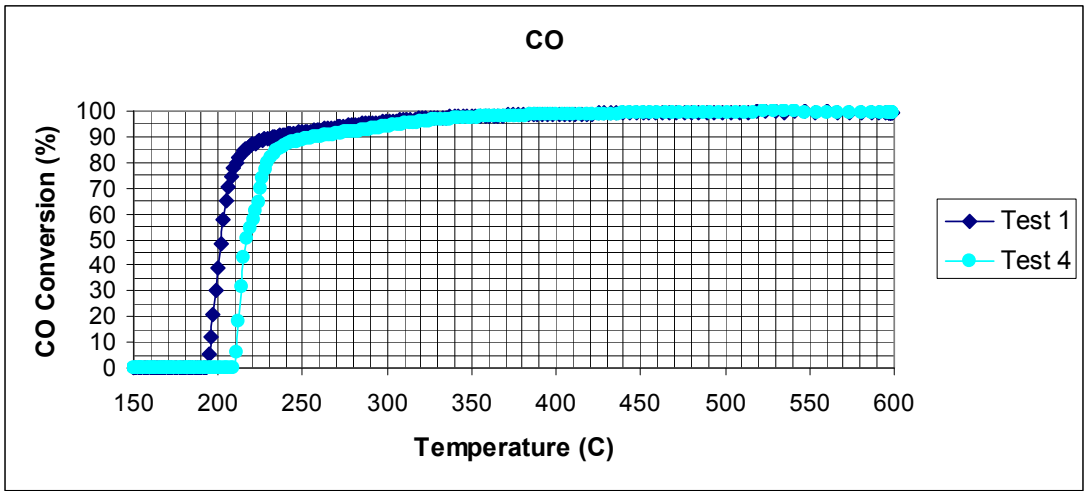

Figure D. 1 CO Catalytic Activity of CZO-CI+AO-(1) Monolithic Catalyst During Tests 1 & 4

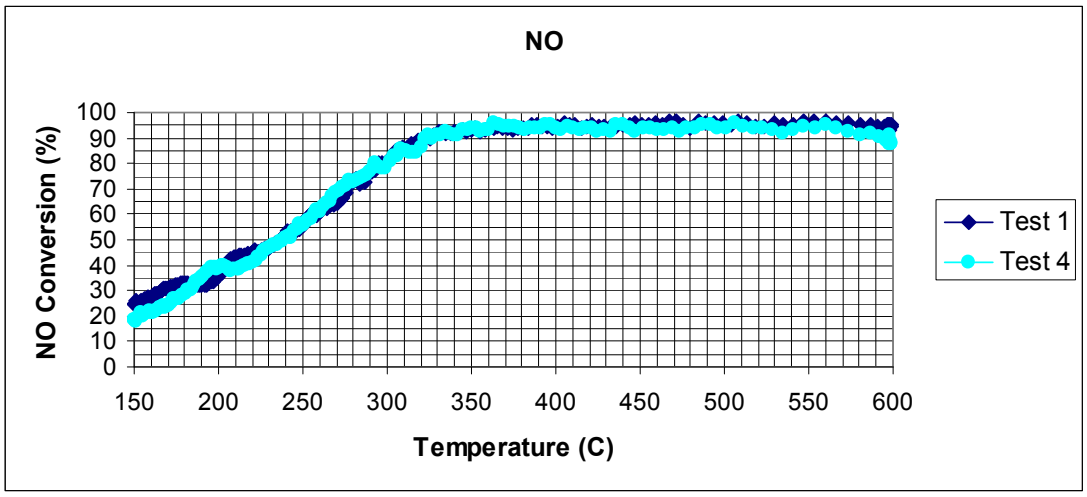

Figure D. 2 NO Catalytic Activity of CZO-CI+AO-(1) Monolithic Catalyst During Tests 1 & 4

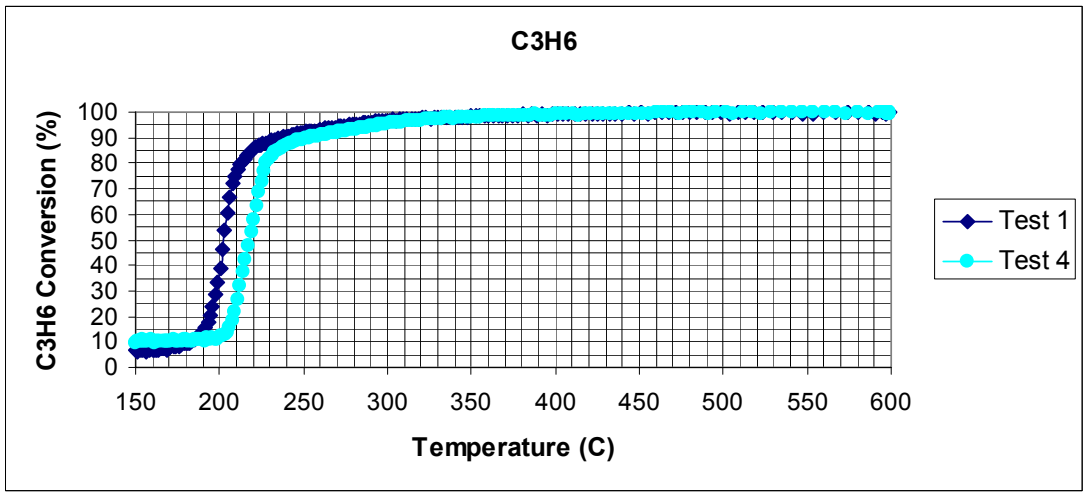

Figure D. 3 C_3H_6 Catalytic Activity of CZO-CI+AO-(1) Monolithic Catalyst During Tests 1 & 4

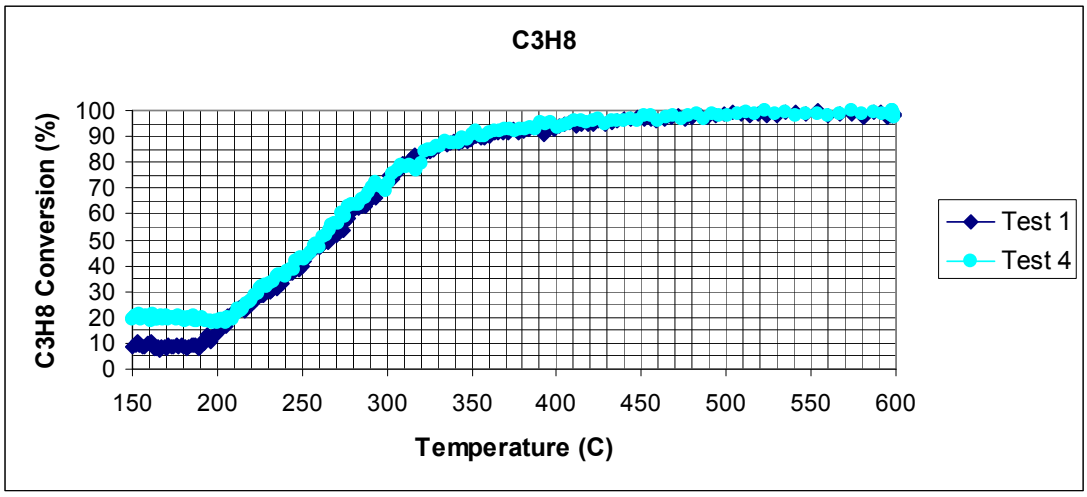

Figure D. 4 C_3H_8 Catalytic Activity of CZO-CI+AO-(1) Monolithic Catalyst During Tests 1 & 4

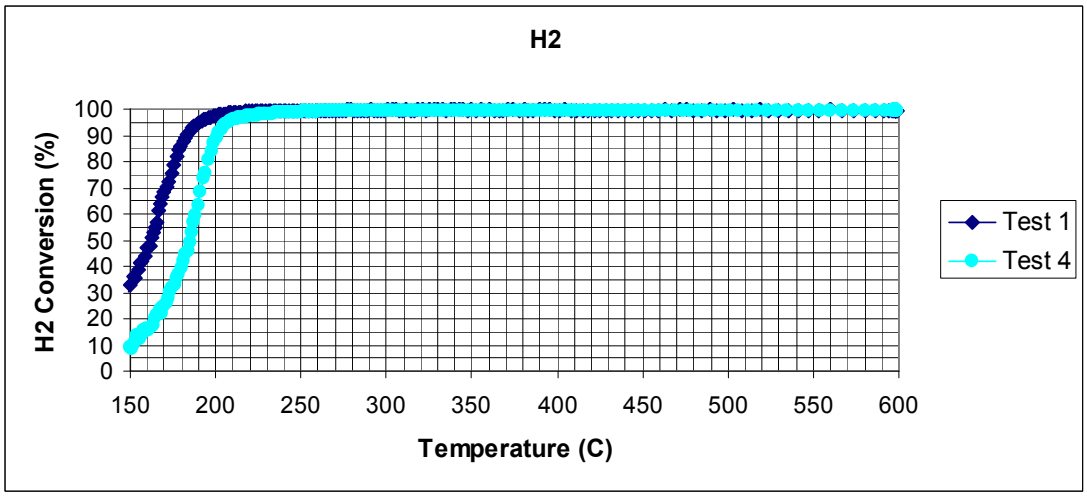

Figure D. 5 H_2 Catalytic Activity of CZO-CI+AO-(1) Monolithic Catalyst During Tests 1 & 4

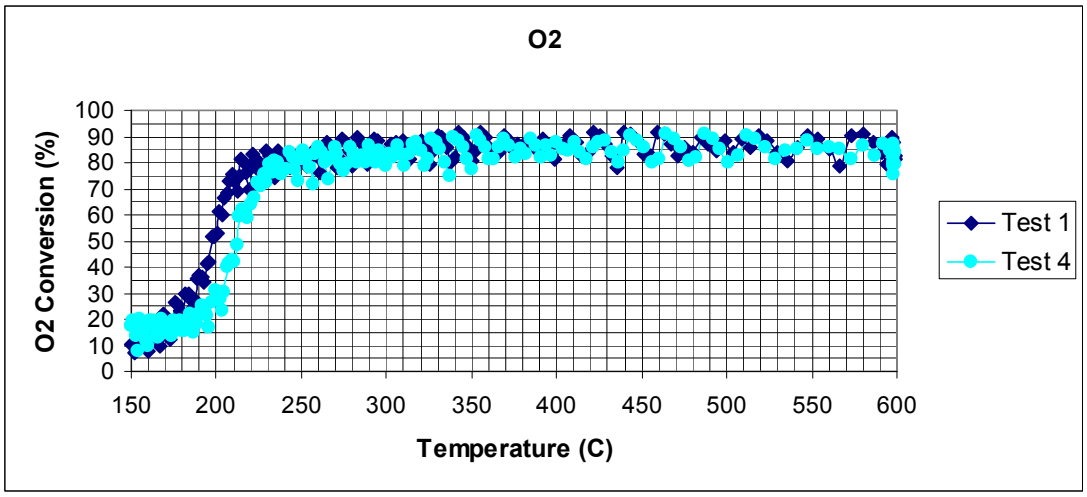

Figure D. 6 O_2 Catalytic Activity of CZO-CI+AO-(1) Monolithic Catalyst During Tests 1 & 4

D.1.2 CZAO-S-(1) Monolithic Catalyst

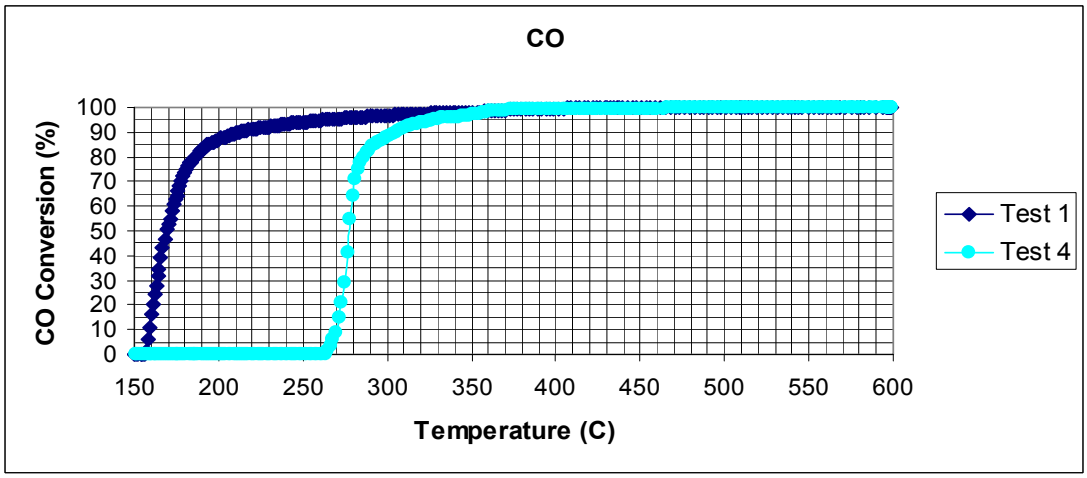

Figure D. 7 CO Catalytic Activity of CZAO-S-(1) Monolithic Catalyst During Tests 1 & 4

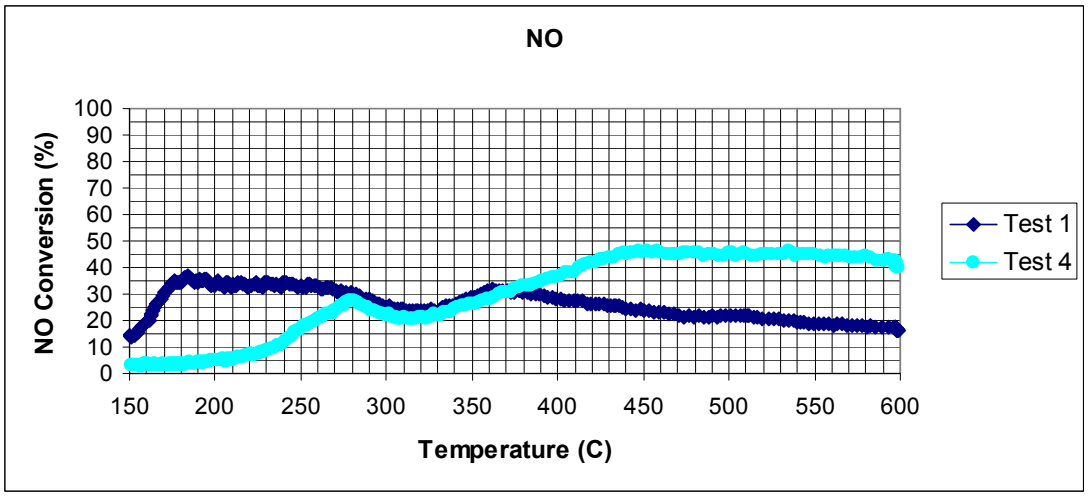

Figure D. 8 NO Catalytic Activity of CZAO-S-(1) Monolithic Catalyst During Tests 1 & 4

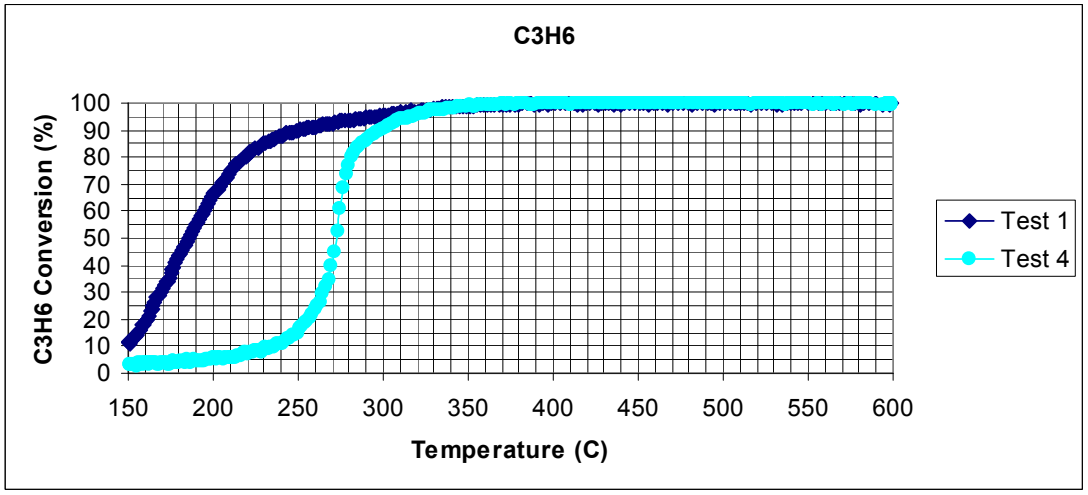

Figure D. 9 C_3H_6 Catalytic Activity of CZAO-S-(1) Monolithic Catalyst During Tests 1 & 4

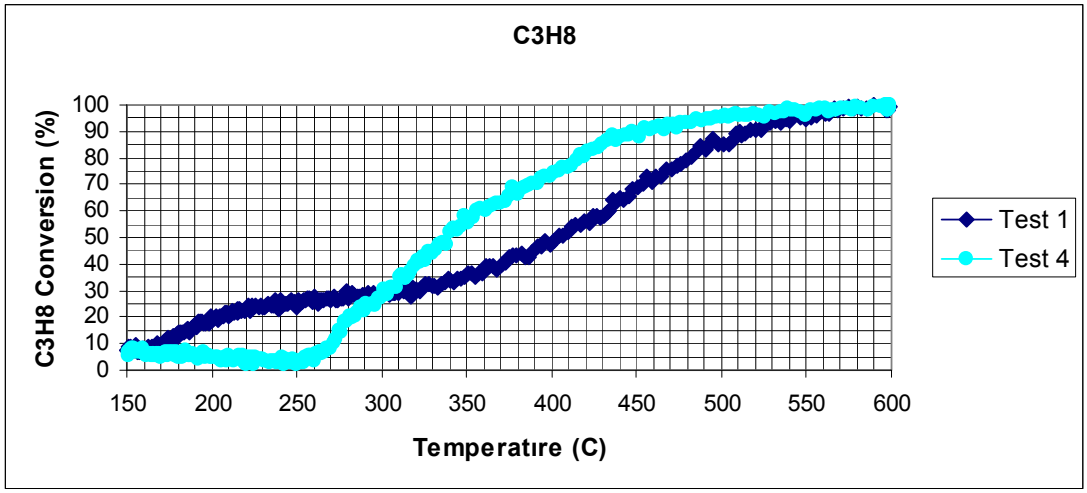

Figure D. 10 C_3H_8 Catalytic Activity of CZAO-S-(1) Monolithic Catalyst During Tests 1 & 4

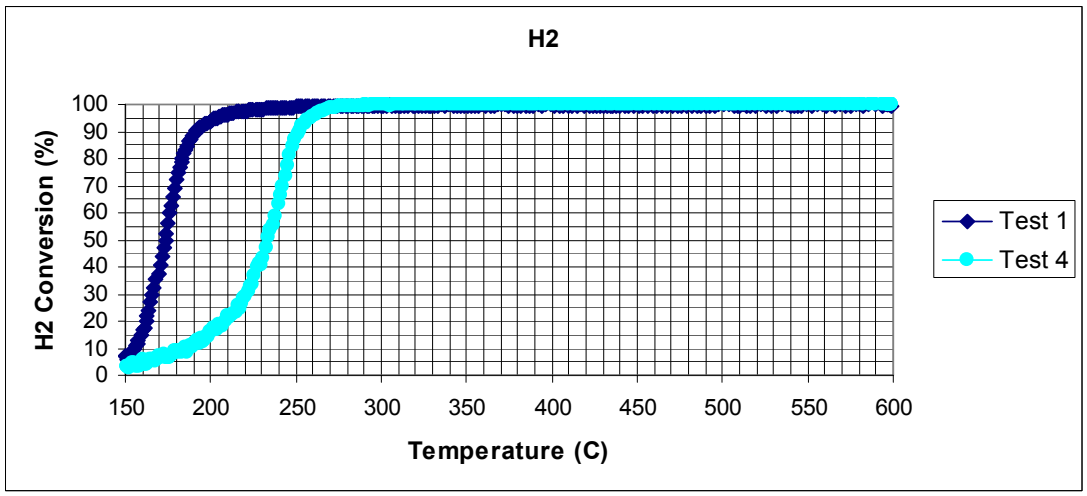

Figure D. 11 H_2 Catalytic Activity of CZAO-S-(1) Monolithic Catalyst During Tests 1 & 4

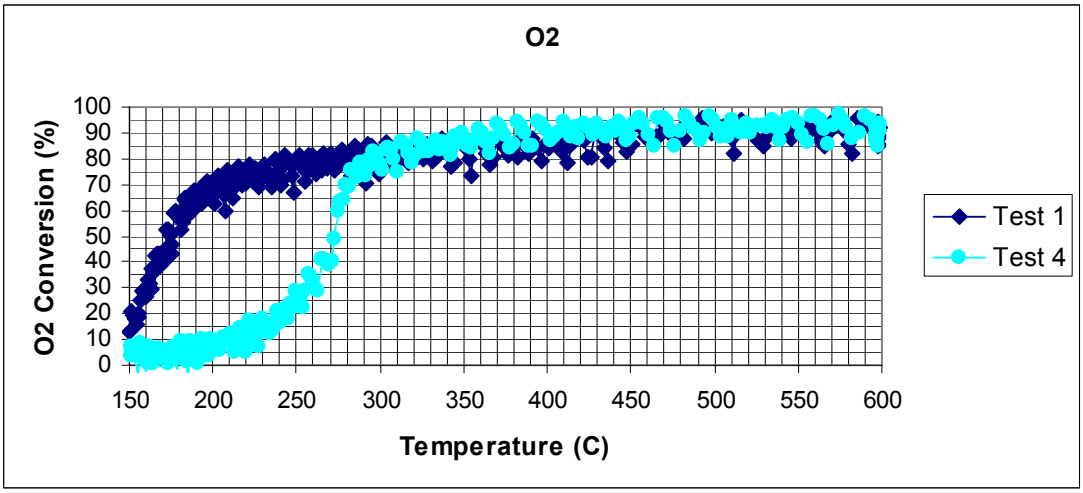

Figure D. 12 O_2 Catalytic Activity of CZAO-S-(1) Monolithic Catalyst During Tests 1 & 4

D.1.3 CZAO-Cl-(1) Monolithic Catalyst

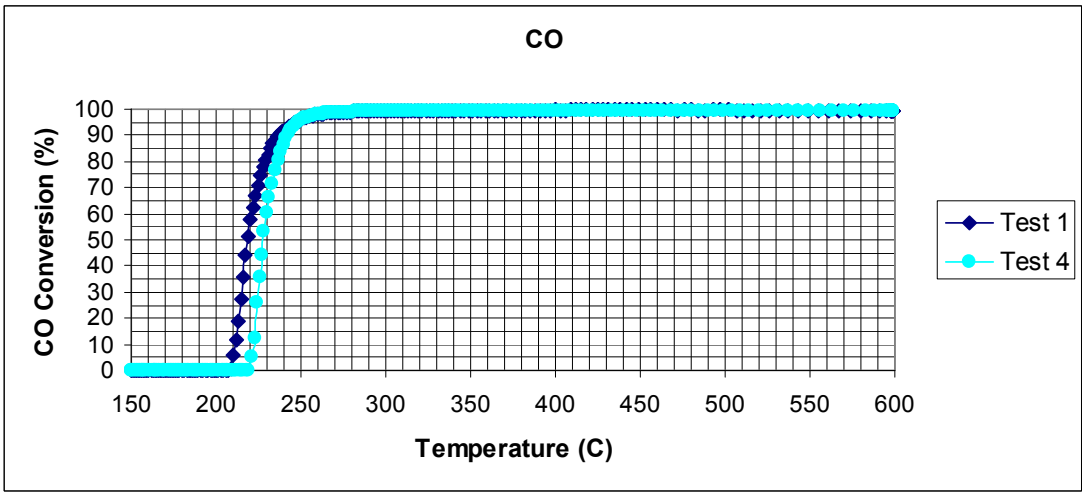

Figure D. 13 CO Catalytic Activity of CZAO-Cl-(1) Monolithic Catalyst During Tests 1 & 4

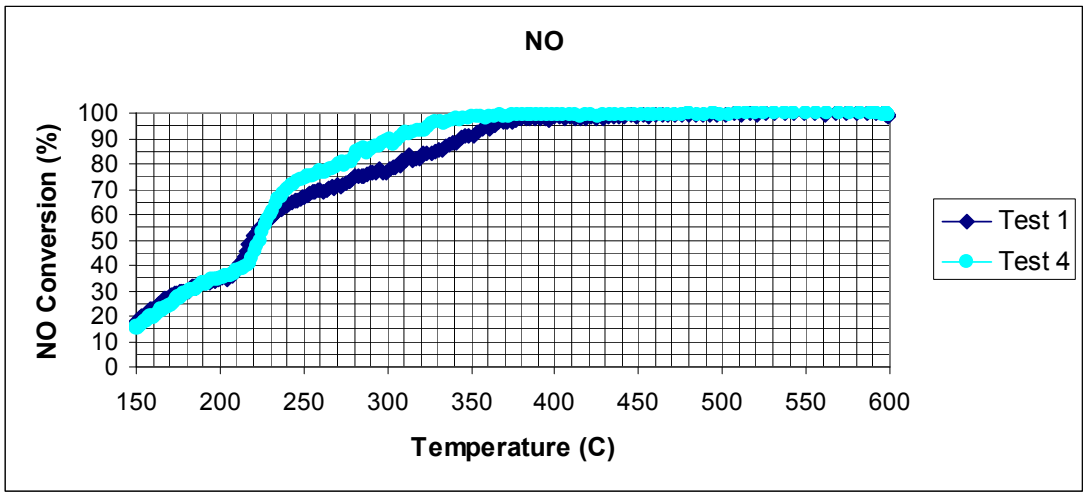

Figure D. 14 NO Catalytic Activity of CZAO-CI-(1) Monolithic Catalyst During Tests 1 & 4

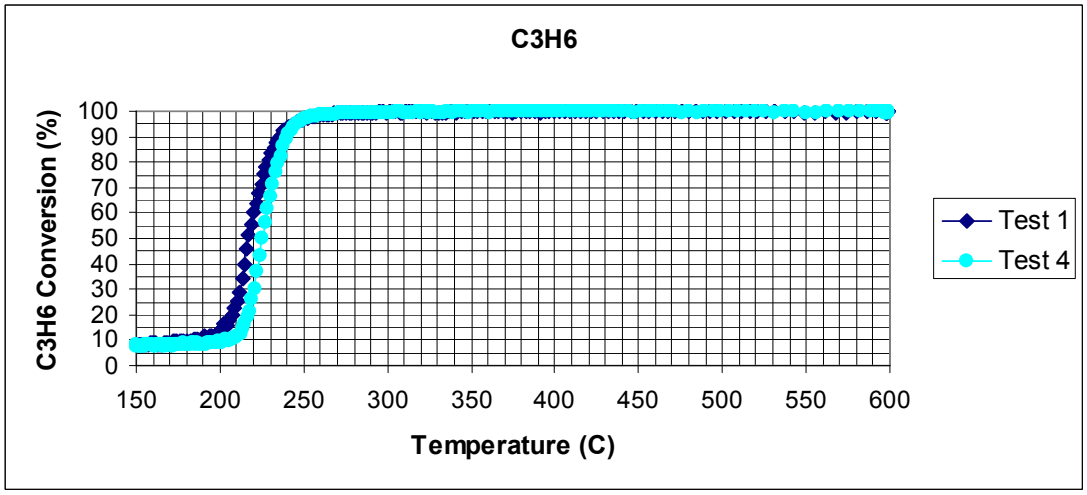

Figure D. 15 C_3H_6 Catalytic Activity of CZAO-CI-(1) Monolithic Catalyst During Tests 1 & 4

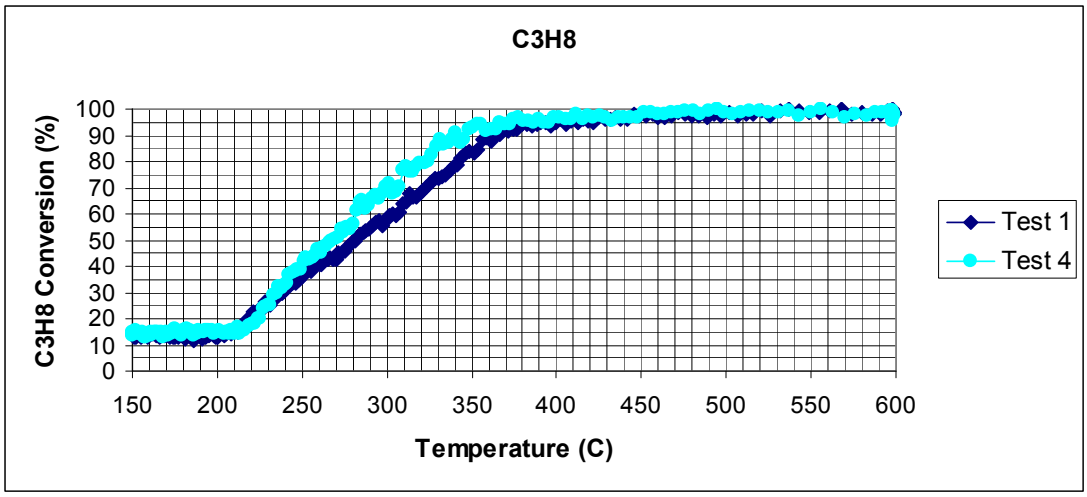

Figure D. 16 C_3H_8 Catalytic Activity of CZAO-CI-(1) Monolithic Catalyst During Tests 1 & 4

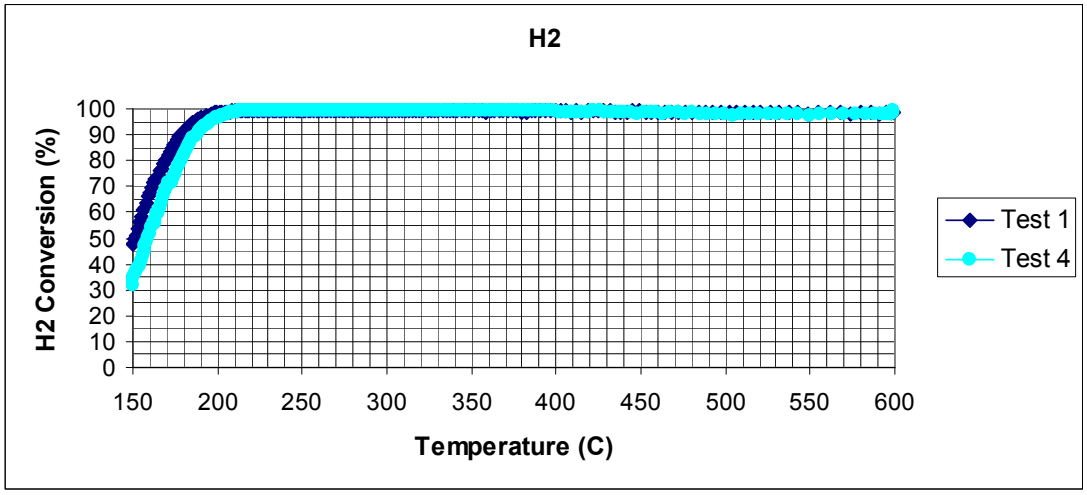

Figure D. 17 H_2 Catalytic Activity of CZAO-CI-(1) Monolithic Catalyst During Tests 1 & 4

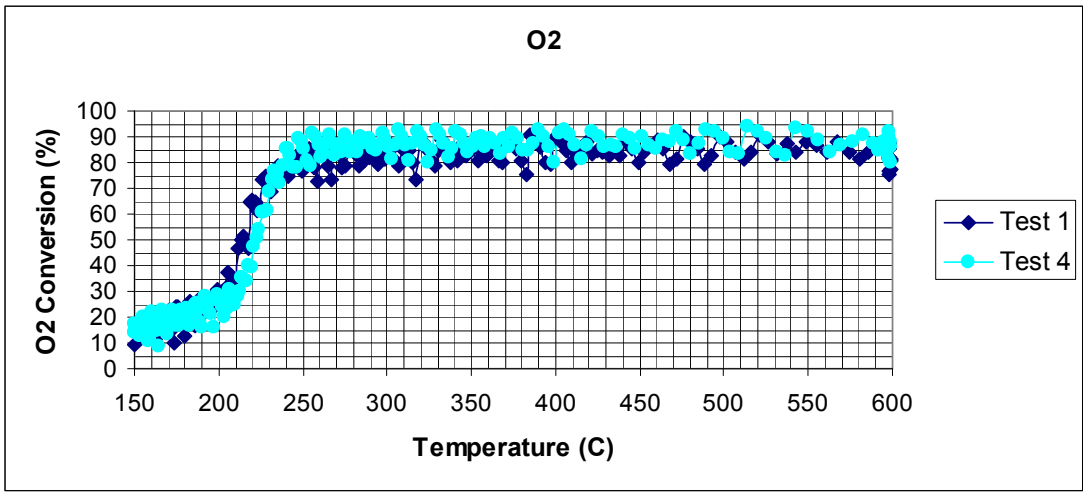

Figure D. 18 O_2 Catalytic Activity of CZAO-Cl-(1) Monolithic Catalyst During Tests 1 & 4

D.1.4 COM-M3 Monolithic Catalyst

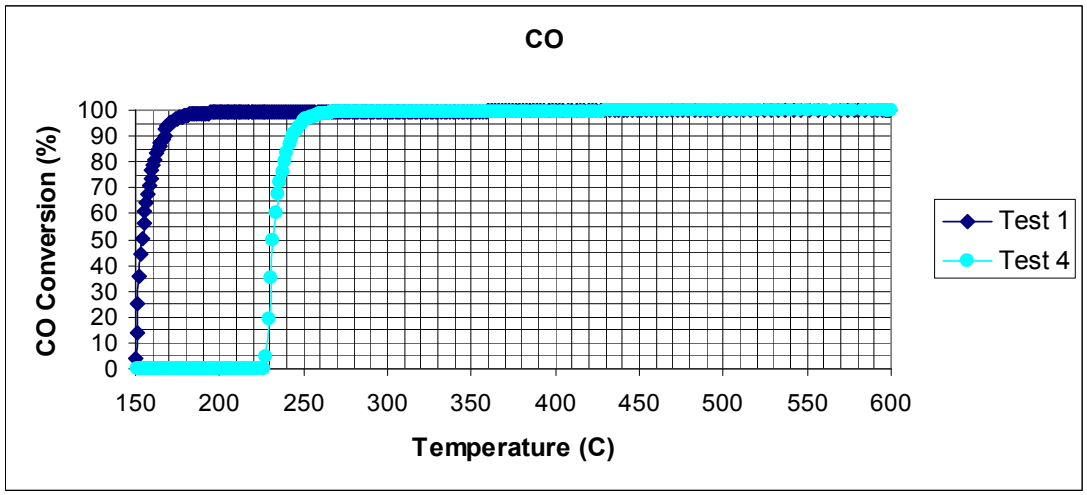

Figure D. 19 CO Catalytic Activity of COM-M3 Monolithic Catalyst During Tests 1 & 4

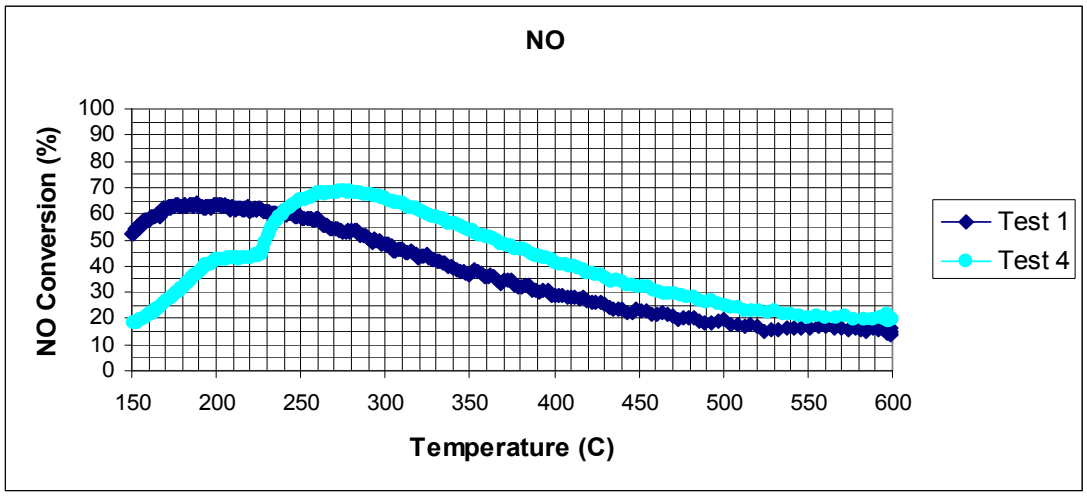

Figure D. 20 NO Catalytic Activity of COM-M3 Monolithic Catalyst During Tests 1 & 4

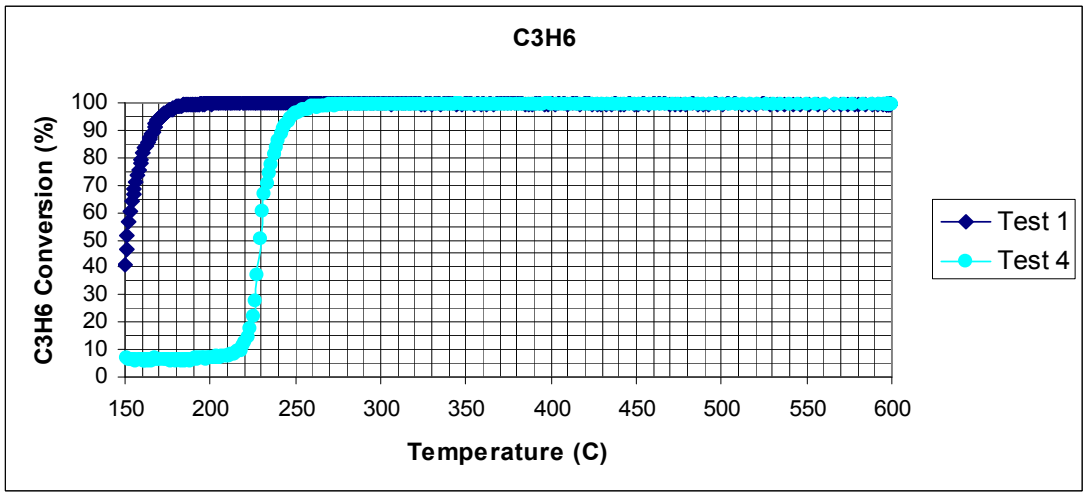

Figure D. 21 C_3H_6 Catalytic Activity of COM-M3 Monolithic Catalyst During Tests 1 & 4

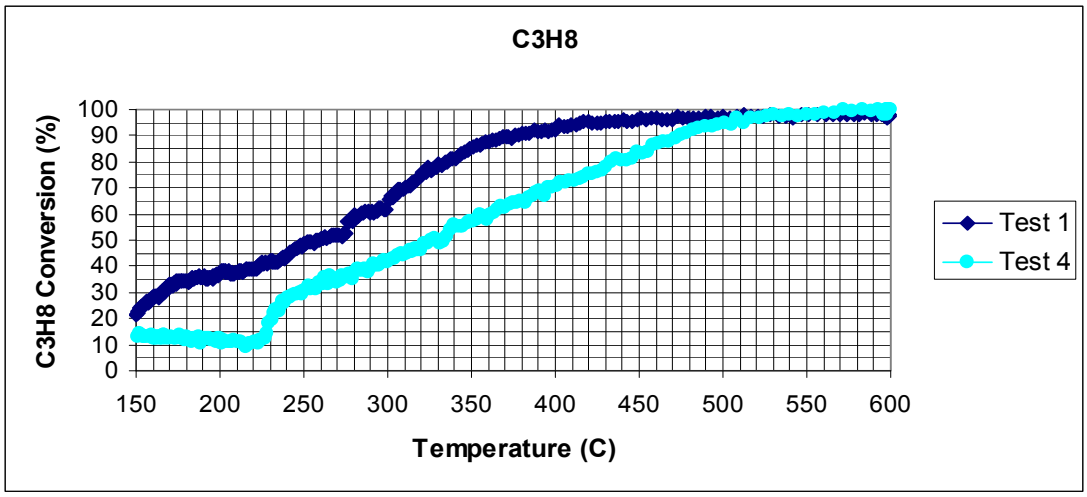

Figure D. 22 C_3H_8 Catalytic Activity of COM-M3 Monolithic Catalyst During Tests 1 & 4

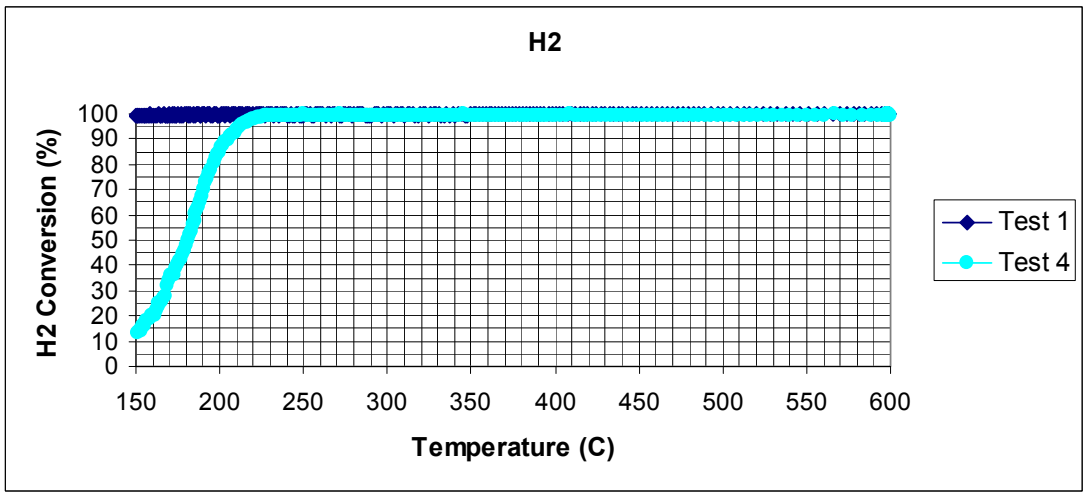

Figure D. 23 H_2 Catalytic Activity of COM-M3 Monolithic Catalyst During Tests 1 & 4

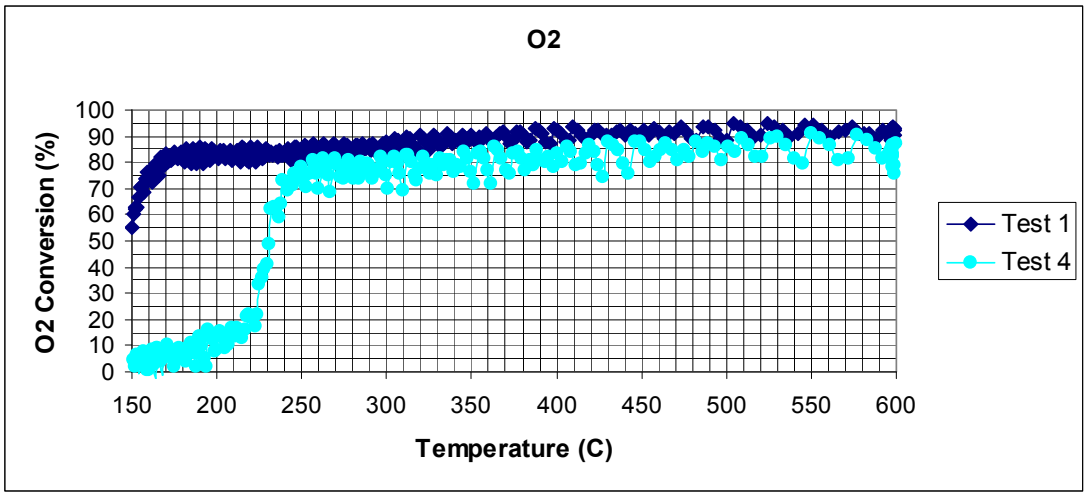

Figure D. 24 O_2 Catalytic Activity of COM-M3 Monolithic Catalyst During Tests 1 & 4

D.2 Results of Catalytic Activity Tests to Determine the Effect of Thermal Aging

D.2.1 CZAO-CI-(2) Monolithic Catalyst

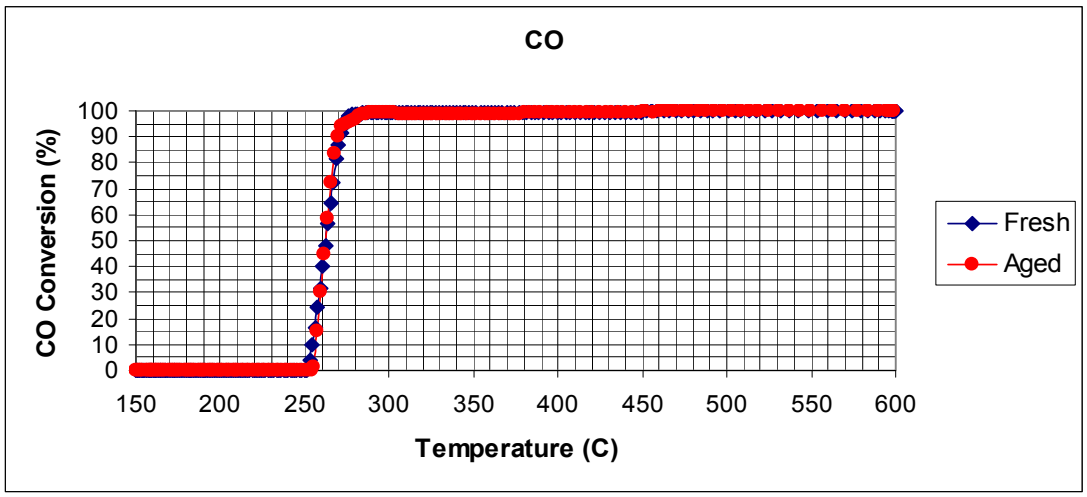

Figure D. 25 CO Catalytic Activity of Fresh and Aged (900 ºC) CZAO-CI-(2) Monolithic Catalyst

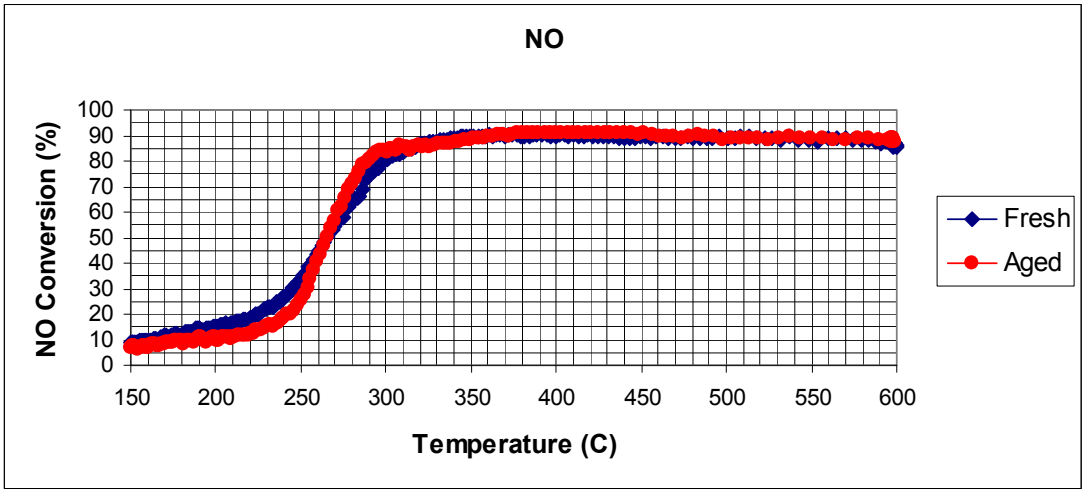

Figure D. 26 NO Catalytic Activity of Fresh and Aged (900 ºC) CZAO-CI-(2) Monolithic Catalyst

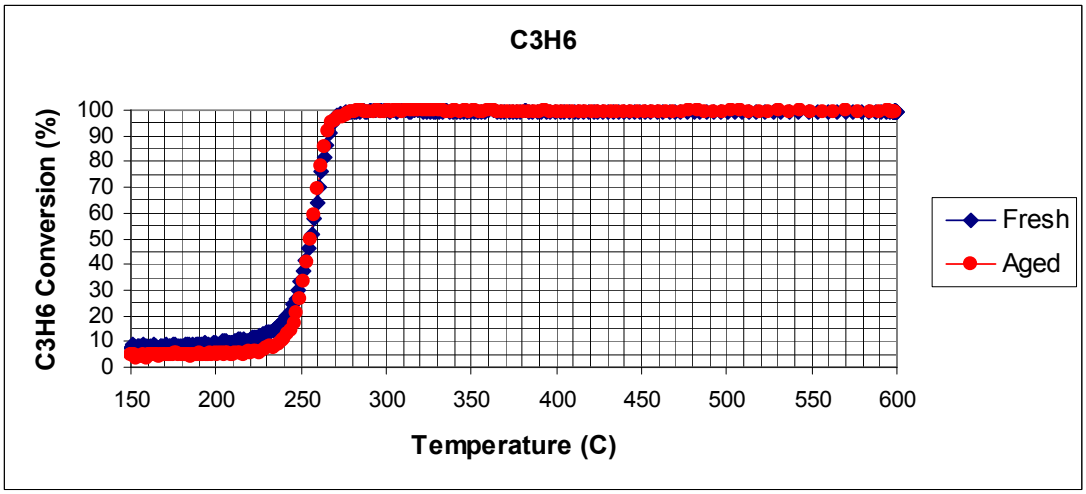

Figure D. 27 C_3H_6 Catalytic Activity of Fresh and Aged (900 ºC) CZAO-CI-(2) Monolithic Catalyst

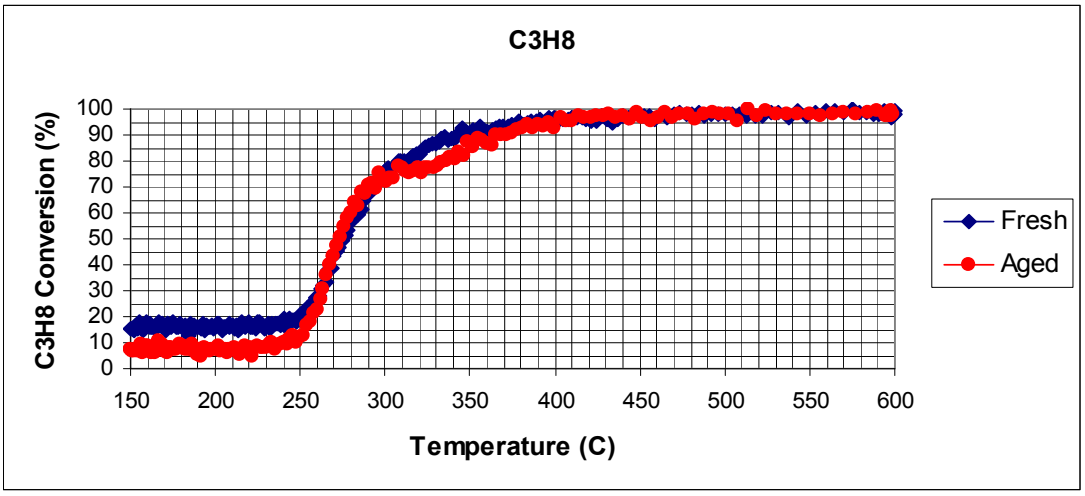

Figure D. 28 C_3H_8 Catalytic Activity of Fresh and Aged (900 ºC) CZAO-CI-(2) Monolithic Catalyst

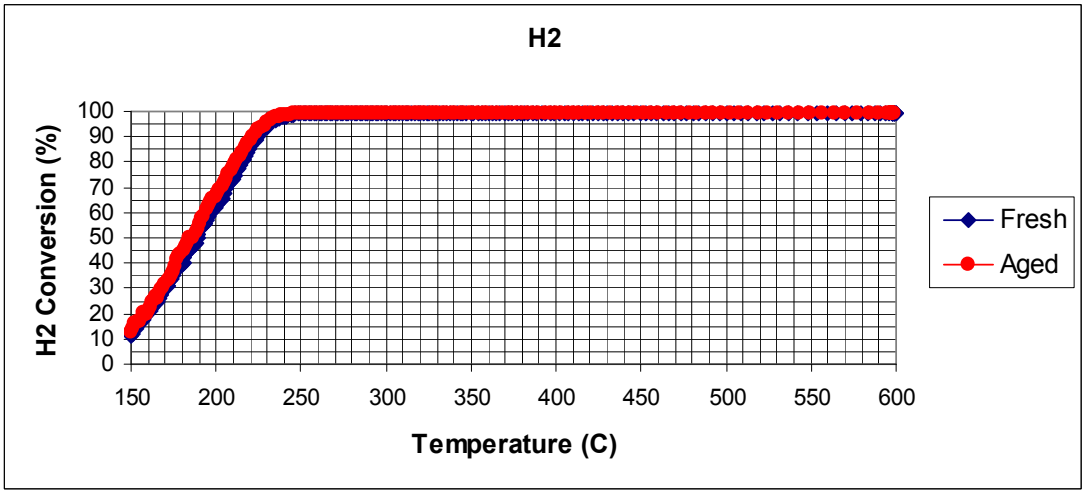

Figure D. 29 H_2 Catalytic Activity of Fresh and Aged (900 ºC) CZAO-CI-(2) Monolithic Catalyst

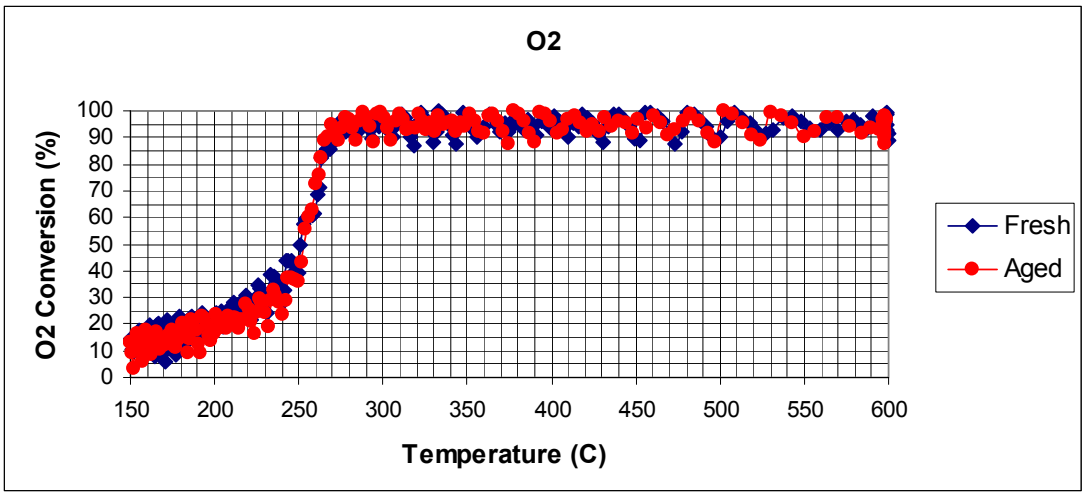

Figure D. 30 O_2 Catalytic Activity of Fresh and Aged (900 ºC) CZAO-CI-(2) Monolithic Catalyst

D.2.2 CZO-CI+AO-(2)-M1 Monolithic Catalyst

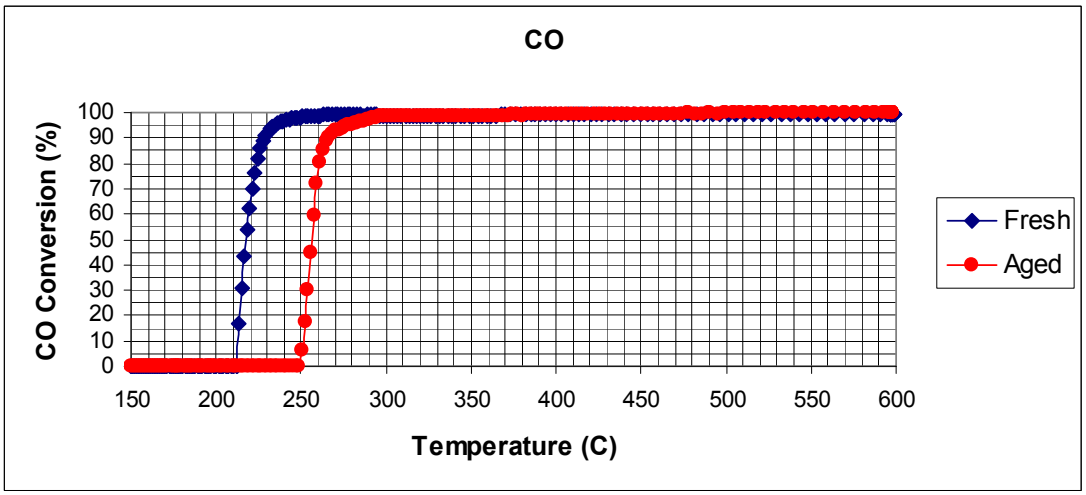

Figure D. 31 CO Catalytic Activity of Fresh and Aged (900 ºC) CZO-CI+AO-(2)-M1 Monolithic Catalyst

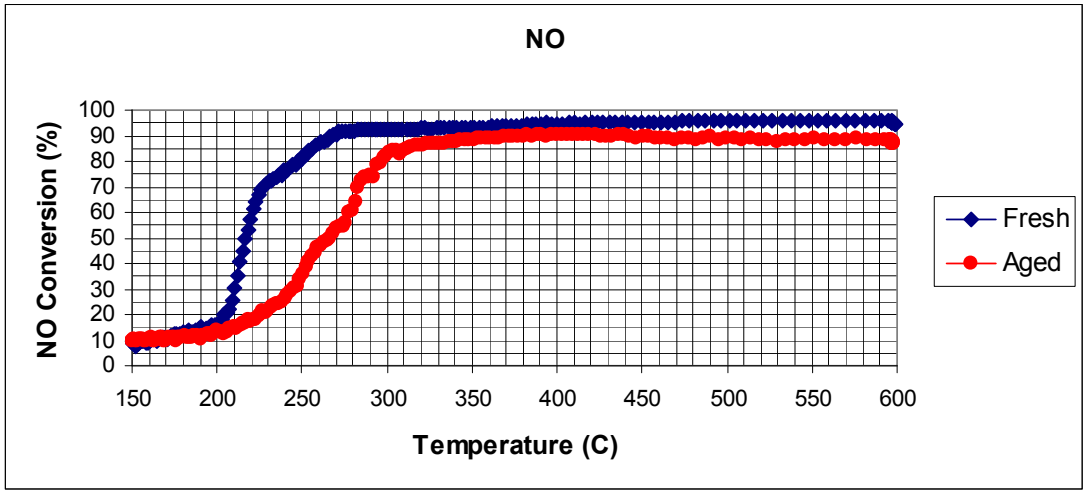

Figure D. 32 NO Catalytic Activity of Fresh and Aged (900 ºC) CZO-CI+AO-(2)-M1 Monolithic Catalyst

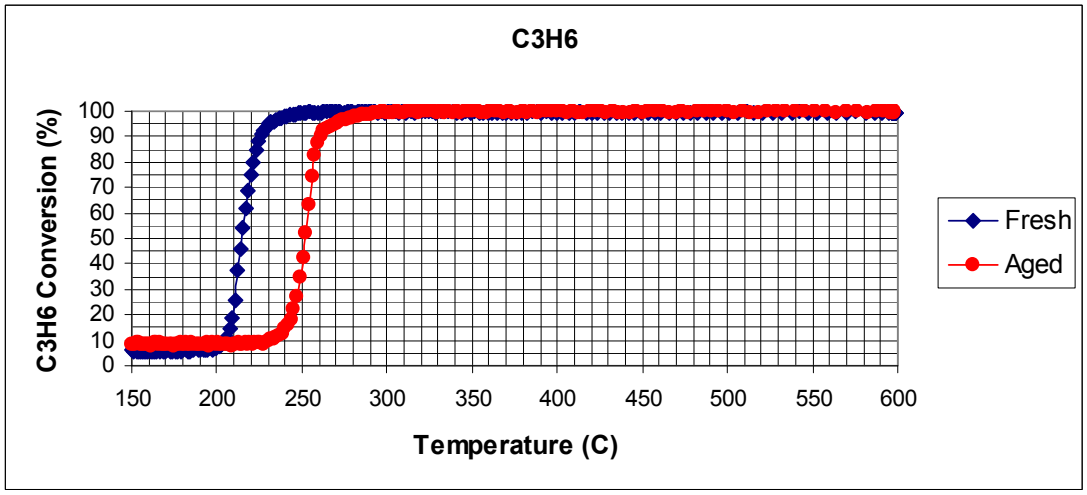

Figure D. 33 C_3H_6 Catalytic Activity of Fresh and Aged (900 ºC) CZO-CI+AO-(2)-M1 Monolithic Catalyst

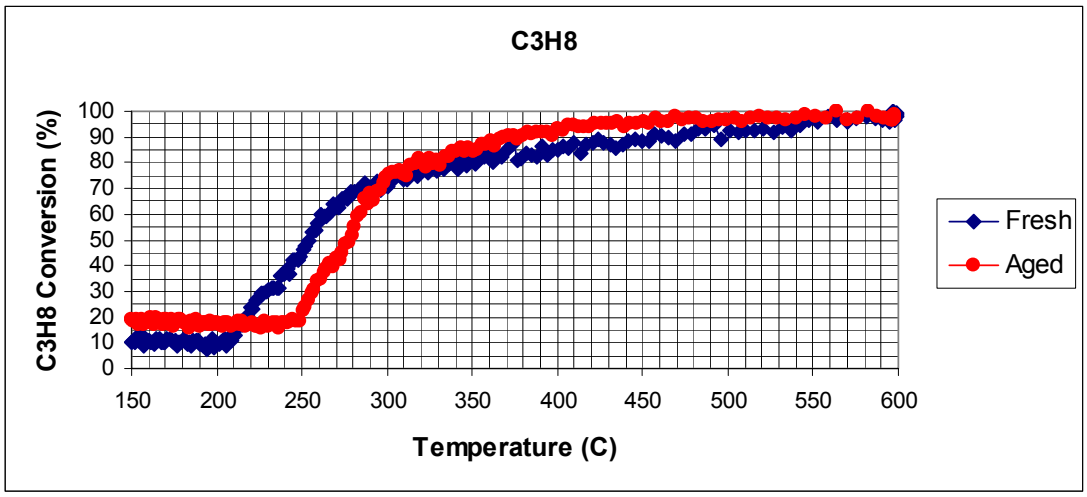

Figure D. 34 C_3H_8 Catalytic Activity of Fresh and Aged (900 ºC) CZO-CI+AO-(2)-M1 Monolithic Catalyst

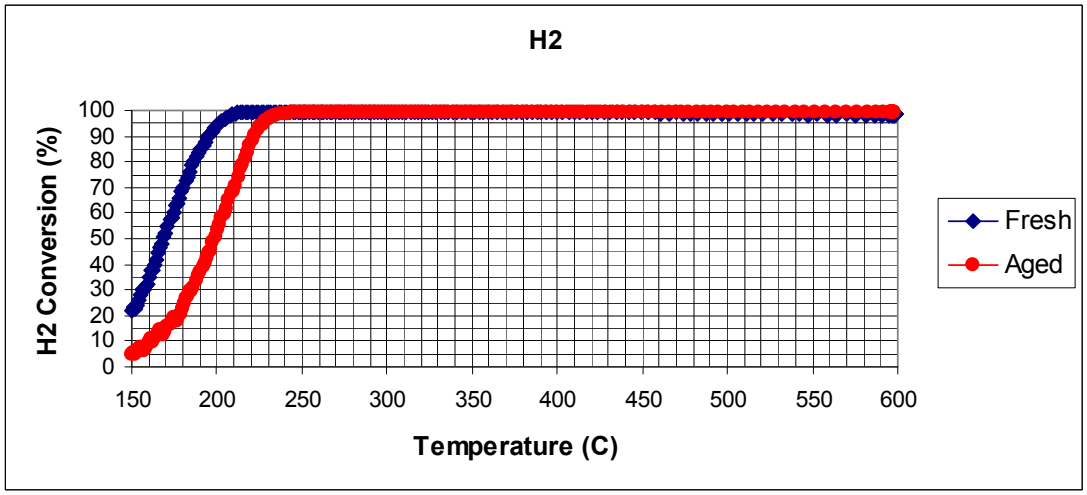

Figure D. 35 H_2 Catalytic Activity of Fresh and Aged (900 ºC) CZO-CI+AO-(2)-M1 Monolithic Catalyst

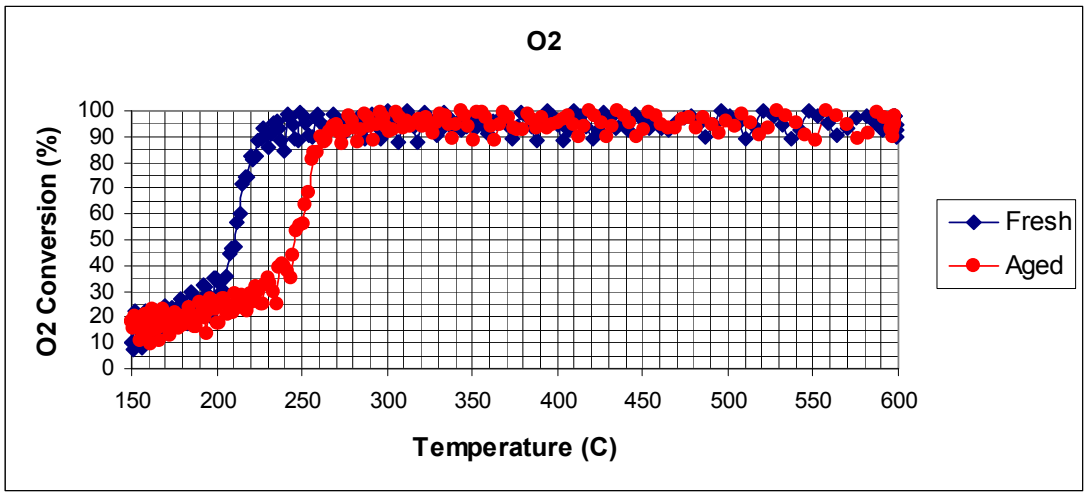

Figure D. 36 O_2 Catalytic Activity of Fresh and Aged (900 ºC) CZO-CI+AO-(2)-M1 Monolithic Catalyst

D.2.3 CZO-SI+AO-(2)-M1 Monolithic Catalyst

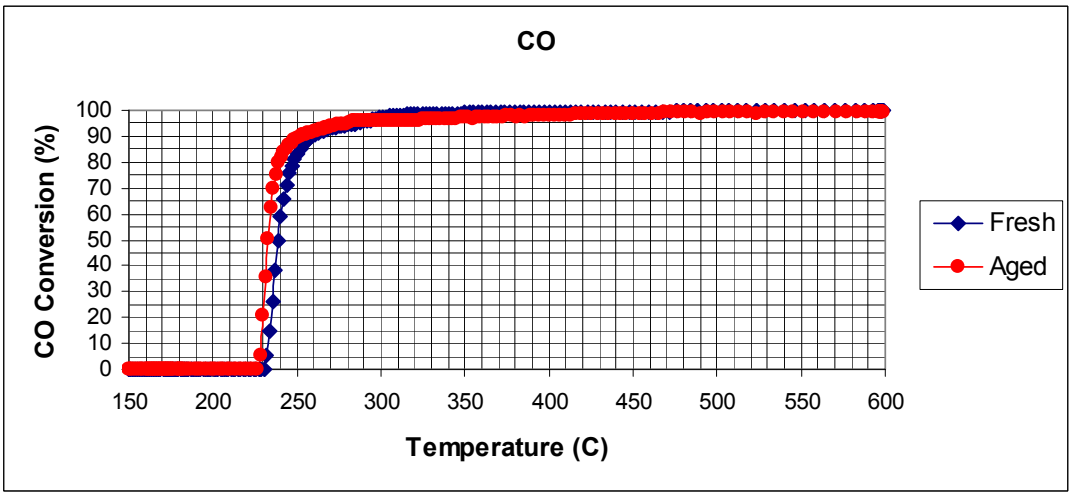

Figure D. 37 CO Catalytic Activity of Fresh and Aged (900 ºC) CZO-SI+AO-(2)-M1 Monolithic Catalyst

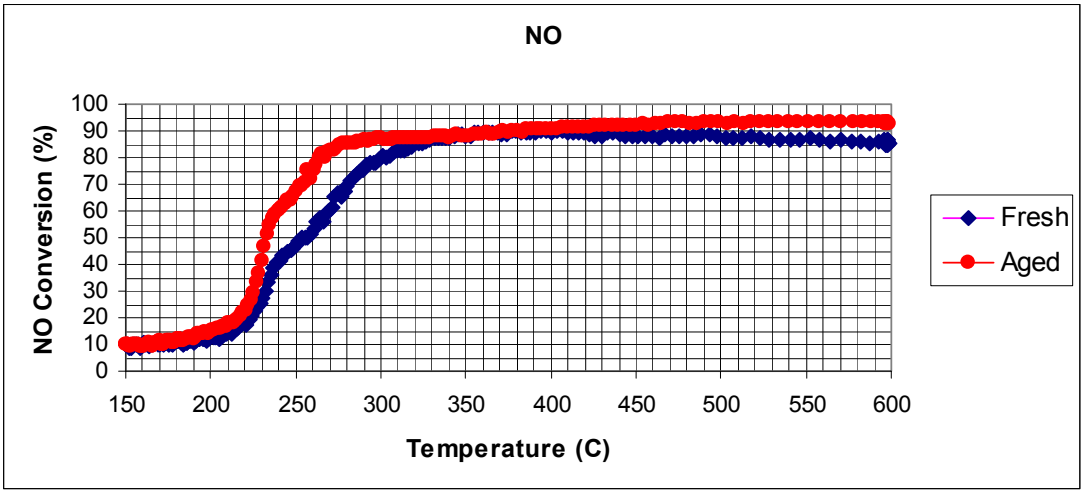

Figure D. 38 NO Catalytic Activity of Fresh and Aged (900 ºC) CZO-SI+AO-(2)-M1 Monolithic Catalyst

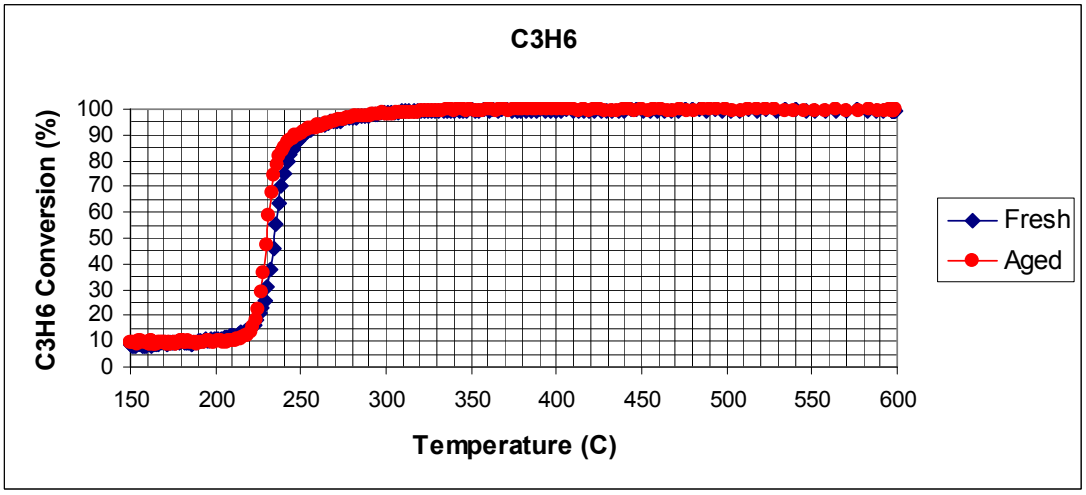

Figure D. 39 C_3H_6 Catalytic Activity of Fresh and Aged (900 ºC) CZO-SI+AO-(2)-M1 Monolithic Catalyst

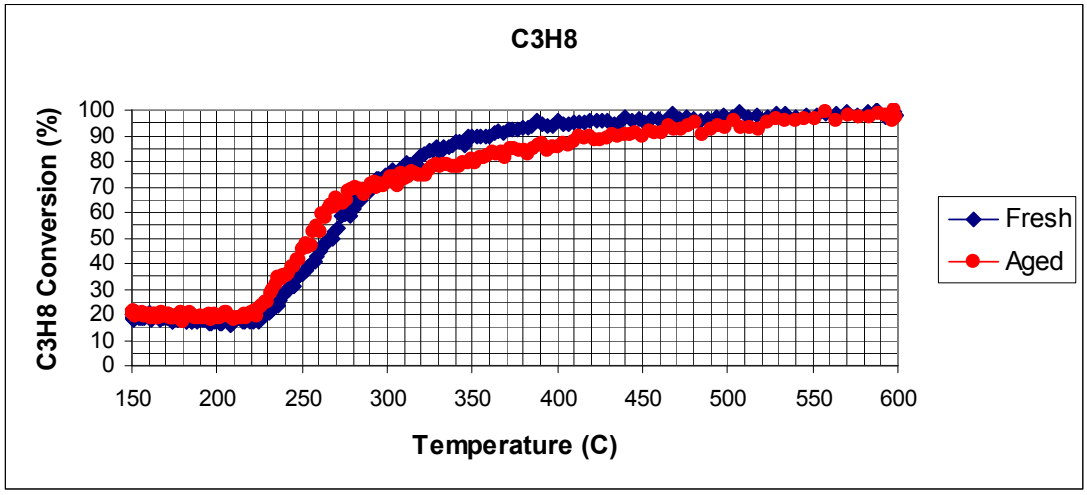

Figure D. 40 C_3H_8 Catalytic Activity of Fresh and Aged (900 ºC) CZO-SI+AO-(2)-M1 Monolithic Catalyst

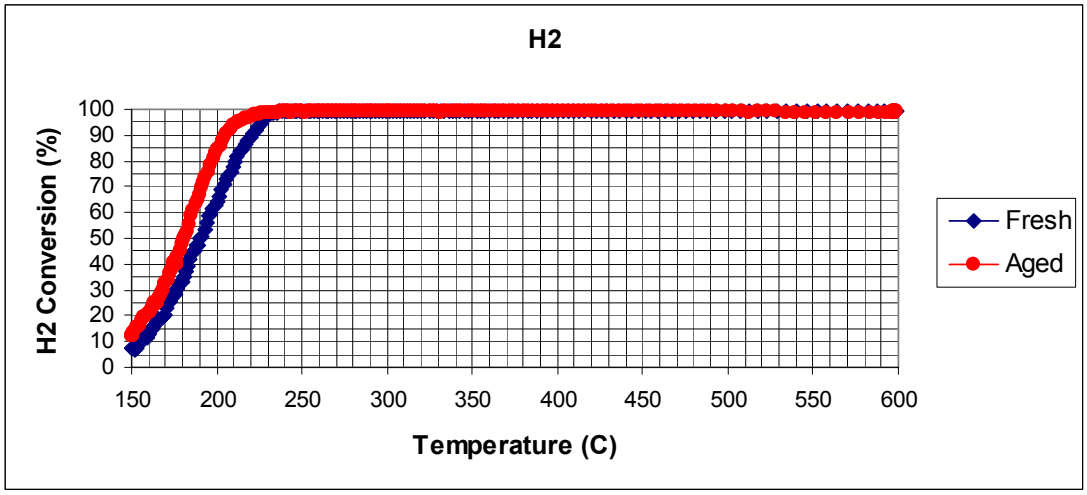

Figure D. 41 H_2 Catalytic Activity of Fresh and Aged (900 ºC) CZO-SI+AO-(2)-M1 Monolithic Catalyst

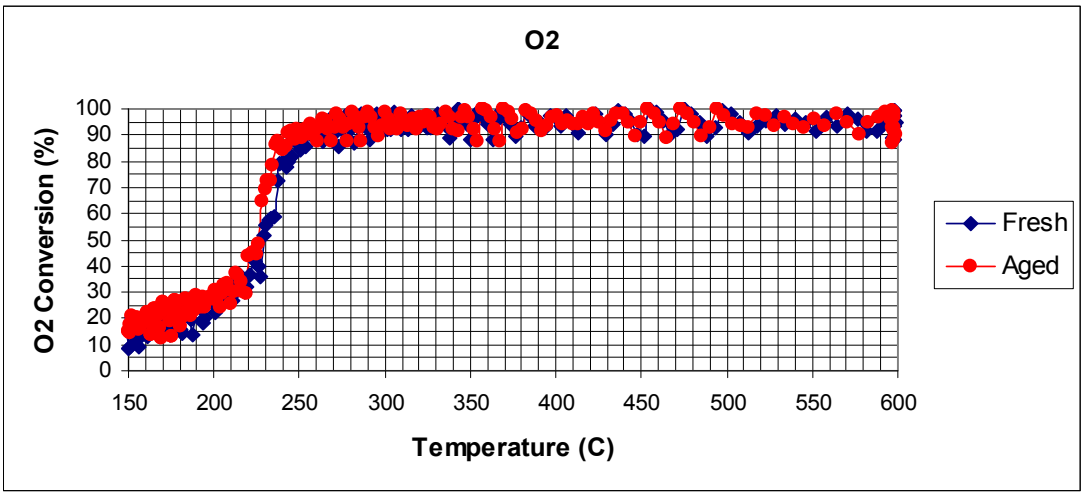

Figure D. 42 O_2 Catalytic Activity of Fresh and Aged (900 ºC) CZO-SI+AO-(2)-M1 Monolithic Catalyst

D.2.4 COM-M5 Monolithic Catalyst

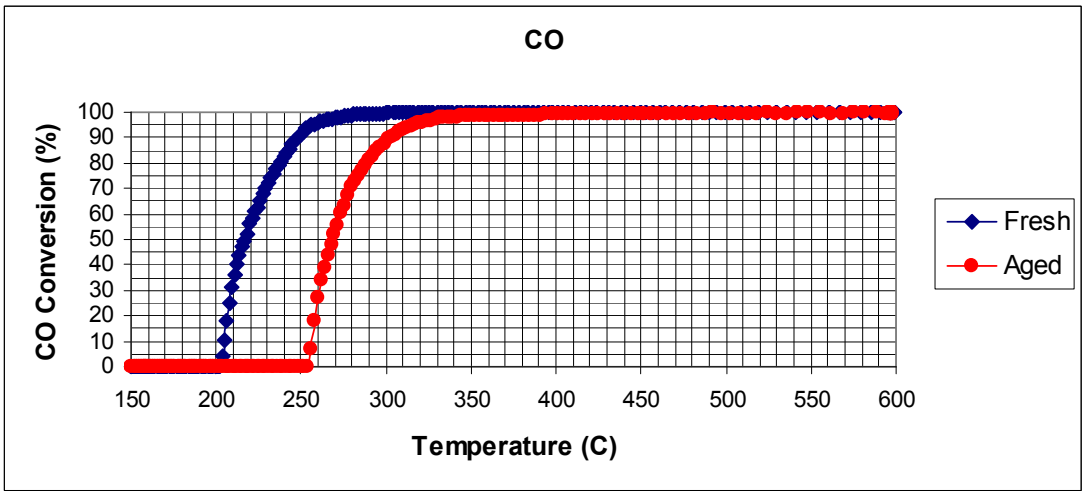

Figure D. 43 CO Catalytic Activity of Fresh and Aged (900 ºC) COM-M5 Monolithic Catalyst During

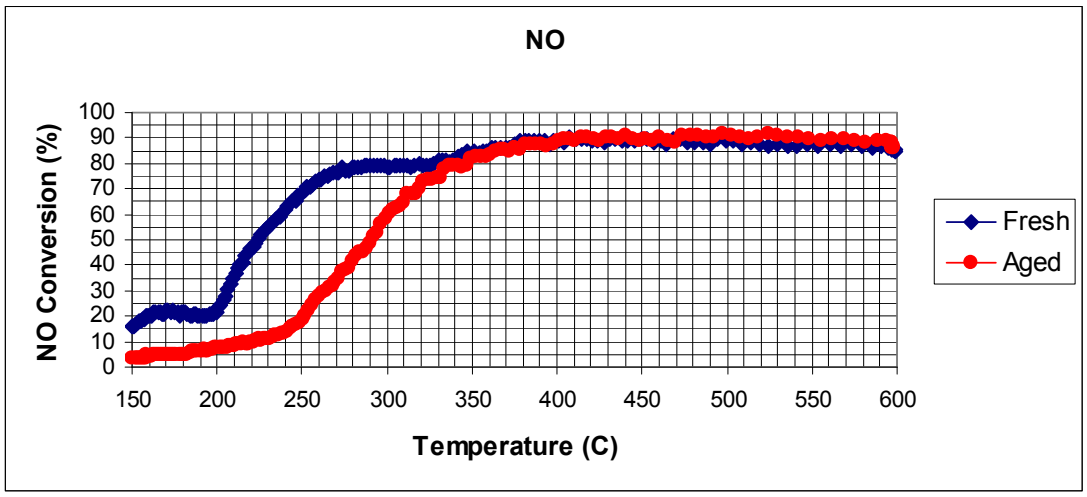

Figure D. 44 NO Catalytic Activity of Fresh and Aged (900 ºC) COM-M5 Monolithic Catalyst

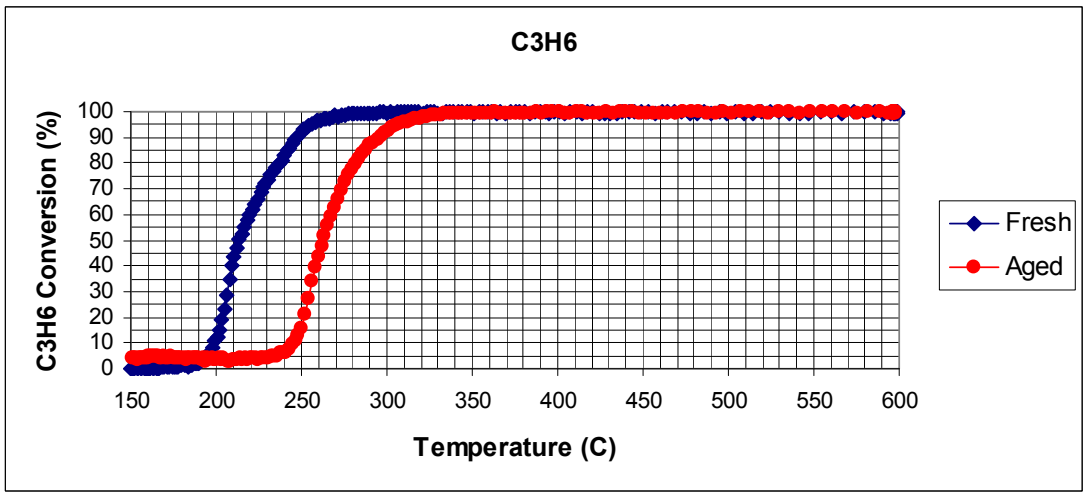

Figure D. 45 C_3H_6 Catalytic Activity of Fresh and Aged (900 ºC) COM-M5 Monolithic Catalyst

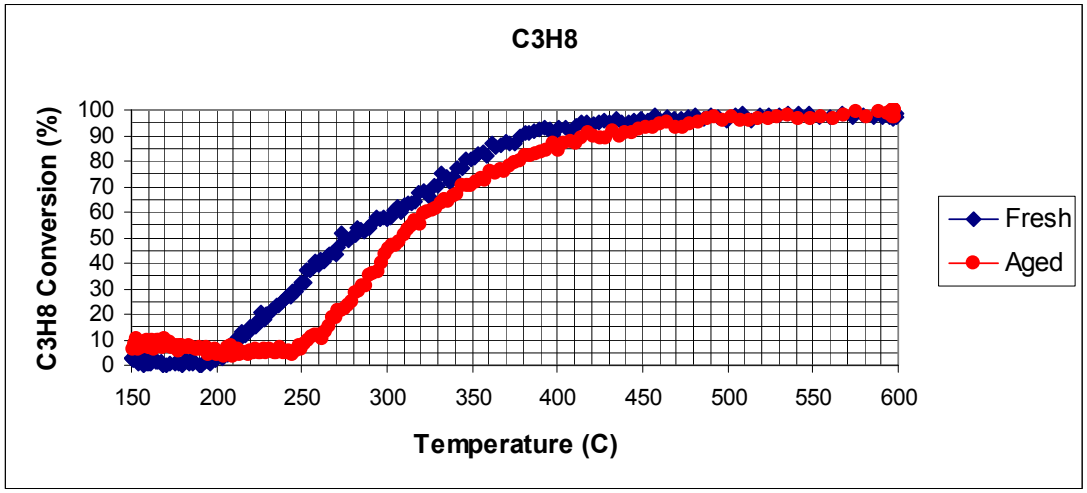

Figure D. 46 C_3H_8 Catalytic Activity of Fresh and Aged (900 ºC) COM-M5 Monolithic Catalyst

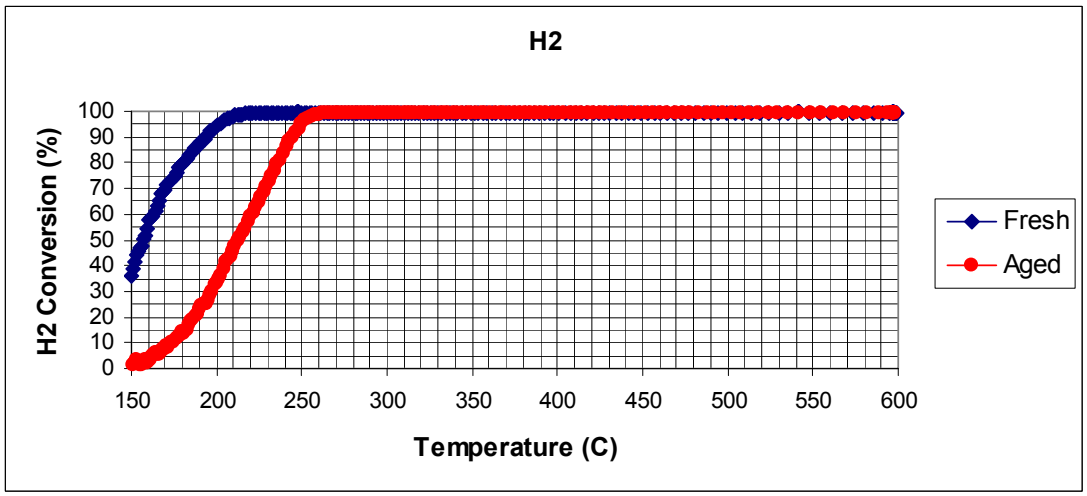

Figure D. 47 H_2 Catalytic Activity of Fresh and Aged (900 ºC) COM-M5 Monolithic Catalyst

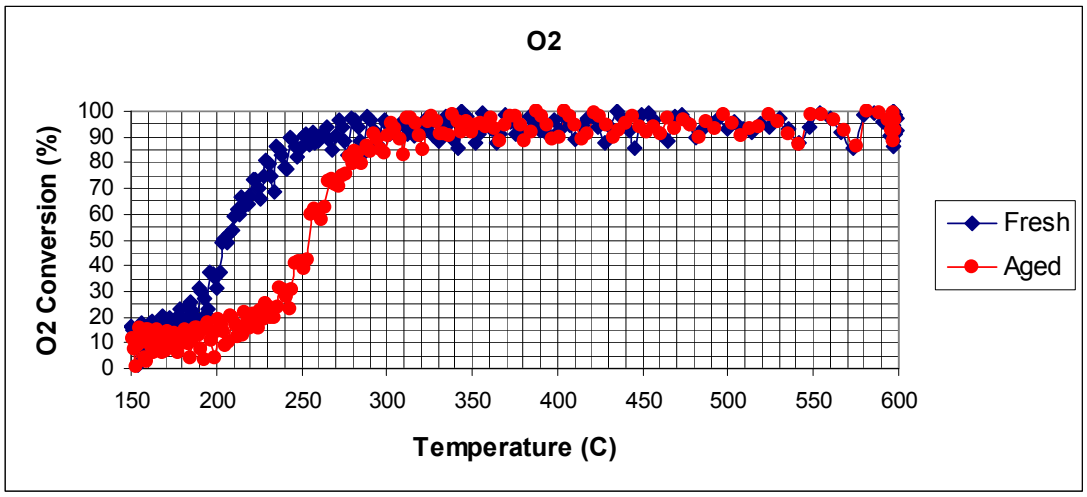

Figure D. 48 O_2 Catalytic Activity of Fresh and Aged (900 ºC) COM-M5 Monolithic Catalyst

D.2.5 CZO-CI+AO-(2)-M2 Monolithic Catalyst

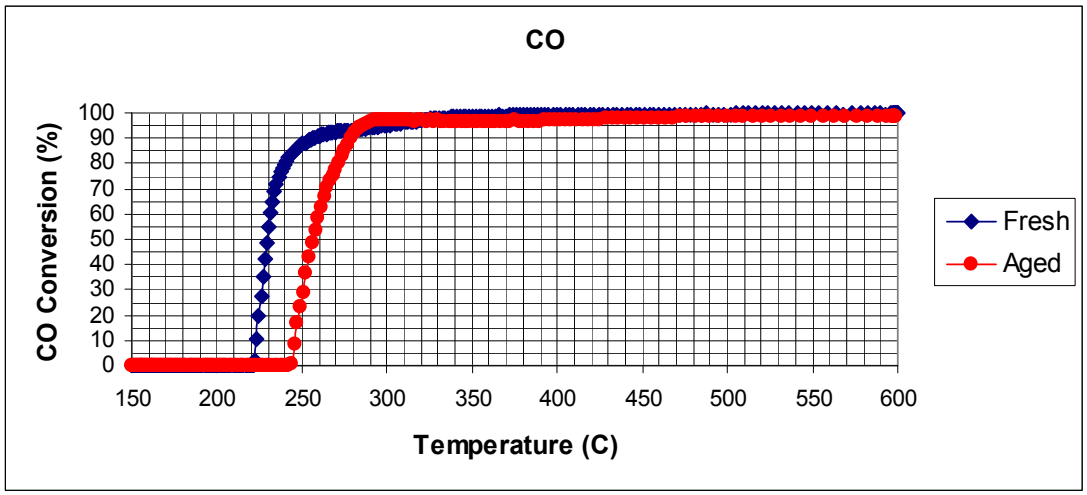

Figure D. 49 CO Catalytic Activity of Fresh and Aged (1000 ºC)
CZO-CI+AO-(2)-M2 Monolithic Catalyst

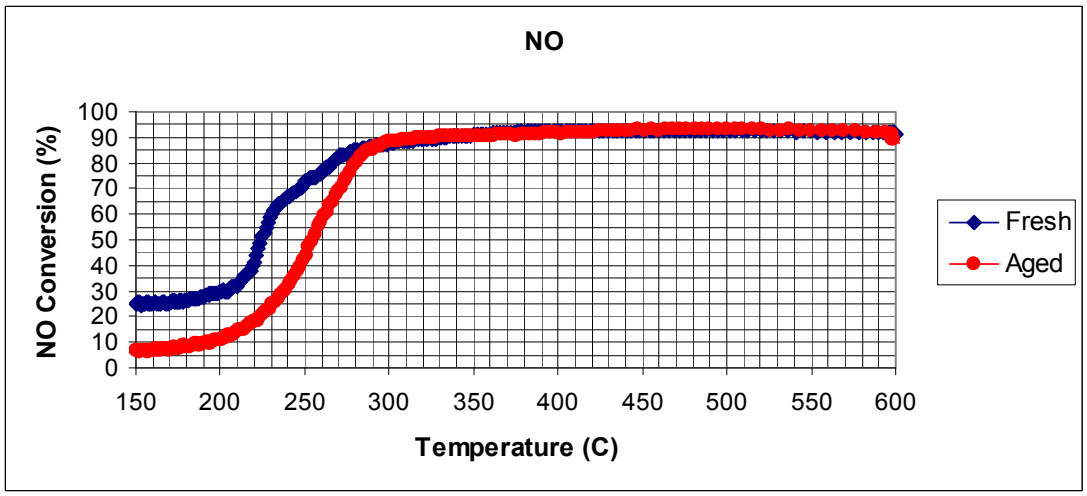

Figure D. 50 NO Catalytic Activity of Fresh and Aged (1000 ºC)
CZO-CI+AO-(2)-M2 Monolithic Catalyst

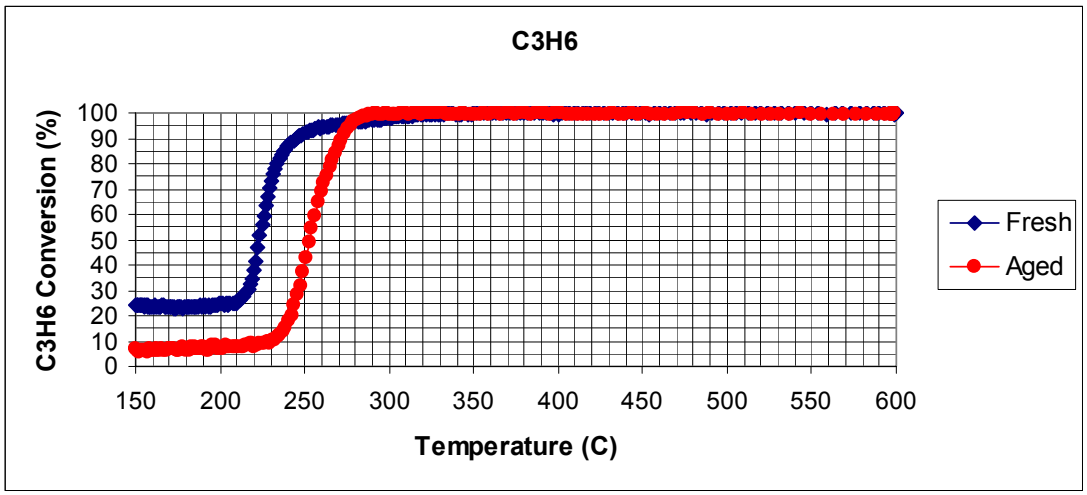

Figure D. 51 C_3H_6 Catalytic Activity of Fresh and Aged (1000 ºC) CZO-CI+AO-(2)-M2 Monolithic Catalyst

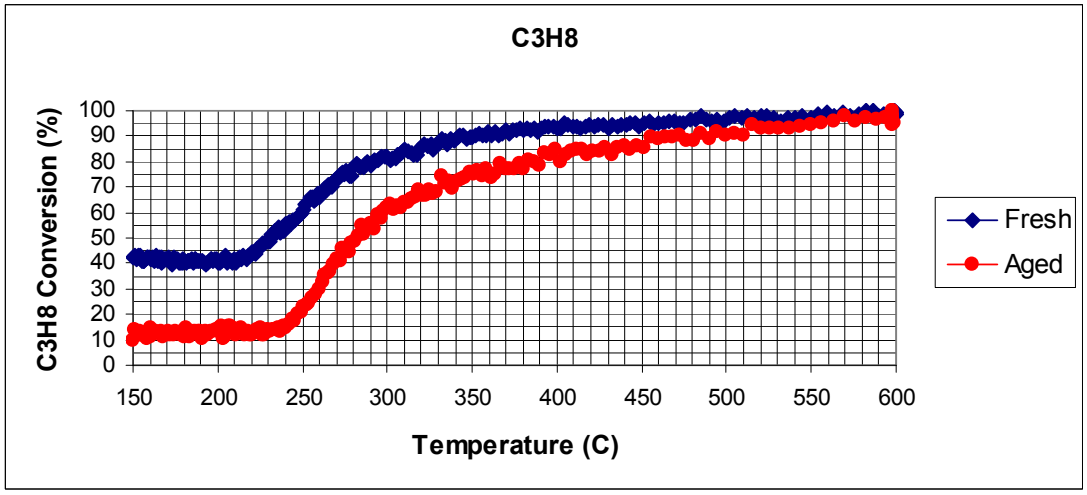

Figure D. 52 C_3H_8 Catalytic Activity of Fresh and Aged (1000 ºC) CZO-CI+AO-(2)-M2 Monolithic Catalyst

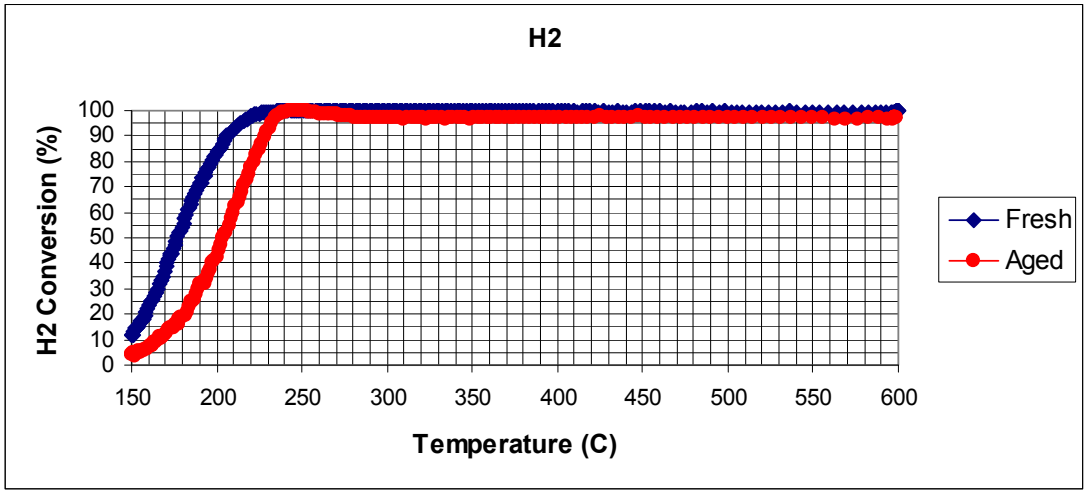

Figure D. 53 H_2 Catalytic Activity of Fresh and Aged (1000 ºC) CZO-CI+AO-(2)-M2 Monolithic Catalyst

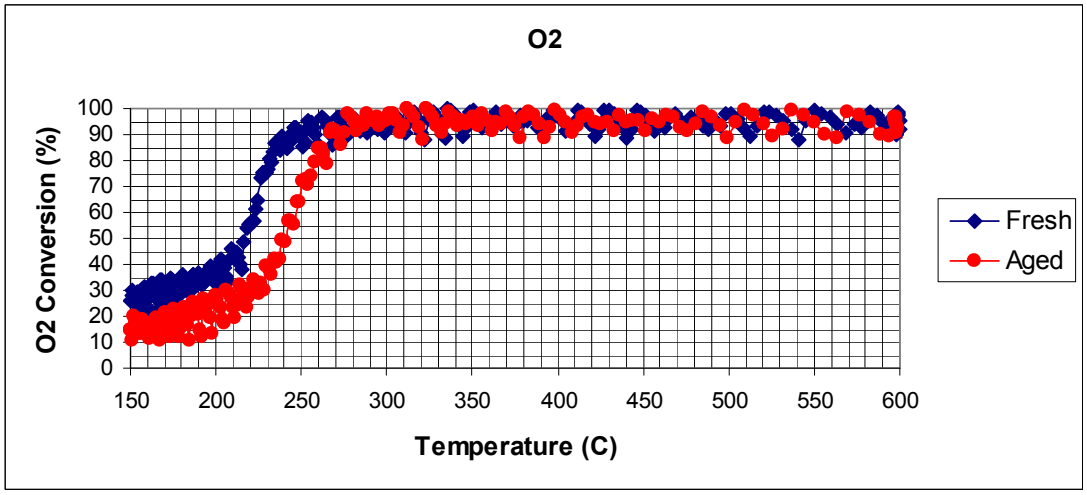

Figure D. 54 O_2 Catalytic Activity of Fresh and Aged (1000 ºC) CZO-CI+AO-(2)-M2 Monolithic Catalyst

D.2.6 CZO-SI+AO-(2)-M2 Monolithic Catalyst

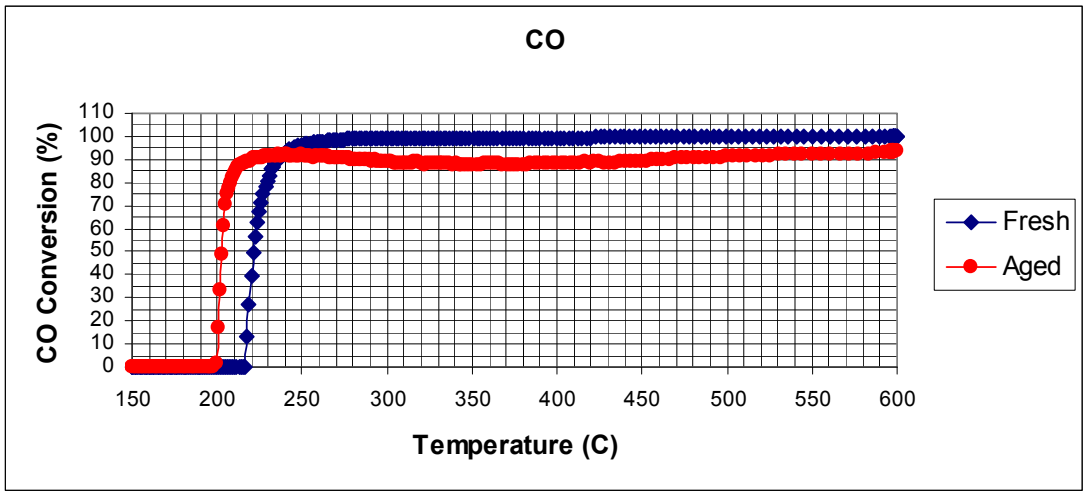

Figure D. 55 CO Catalytic Activity of Fresh and Aged (1000 ºC)
CZO-SI+AO-(2)-M2 Monolithic Catalyst

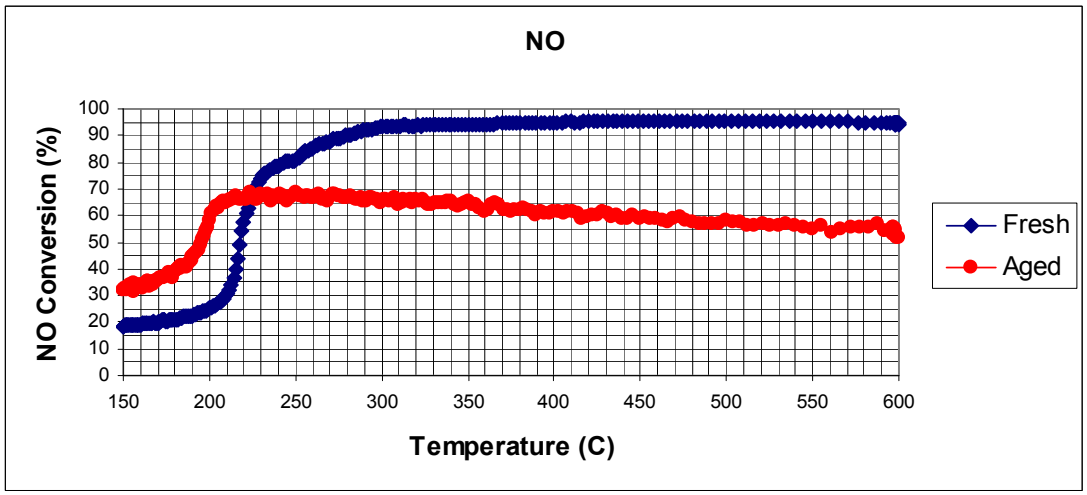

Figure D. 56 NO Catalytic Activity of Fresh and Aged (1000 ºC)
CZO-SI+AO-(2)-M2 Monolithic Catalyst

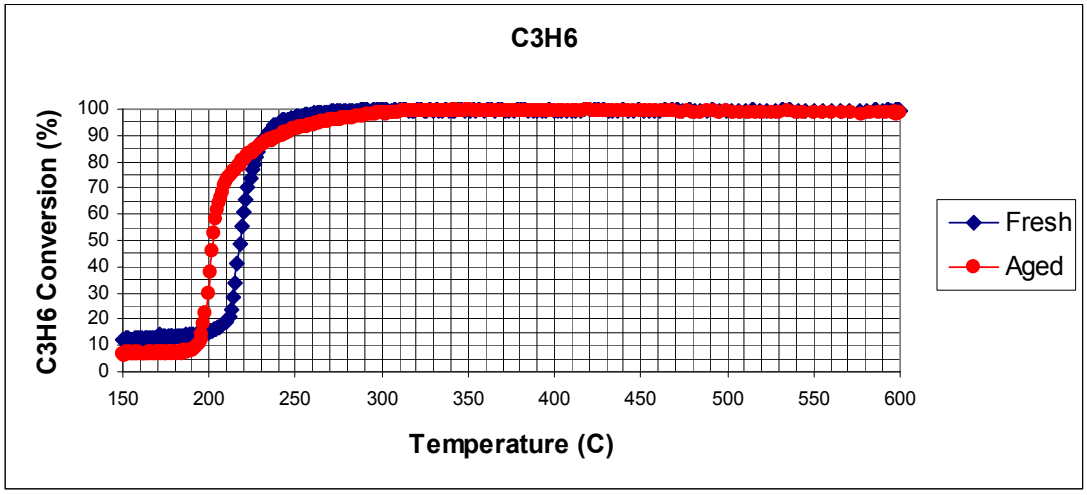

Figure D. 57 C_3H_6 Catalytic Activity of Fresh and Aged (1000 ºC) CZO-SI+AO-(2)-M2 Monolithic Catalyst

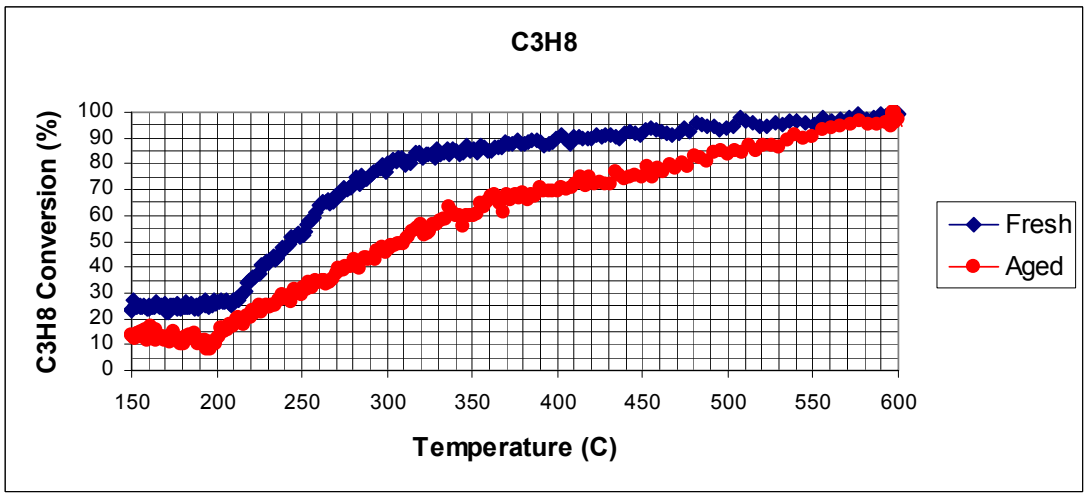

Figure D. 58 C_3H_8 Catalytic Activity of Fresh and Aged (1000 ºC) CZO-SI+AO-(2)-M2 Monolithic Catalyst

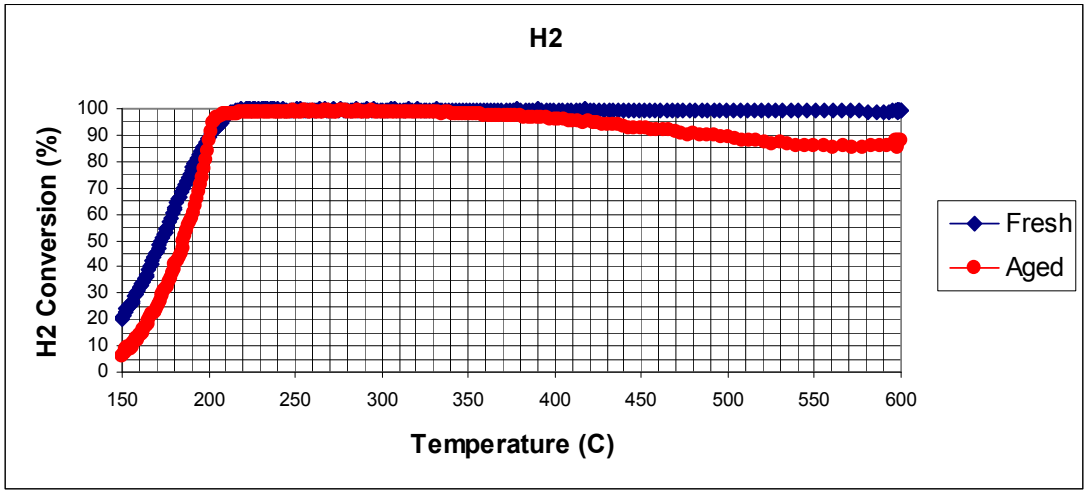

Figure D. 59 H_2 Catalytic Activity of Fresh and Aged (1000 ºC) CZO-SI+AO-(2)-M2 Monolithic Catalyst

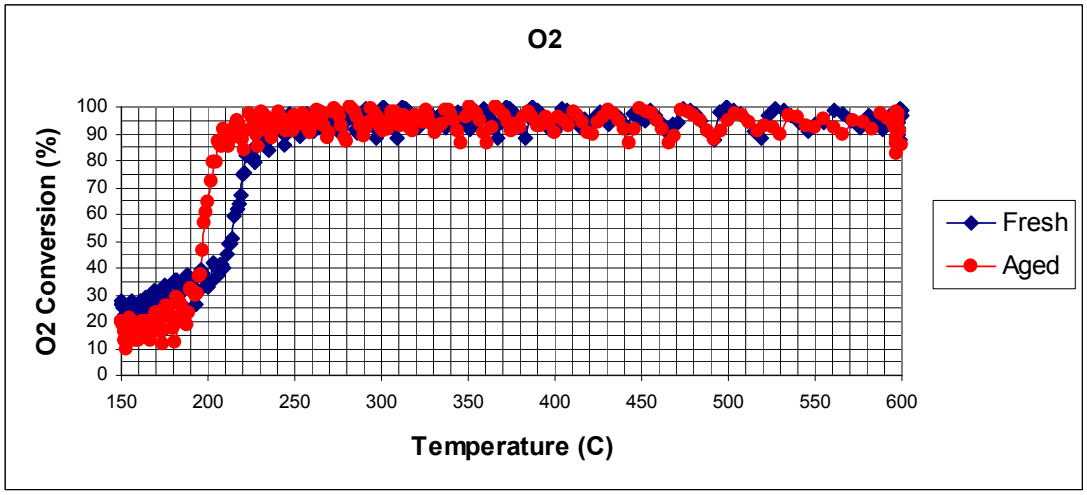

Figure D. 60 O_2 Catalytic Activity of Fresh and Aged (1000 ºC) CZO-SI+AO-(2)-M2 Monolithic Catalyst

D.2.7 COM-M6 Monolithic Catalyst

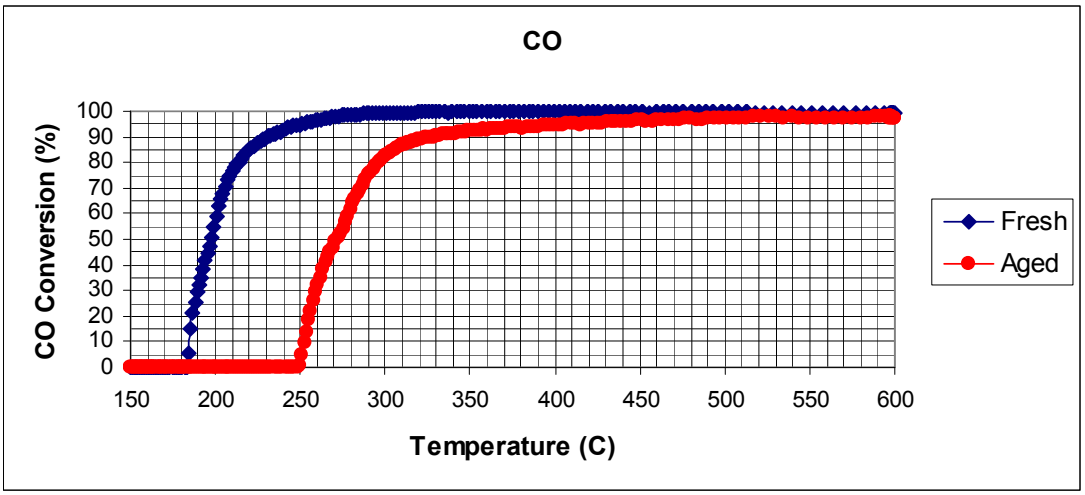

Figure D. 61 CO Catalytic Activity of Fresh and Aged (1000 ºC) COM-M6 Monolithic Catalyst

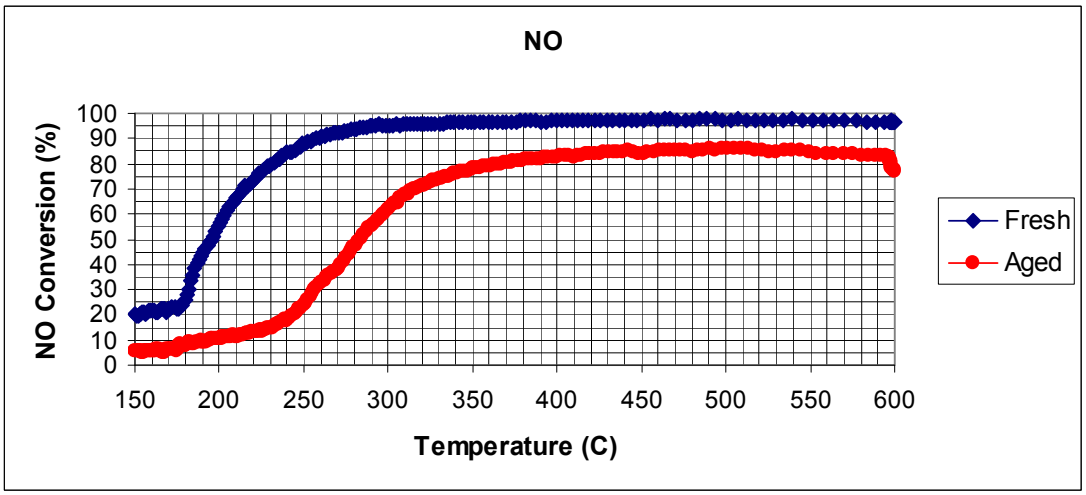

Figure D. 62 NO Catalytic Activity of Fresh and Aged (1000 ºC) COM-M6 Monolithic Catalyst

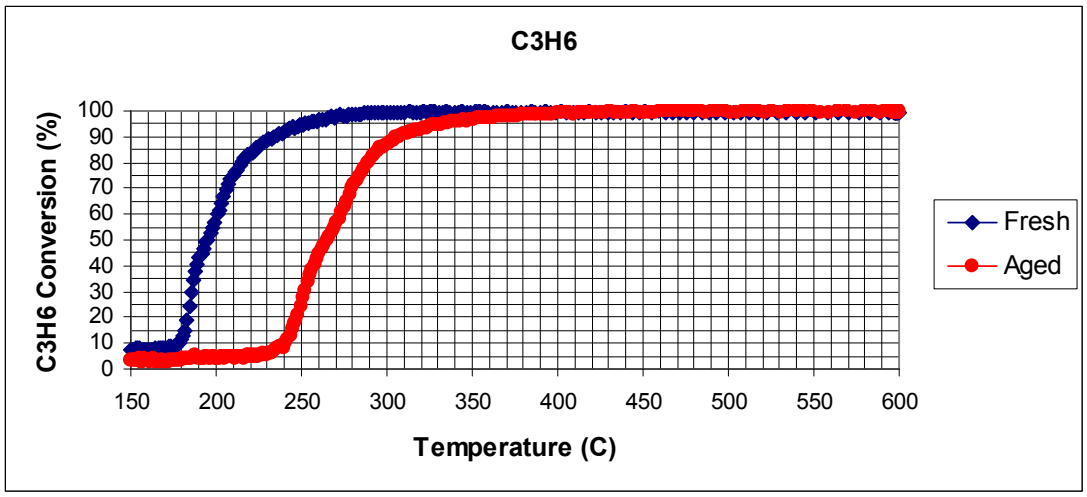

Figure D. 63 C_3H_6 Catalytic Activity of Fresh and Aged (1000 ºC) COM-M6 Monolithic Catalyst

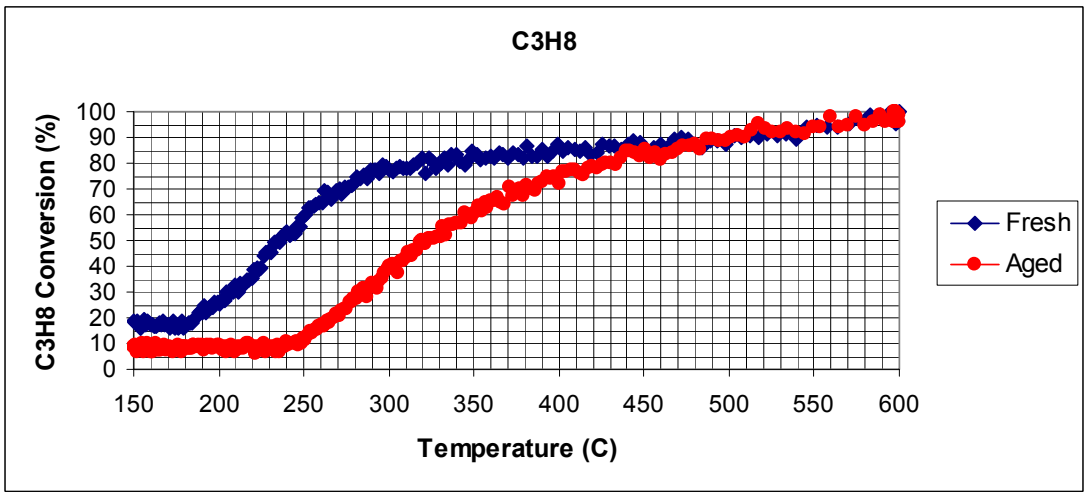

Figure D. 64 C_3H_8 Catalytic Activity of Fresh and Aged (1000 ºC) COM-M6 Monolithic Catalyst

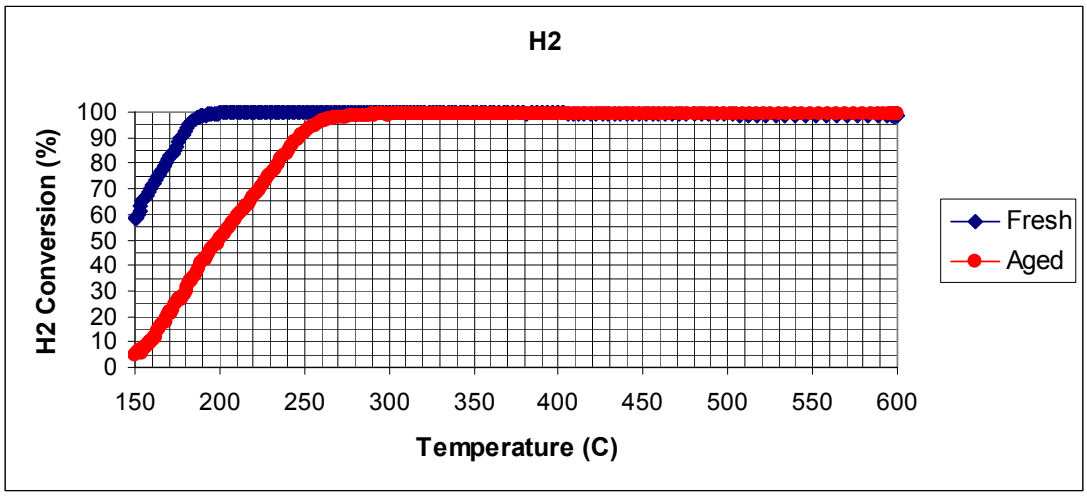

Figure D. 65 H_2 Catalytic Activity of Fresh and Aged (1000 ºC) COM-M6 Monolithic Catalyst

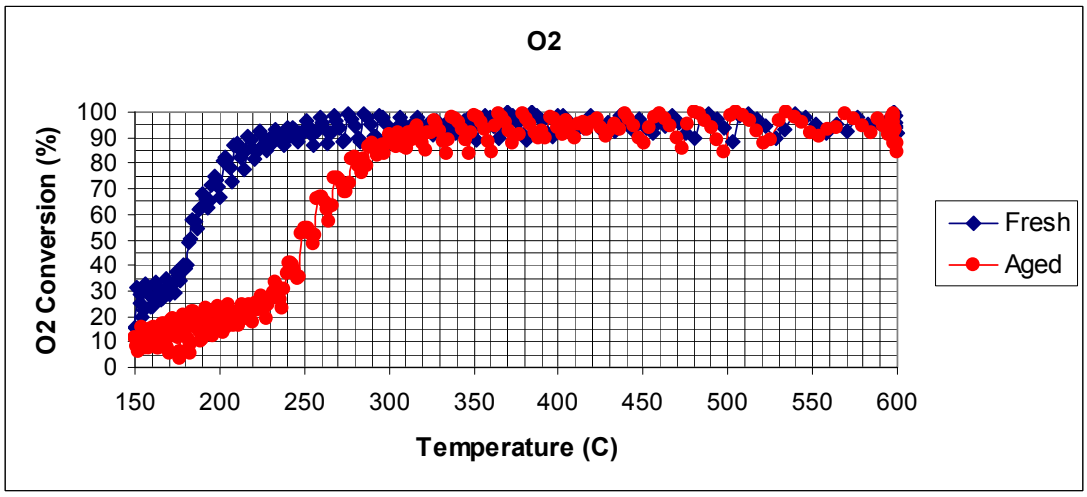

Figure D. 66 O_2 Catalytic Activity of Fresh and Aged (1000 ºC) COM-M6 Monolithic Catalyst

APPENDIX E

ESTIMATION OF PARTICLE SIZE AND XRD DIFFRACTOGRAMS

E.1 Estimation of Particle Size

Particle size of the powder catalysts are estimated using Scherrer equation (Equation E.1) (Cullity & Stock, 2001). In Scherrer equation, "t" is particle size, "λ" is wavelength in nm, "B" is full width of the peak at half of maximum Bragg peak in radians and "θ_B" is Bragg angle. The wavelength of the Cu Kα X-ray is 0.154 nm.

$$t = \frac{0.9\,\lambda}{B\cos(\theta_B)} \qquad \text{(E.1)}$$

For B = 1.46º and $2\theta_B$ = 29.39º, particle size is found as 17 nm.

$$B = 1.46° = 1.46° \times \frac{\pi}{360} = 0.0126\,radians$$

$$2\theta_B = 29.39°$$

$$\theta_B = 14.695°$$

$$t = \frac{(0.90) \times (0.154\,nm)}{(0.0126) \times \left|\cos(14.695)\right|} = 17\,nm$$

E.2 XRD Diffractograms of Fresh Powdered Slurries of Second Set of Catalysts

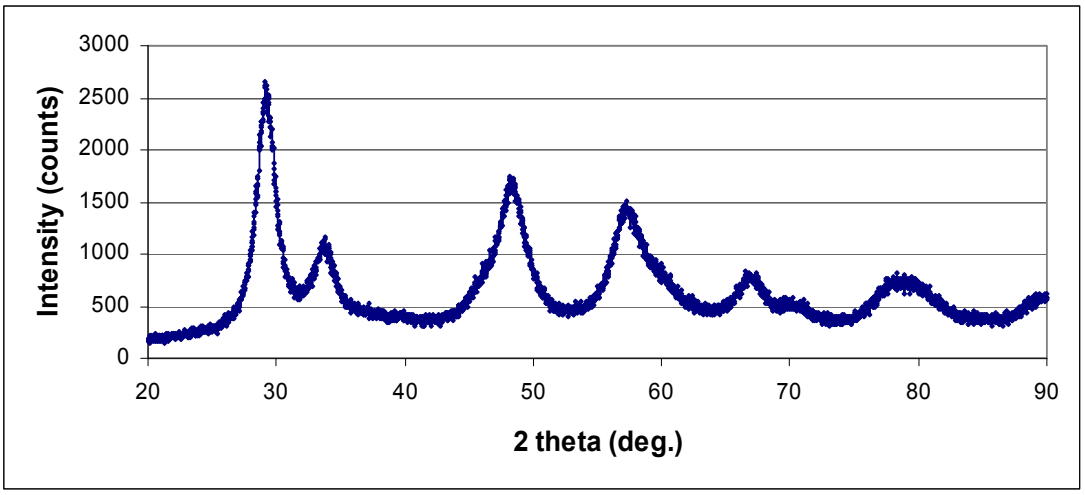

Figure E. 1 XRD Diffractogram of Fresh Powdered Slurry of CZAO-CI-(2) Catalyst

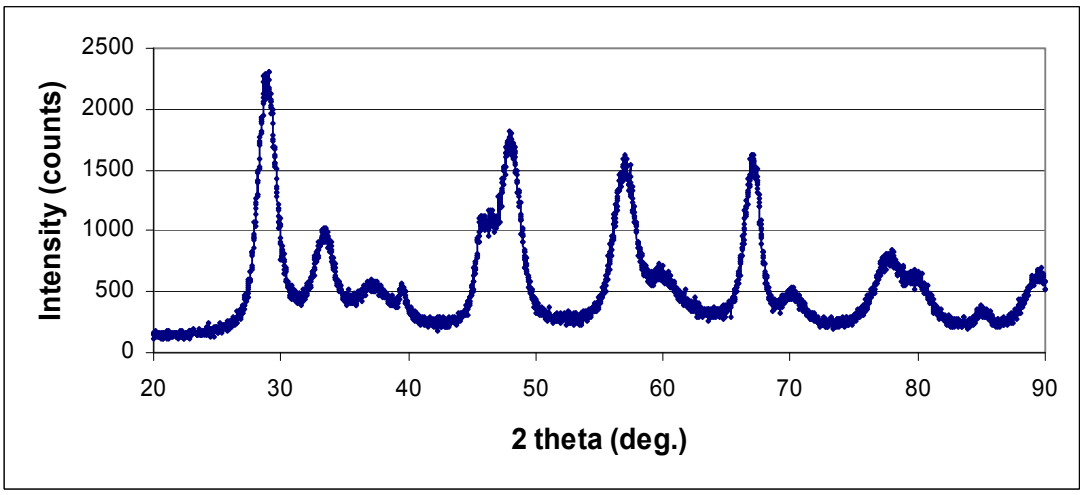

Figure E. 2 XRD Diffractogram of Fresh Powdered Slurry of CZO-CI+AO-(2) Catalyst

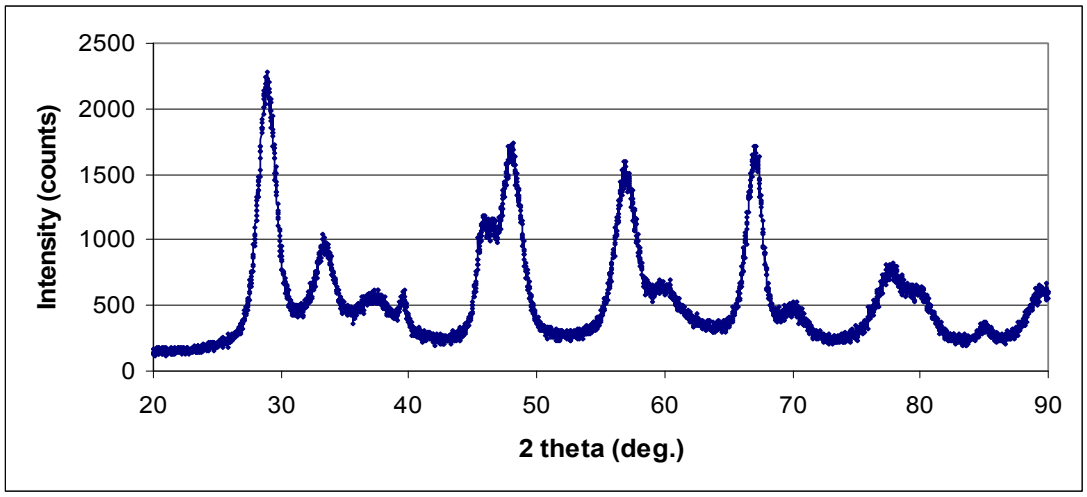

Figure E. 3 XRD Diffractogram of Fresh Powdered Slurry of CZO-SI+AO-(2) Catalyst

E.3 XRD Diffractograms of Aged Powdered Slurries of Second Set of Catalysts

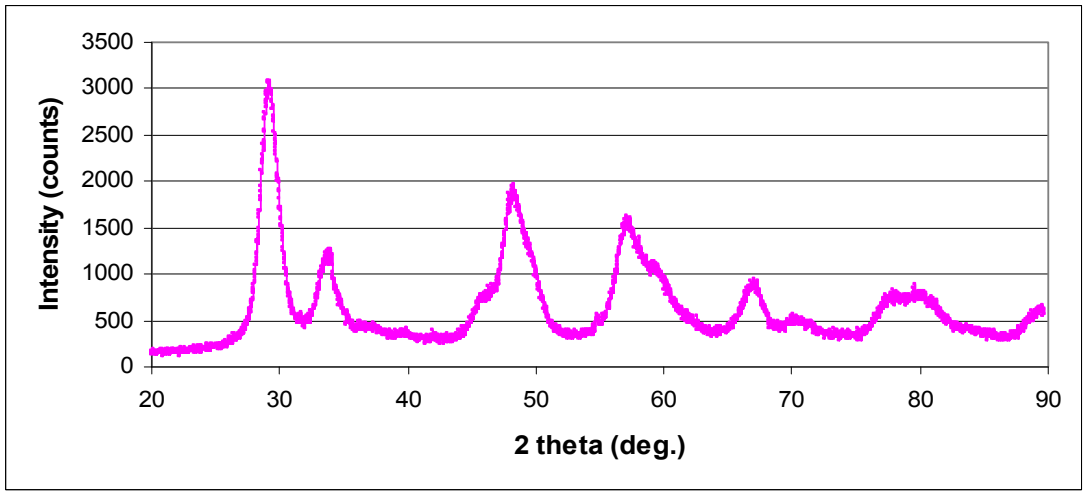

Figure E. 4 XRD Diffractogram of Aged Powdered Slurry of CZAO-CI-(2) Catalyst at 900 ºC

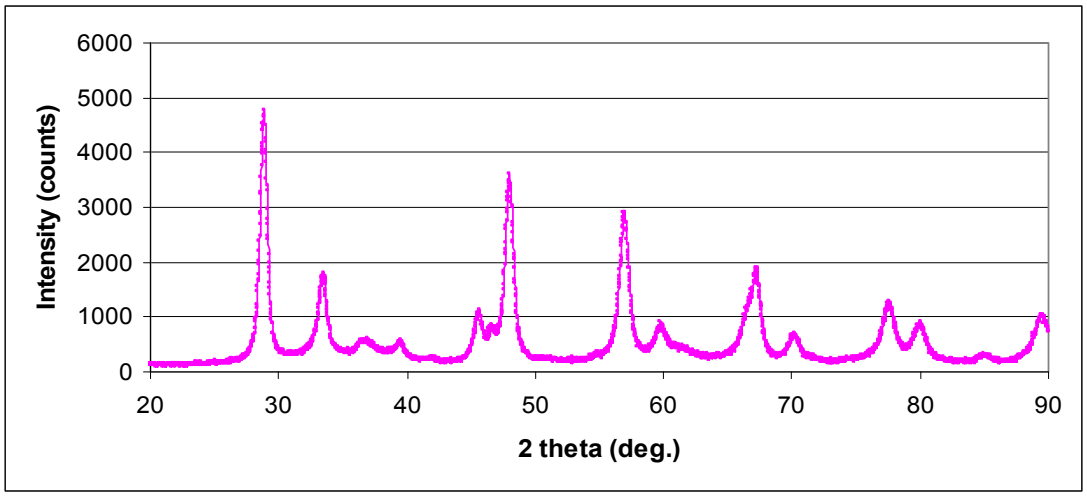

Figure E. 5 XRD Diffractogram of Aged Powdered Slurry of CZO-CI+AO-(2) Catalyst at 900 ºC

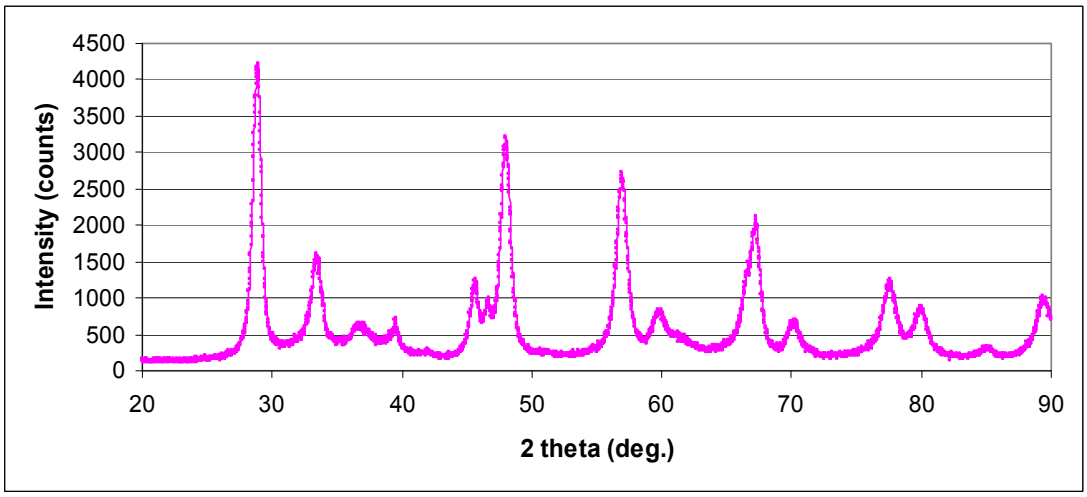

Figure E. 6 XRD Diffractogram of Aged Powdered Slurry of CZO-SI+AO-(2) Catalyst at 900 ºC

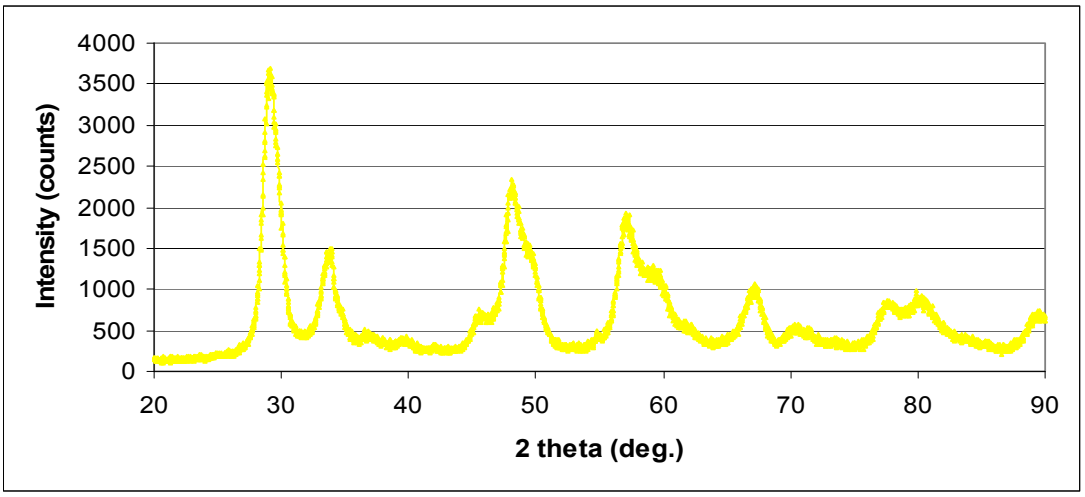

Figure E. 7 XRD Diffractogram of Aged Powdered Slurry of CZAO-CI-(2) Catalyst at 1000 ºC

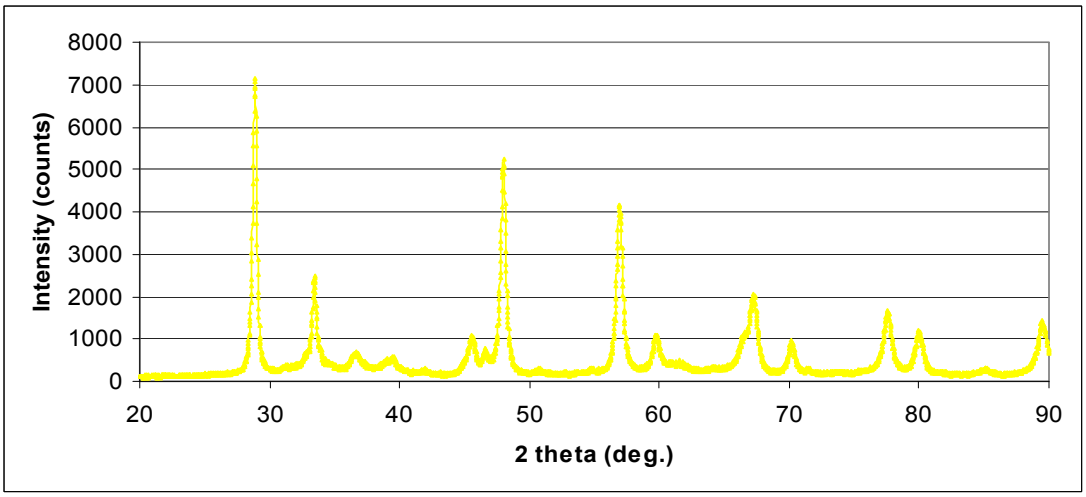

Figure E. 8 XRD Diffractogram of Aged Powdered Slurry of CZO-CI+AO-(2) Catalyst at 1000 ºC

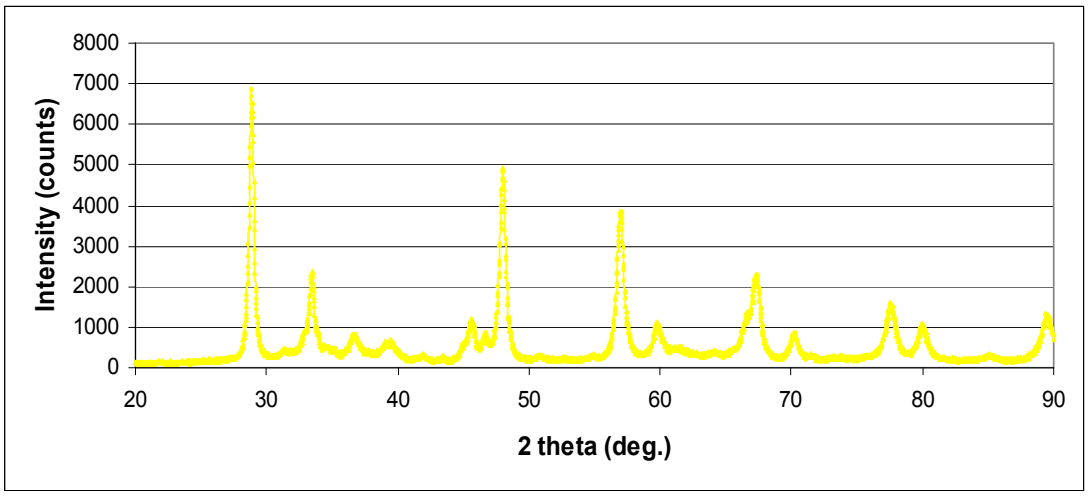

Figure E. 9 XRD Diffractogram of Aged Powdered Slurry of CZO-SI+AO-(2) Catalyst at 1000 ºC